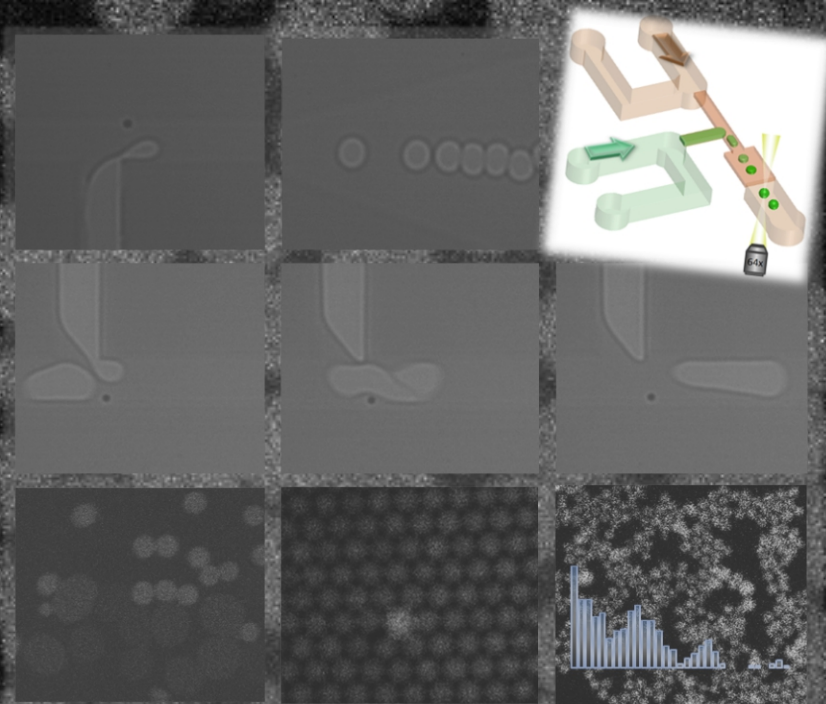


Toward Single Enzyme Analysis in a Droplet-based Micro and Nanofluidic System



Rerngchai Arayanarakool



Toward Single Enzyme Analysis in a Droplet-based Micro and Nanofluidic System

UNIVERSITY OF TWENTE.



The research described in this thesis has been carried out at the “Miniaturized systems for Biomedical and Environmental Applications” (BIOS/Lab-on-a-Chip) group of the MESA+ Institute for nanotechnology at the University of Twente, Enschede, the Netherlands. The research was financially supported by the European Research Council ERC (elab4life) and the European Union’s Seventh Framework Programme FP7 (Brainstorm Project).

Members of the committee:

Chairman	Prof. Dr. Ir. A.J. Moutaah	University of Twente
Promotor	Prof. Dr. Ir. A. van den Berg	University of Twente
	Prof. Dr. J.C.T. Eijkel	University of Twente
Members	Prof. Dr. Ir. R.G.H. Lammertink	University of Twente
	Prof. Dr. Ir. G.J.M. Krijnen	University of Twente
	Prof. Dr. J. van der Oost	Wageningen University
	Prof. Dr. C. Baroud	École Polytechnique (FR)
	Dr. L. Shui	South China Normal University (CN)

Title: Toward Single Enzyme Analysis in a Droplet-based Micro and Nanofluidic System

Author: Rerngchai Arayanarakool

ISBN: 978-90-365-3431-4

DOI: 10.3990./1.9789036534314

Publisher: Woermann Print Service, Zutphen, the Netherlands

Copyright © 2012 Rerngchai Arayanarakool, Enschede, the Netherlands

**TOWARD SINGLE ENZYME ANALYSIS IN
A DROPLET-BASED MICRO AND
NANOFLUIDIC SYSTEM**

DISSERTATION

to obtain
the degree of doctor at the University of Twente,
on the authority of the rector magnificus,
prof.dr. H. Brinksma,
on account of the decision of the graduation committee,
to be publicly defended
on Thursday the 18th of October at 14:45 hrs.

by

Rerngchai Arayanarakool
born on the 4th of February 1981
in Nakorn Ratchasima, Thailand

Table of Contents

1. Aim and outline of thesis	1
<i>I. Introduction</i>	2
<i>II. Main objective of thesis</i>	3
<i>III. Thesis outline</i>	3
<i>References</i>	4
2. Review of droplet microfluidics and enzyme kinetics	6
<i>I. Droplet-based Microfluidics</i>	7
a. Characteristics of droplet-based microfluidics.....	7
b. Droplet generation.....	10
(1) T-junction system.....	10
(2) Flow-focusing system.....	11
(3) Co-axial focusing system.....	13
(4) Electrically-induced droplet generating system.....	14
c. Droplet manipulation.....	14
(1) Active approach.....	15
(2) Passive approach.....	24
(3) Droplet fusion.....	30
d. Conclusion.....	34
<i>II. Enzyme and enzyme kinetics</i>	34
<i>References</i>	36
3. Design, Material and Realization	40
<i>I. Conceptual design</i>	41
a. Miniaturization of the carriers.....	41
b. Regulation of a small flow rate.....	42
c. Droplet fusion concept.....	43
d. Concept of detection channel.....	45
<i>II. Material selection</i>	46
<i>III. Polydimethylsiloxane (PDMS)based microfluidic device</i>	49
<i>IV. Glass-based microfluidic device</i>	53
<i>V. Fluidic and optical setups</i>	55
a. Fluidic connection.....	55
b. Optical setup.....	55
<i>VI. Simulation</i>	57
<i>References</i>	61

4. Low-temperature, simple and fast integration technique of microfluidic chips using a UV-curable adhesive.....	63
<i>I. Introduction</i>	64
<i>II. Experimental details</i>	66
a. Chip bonding.....	66
b. Characterization.....	67
(1) Homogeneity of the gluing layer.....	67
(2) Thickness of the gluing layer.....	67
(3) Chemical test.....	67
(4) Fluidic test.....	67
<i>III. Results and Discussion</i>	68
(1) Optimization of the bonding method.....	68
(2) Bonding characterization.....	69
<i>IV. Conclusion</i>	71
<i>References</i>	71
5. In-channel UV-patternable hydrophobization of micro- and nanofluidic networks.....	74
<i>I. Introduction</i>	75
<i>II. Experimental details</i>	77
a. Surface modification.....	77
b. Characterization.....	77
(1) Contact angle measurement.....	77
(2) X-ray Photoelectron Spectroscopy (XPS).....	78
(3) W/O emulsion generation.....	78
(4) Hydrophobic patterning.....	78
<i>III. Results and discussion</i>	79
a. Characterization.....	79
(1) Contact angle measurement.....	79
(2) X-ray Photoelectron Spectroscopy (XPS).....	81
(3) Stability.....	82
(4) In-channel modified surface.....	83
(5) Homogeneity of hydrophobization (W/O emulsion).....	84
(6) Hydrophobic patterning.....	85
b. Discussion.....	86
<i>IV. Conclusion</i>	88
<i>References</i>	88

6. Single-molecule encapsulation and detection in a droplet-based micro and nanofluidic device	91
<i>I. Single-molecule detection</i>	92
<i>II. Kinetic activity in the bulk experiment determined from a fluorescence spectrometer</i>	97
<i>III. Single-enzyme kinetics on a droplet-based microfluidics</i>	98
a. Experimental Details.....	99
b. Experimental Results.....	100
(1) Enzyme kinetics in the presence of n-propyl gallate.....	100
(2) Enzyme kinetics in the absence of n-propyl gallate.....	103
<i>IV. Discussion</i>	106
<i>V. Conclusion</i>	108
<i>References</i>	109
7. Summary and perspectives	110
<i>I. Summary</i>	111
<i>II. Perspective</i>	112
a. Droplet fusion.....	112
b. Expansion chamber to enhance the efficiency of droplet fusion.....	113
c. Study of the effect of inhibitors.....	114
d. Break-up of a large droplet to generate small droplets.....	114
e. Reduced background from a device.....	116
f. Enzymatic reaction at elevated temperature.....	117
g. Surfactant and oil.....	117
<i>References</i>	117
Appendix A	118
Appendix B	123
Appendix C	129
Acknowledgements	133
Curriculum Vitae	136
Publications	137

CHAPTER 1:

Introduction

This chapter introduces the aim of this thesis, which is to perform single enzyme kinetic analysis using microfluidics and droplet-based microfluidic technology. Short introductions into these subjects are followed by a brief description of each chapter.

I. Introduction

Microfluidics is a relatively new multidisciplinary research field dealing with transport phenomena in fluid-based devices at scales reaching from single cells to the dimension of biomolecules. The potential characteristics of micro- or nano-scaled devices are, for instance, low consumption of reagents, precise control of fluids, and high-throughput results. These benefits enabled this technology gaining more and more popularity in multidisciplinary research areas during the last few decades.¹

Droplet-based microfluidics

Droplet-based microfluidic is a subcategory of microfluidic technology by which two or more immiscible fluids (i.e. oil and water) are loaded into a microfluidic device to generate compartmented and well-confined carriers of one fluid in the other fluid (e.g. oil-in-water or water-in-oil emulsions). Generated carriers can be used for diverse applications such as bioanalysis, polymerization and so on. In addition, the dimension of the generated carriers can be modulated by changing the flow rates of the two immiscible fluids or the geometry of the fluidic channel in the device. Furthermore, the generated carriers can be simply but precisely manipulated in the microfluidic device.^{2,3}

Single-molecule analysis

Recent single-molecule analysis studies have tried to unravel phenomena that remain hidden in the conventional bulk experiments by encapsulating single molecules into enclosed volumes such as vesicles,⁴⁻⁶ or by attaching a single molecule onto the polymer-coated surface.⁷⁻⁹ However, when the compartmented volume is reduced, the issue of the evaporation of reagent and the precise dimensions as well as the monodispersity¹⁰ of the confining containers can arise. Alternatively, a droplet-based microfluidic device allows a high rate of formation of highly-monodisperse carriers which can be used as containers to encapsulate a single molecule for bioanalysis.

II. Main objective of this thesis

The main objective of this thesis is to develop a micro- and nanofluidic platform for the generation and manipulation of tiny (femtolitre) aqueous droplets in the oil phase (water-in-oil emulsion) for the encapsulation of a single molecule of enzyme to perform an enzyme kinetic analysis.

III. Thesis Outline

In this thesis, we demonstrate the application of a micro- and nanofluidic device for the single-enzyme analysis by encapsulating single enzymes into the generated aqueous droplets in oil. This thesis consists of the introduction (chapter 1), a review of the generation and manipulation of droplets and the basic enzymology (chapter 2), the design and fabrication of our device (chapter 3), the technologies related to our device (chapter 4 and 5), the validation of our device for the single enzyme analysis (chapter 6), and lastly the conclusion and the perspective of our device (chapter 7).

Chapter 2: Theoretical background

In chapter 2, we review and elucidate the formation and manipulation of droplets in a microfluidic device. In addition, the basic concept of enzymology is explained to the non-enzymologist reader.

Chapter 3: Design, materials and realization

Chapter 3 explains the concept of the fluidic manipulation in our device. The design and the materials of our device as well as its fabrication method are discussed. Then, devices which are made of different materials are tested to validate the materials choice for our application. Glass is finally selected as the most appropriate material.

Chapter 4: Low-temperature bonding technique

Chapter 4 proposes the integration method of two substrates which operates at room temperature by using UV light and UV adhesive. Basically, the glass substrates need to be hydrophobized for facilitating water-in-oil emulsion for our application. One idea is to

Chapter: 1

hydrophobize two patterned glass substrates and subsequently bond them by using this bonding method since the conventional bonding approaches can ruin the surface layer of modified substrates. This bonding approach can be applied for different materials with a thin layer of a gluing layer. However, this technique is unsuitable for a device comprising nanofluidic channels.

Chapter 5: In-channel hydrophobization

In this chapter, a new hydrophobization method is described to manufacture hydrophobic glass-based devices, needed to prepare water-in-oil emulsions. Surface modification of the micro- and nanofluidic chip is performed in-channel by using UV light and silicone oil. The hydrophobized chip is characterized by different methods.

Chapter 6: Single-enzyme encapsulation and enzyme kinetics study in a droplet

In chapter 6, the hydrophobized fluidic chip is used to generate droplets for the single-enzyme analysis via a fluorescence measurement. The optical background noise is considered and discussed for the enzymatic reaction in our study. Then, the encapsulation of single enzymes is validated from the observed distribution of the increasing fluorescence intensity of the product molecule. The obtained enzyme kinetic activity was compared to the value obtained from the experiment in bulk by a fluorescence spectrometer.

Chapter 7: Summary and perspective

Eventually, all aspects in this thesis are summed up. In addition, the outlook of our device is detailed such as further experiments on droplet fusion, the improvement of the droplet fusion and the further reduction of the optical background noise. Also, promising applications of our device are exemplified and discussed in the last chapter.

References

1. A. van den Berg and T. S. J. Lammerink, *Top Curr Chem*, 1998, **194**, 21-49.
2. A. B. Theberge, F. Courtois, Y. Schaerli, M. Fischlechner, C. Abell, F. Hollfelder and W. T. S. Huck, *Angew Chem Int Edit*, 2010, **49**, 5846-5868.
3. S. Y. Teh, R. Lin, L. H. Hung and A. P. Lee, *Lab Chip*, 2008, **8**, 198-220.

4. S. M. Christensen, P. Y. Bolinger, N. S. Hatzakis, M. W. Mortensen and D. Stamou, *Nat Nanotechnol*, 2012, **7**, 51-55.
5. Q. Chen, H. Schonherr and G. J. Vancso, *Small*, 2009, **5**, 1436-1445.
6. T. M. Hsin and E. S. Yeung, *Angew Chem Int Edit*, 2007, **46**, 8032-8035.
7. H. P. Lu, L. Y. Xun and X. S. Xie, *Science*, 1998, **282**, 1877-1882.
8. W. Min, I. V. Gopich, B. P. English, S. C. Kou, X. S. Xie and A. Szabo, *J Phys Chem B*, 2006, **110**, 20093-20097.
9. K. Velonia, O. Flomenbom, D. Loos, S. Masuo, M. Cotlet, Y. Engelborghs, J. Hofkens, A. E. Rowan, J. Klafter, R. J. M. Nolte and F. C. de Schryver, *Angew Chem Int Edit*, 2005, **44**, 560-564.
10. B. Rotman, *Biochemistry*, 1961, **47**, 1981-1991.

CHAPTER 2:

Brief review of droplet microfluidics and enzyme kinetics

This chapter summarizes the theoretical background used in this thesis. First of all, the droplet-based microfluidics which is the major technology used in this work is detailed in aspects of (i) its potential characteristics which have attracted many researchers to employ this technology for a wealth of applications; (ii) droplet generation which is explained in three categories for different fluidic configurations; and lastly (iii) droplet manipulation which is briefly reviewed to give an overview of the recent methods that people have utilized to control the droplets in microfluidic systems. In addition, the basic concepts needed to describe the enzymatic reaction and related technical terms are provided.

Theoretical Background

I. Droplet-based microfluidics

a. Characteristics of droplet-based microfluidics

Droplet-based microfluidics is one subcategory of microfluidics focusing on the creation of confined volumes from two (or more) immiscible phases. In general, the dimensions of the microscopic patterns or channels in microfluidic devices are limited by the resolution and the cost of microfabrication technology which hinders their usage in the miniaturization of fluidic volumes. In addition, miniaturized fluidic channels can cause problems during fluidic operation such as channel clogging. To avoid these limitations, microdroplets generated in a microfluidic device offer an alternative approach to reproducibly generate confined discrete volumes of fluid down to submicron scales.¹ The essential characteristics of the droplet-based microfluidic system are discussed below.

Compartmentalization

The compartmentalized droplet can be used as a platform for a vast range of experiments e.g. biological or (bio)chemical reactions and analysis. Individual droplets of water containing all ingredients of the reaction are isolated in an immiscible continuous phase, as a result of which the reaction occurring inside a microdroplet is (generally) not perturbed by contamination. Also, the product of the reaction is accumulated in a single droplet allowing the time-resolved measurement of product for the determination of kinetic activity of the reaction. Numerous researchers have recently demonstrated the considerable potential of the droplet-based microfluidic technology for varied bio-analysis experiments i.e. enzymatic reactions,²⁻¹¹ the polymerase chain reaction (PCR),¹²⁻¹⁵ cell-encapsulated assay,¹⁶⁻²² as well as for the fabrication of monodisperse microparticles²³⁻³⁰ on microfluidic devices.

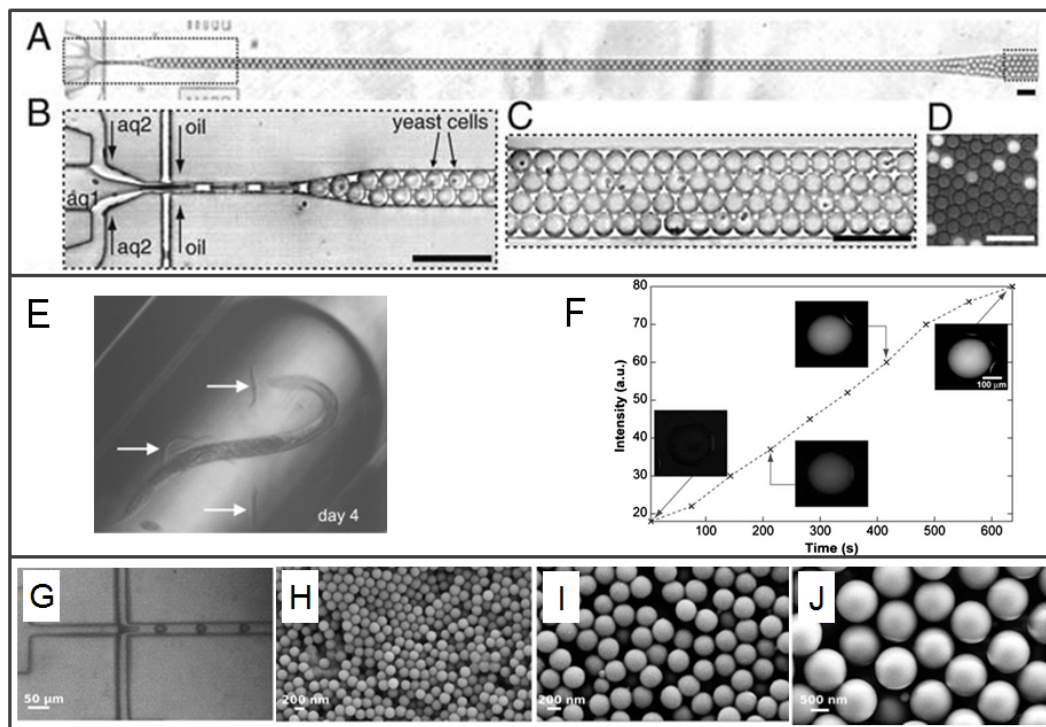


Figure 2-1: Applications of droplet-based microfluidics; (A)-(D) cell-encapsulated assay [ref.16], (E) the single-cell experiment [ref.22] (Reprinted from *Chemical Biology*, 15, 427-437, 2008 with permission from Elsevier); (F) the study of the enzymatic reaction [ref.11], and (G)-(J) the synthesis of monodisperse microparticles with tunable dimensions [ref.30]. (Reproduced figure. F-J by permission of *The Royal Society of Chemistry*).

Precisely controlled vessels

Once formed, the droplets can be manipulated either by passive or active approaches to maneuver them such as sorting, trapping and coalescing which will be discussed in the next section. Capable to be precisely manipulated, the droplet is thus used as a vessel to carry the reagent(s) to the targeted place. In addition, droplets have an advantage considering mass transport. Due to the low Reynolds number regime in microchannels, mixing of two flows of reagents occurs predominantly by diffusion along the surface area between two flows. Without turbulent mixing, the reagent molecules take long time to reach the region of another reagent causing mixing. On the contrary, droplet-based microfluidics can generate a tiny carrier containing two (or multiple) reagents. When traveling through a microchannel, droplets experience an internal recirculation in the droplets greatly enhancing the surface contact area between the volumes containing the two reagents.^{31, 32} The enhanced contact

surface area makes the mixing of two reagents inside the droplet more rapidly compared to that in the microchannel. Moreover, this rapid mixing in droplets can still be enhanced when droplets travel in a winding channel (See Fig.2-2). Not only the mass transfer is enhanced in this manner but also heat transfer can quickly occur in the droplet.³³

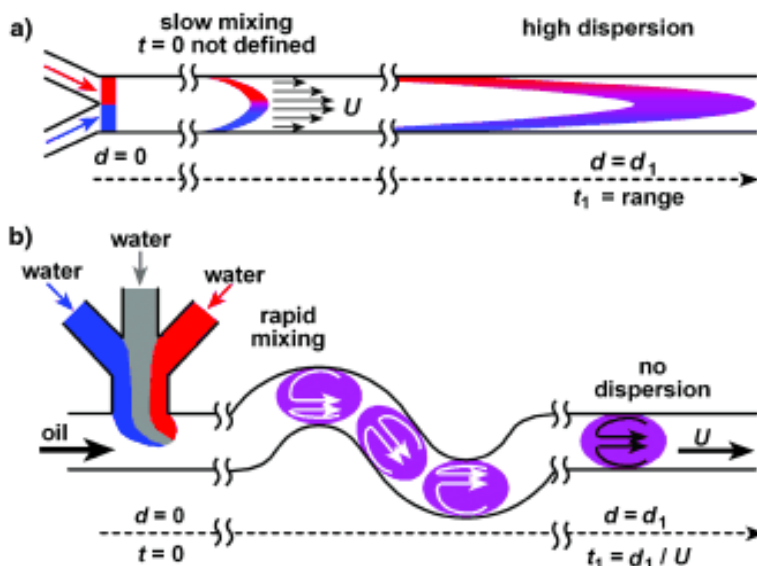


Figure 2-2: (A) Mixing between two (or more) reagents in the conventional microchannel dominated by diffusion is slower than that in the droplet encapsulated in the continuous phase (B) at which the chaotic advection takes place when travelling in the winding channel [ref.31]. (Reproduced by the permission of Wiley Company).

Miniaturization in a confined volume

The fluidic flows inside a microchannel can be delicately regulated enabling precise control in the fluidic volume of the generated droplet, as will be reviewed below. In addition, a great variety of volumes of droplets can be modulated by adjusting the flow rates, the viscosities of two immiscible fluids or the geometry of the fluidic channels.³⁴⁻³⁶ This flexibility provides a great opportunity for droplet-based microfluidics to handle and analyze minute amounts of precious or rare reagents.

High throughput screening

Monodisperse droplets can be generated at high formation rate for usage as reactors or carriers. Therefore reactions in each droplet occur in parallel at the same time in one batch. The obtained high-throughput results express the data from one single droplet and the

Chapter: 2

average data from the whole array of droplets. The high-throughput screening from droplet-based microfluidic device enables for example the determination of the mutated genes in the presence of a 200,000-fold excess of unmutated genes.³⁷

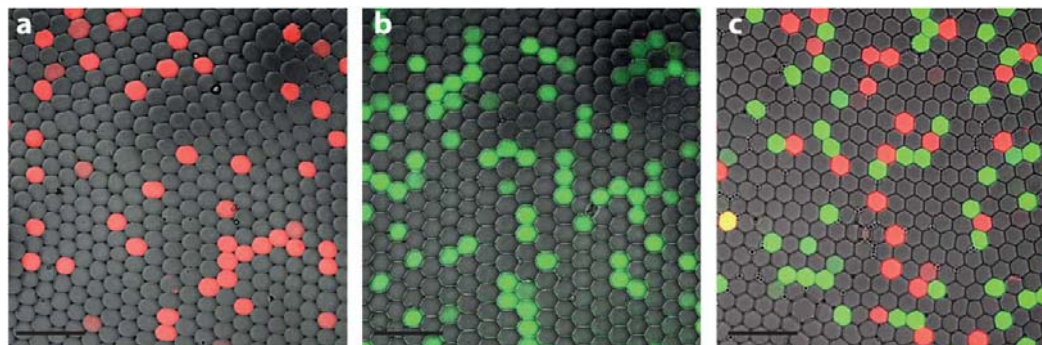


Figure 2-3: Droplets-based microfluidic system used for the study of rare mutations of *KNAS* genes. The droplet color indicates the presence of the normal gene (A-red) or mutated gene (B-green) in droplets. The ratio of green droplets to red droplets provide the determination of the ratio of mutant to unmutated gene in a population (C). The scale bar is 100 μm [ref.37]. (Reproduced by permission of The Royal Society of Chemistry).

b. Droplet generation

In general, droplets can be produced from two immiscible fluids such as water and oil. In case of a water-in-oil emulsion, at the interface the water molecule is attracted to another water molecule on the water side rather than to the oil molecule on the oil side. The molecules at the contact area are thus in a higher energy state, and the system will strive to minimize the surface energy and hence the surface area between the two liquids. The minimization of the surface area creates the spherical shape of a water droplet in oil. To create an emulsion, two (or more) immiscible fluids are required to be used, where the target phase forming droplets is called “dispersed phase” and the phase that forms the surrounding medium is called “continuous phase”. In general, formed droplets can be stabilized in continuous phase by adding amphiphilic molecules such as surfactants which hinder the droplet coalescence.^{38,39} The techniques of the generation of droplets in microfluidic devices can be categorized by their configuration as detailed below.

1. T-junction system

Droplet formation in a T-shaped device was firstly reported by Thorsen *et al.*⁴⁰ In this system, the dispersed phase flows perpendicularly to the main channel containing the

continuous phase. At the T-junction, the tip of the dispersed phase entering the main channel is sheared by a force from the continuous phase creating a droplet as depicted in Fig.2-4A.⁴¹ The dimension of the formed droplets can be modulated by altering the fluid flow rates, the relative viscosity between the two phases^{34, 35} or by changing the geometry (width or depth) of the channels.⁴² Due to the simple configuration of the T-junction, this system is available for multiple inlets or more complicated droplet generation systems.⁴³

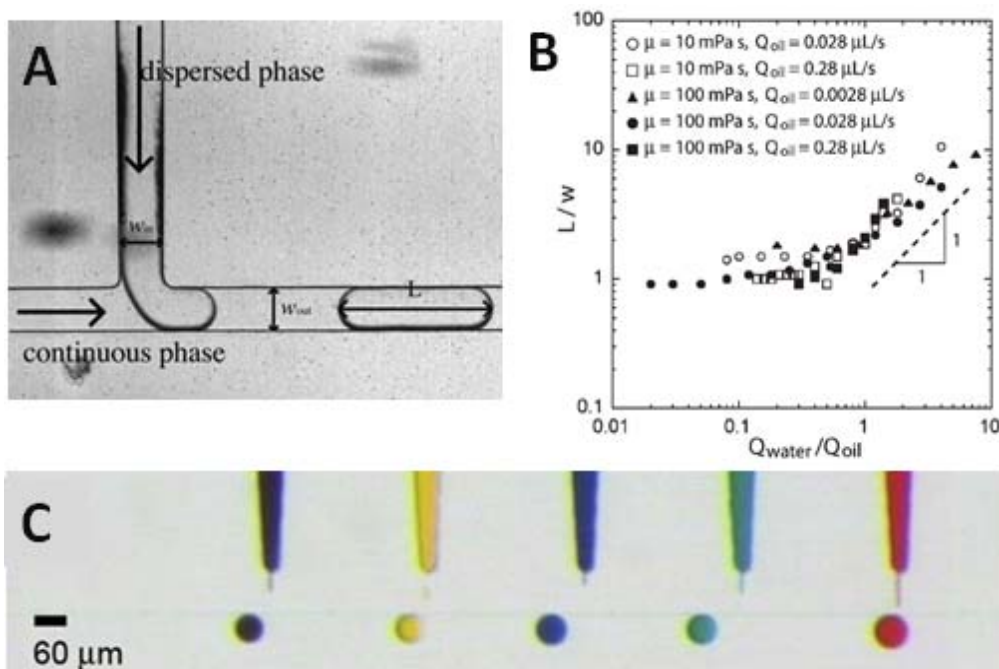


Figure 2-4: (A) T-junction system used for generating droplets in microfluidic devices [ref.41]. (Reproduced by permission of The Royal Society of Chemistry). (B) The dimension of generated droplets is determined by the flow rates of the dispersed aqueous phase and the continuous oil phase and the relative viscosity of the two phases [ref.35]. (Figure A and B reproduced by permission of The Royal Society of Chemistry). (C) T-junction device is used to generate multiple aqueous droplets in a microfluidic device and the continuous phase flows from right to left [ref.43]. (Reprinted from *Anal Chim Acta*, 630, 124-130, 2008 with permission from Elsevier).

2. Flow-focusing system

Droplet generation in a flow-focusing system was firstly demonstrated by Anna *et al.*⁴⁴ In the flow-focusing configuration, the dispersed phase is injected into the center of a nozzle and sheared from two sides by two co-flows of continuous phase to generate droplets. Two symmetric flows of continuous fluid are positioned at one single point around the narrowest region in the nozzle providing the shear force around the stream of dispersed phase. Under

Chapter: 2

such conditions, the dispersed phase is thinned and subsequent broken up forming the droplets (See Fig.2-5A). Like a T-junction system, the break-up mechanism of droplets in flow-focusing systems is based on applying a shear force with the continuous phase. Thus, the size of the generated droplets is dependent on the flow rates and viscosities of dispersed and continuous phases, the geometry of the microchannels as well as the dimension of the nozzle^{36, 41, 44-49} (Fig.2-5).

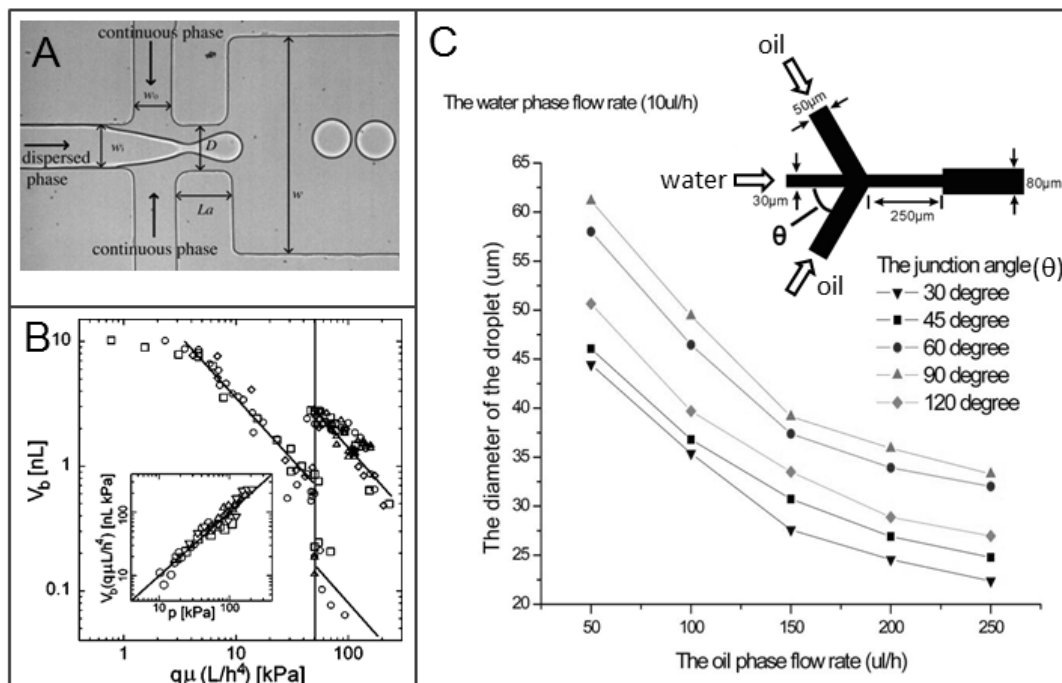


Figure 2-5: (A) The flow-focusing design for generating droplets in a microfluidic device [ref.41]. (Reproduced by permission of The Royal Society of Chemistry). (B) The volume of generated droplet is determined by the flow rates and the viscosities of two immiscible fluids [ref.36]. (Reprinted with permission from Appl Phys Lett, 85, 2649-2651, Copyright 2004, American Institute of Physics). (C) An example of the effect of the geometry of the flow-focusing configuration on the diameter of formed droplets [ref.49]. (Reproduced from © 2011 IEEE)

Abate *et al*⁴⁵ reported that the flow-focusing system can generate monodisperse and stable droplets at moderate and high capillary numbers (Ca) while the T-junction system can do so at low and moderate capillary numbers (Fig.2-6). The capillary number (Ca) is a dimensionless number representing the relative effect from viscosity compared to the interfacial tension as expressed as $Ca = \mu * V / \gamma$ where μ = viscosity of continuous fluid (Pa.s), V = fluidic velocity (ms^{-1}), γ = surface tension (Nm^{-1}).

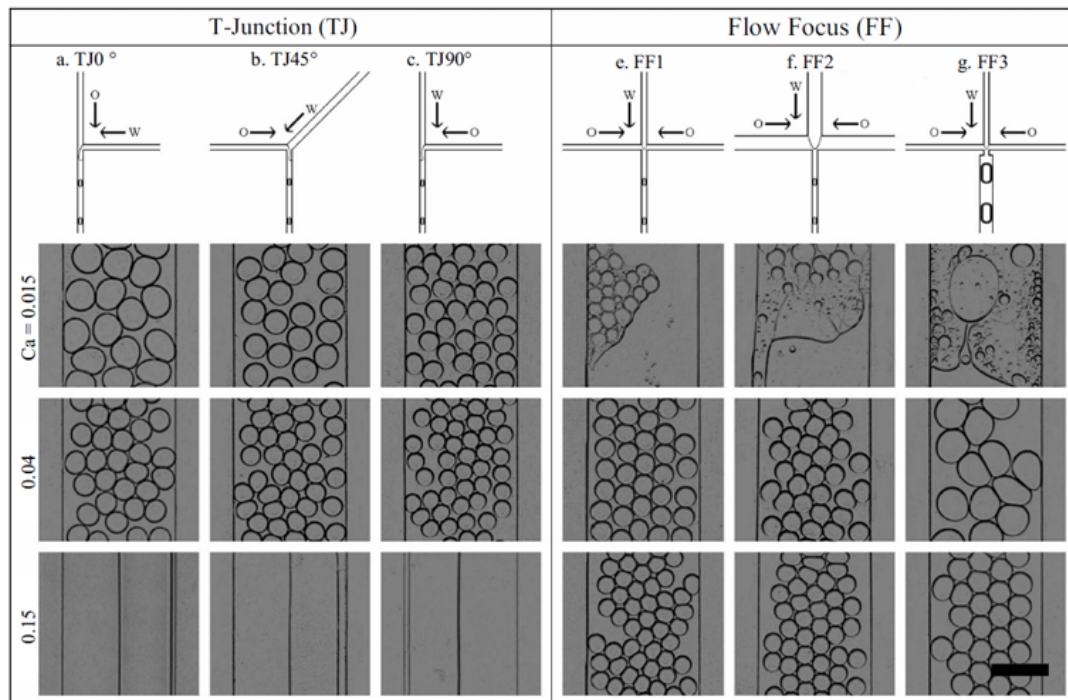


Figure 2-6: Schematic of droplet generators with different inlet channel geometries. The cross section of each channel is $15 \times 15 \mu\text{m}^2$. The emulsion contained water drops in fluorocarbon oil stabilized by fluorosurfactant. Example images of drops generated from each device at different capillary numbers (Ca) are shown in the lower row; $Ca = 0.015$ (second row), 0.04 (third row) and 0.15 (fourth row) [ref.45]. (Reprinted with permission from *Phys Rev E*, 80, Copyright 2009, The American Physical Society).

3. Co-axial focusing system

Droplets can also be produced from microfluidic devices by using a co-axial focusing system. The mechanism is similar to the flow-focusing system but the device is fabricated by inserting a capillary tube into the microchannel. The co-axial focusing system was firstly reported by Umbanhowar *et al.*⁵⁰ The dispersed phase is introduced into a capillary tube while the continuous phase is injected into the microchannel. At the tip of the capillary tube, the head of the dispersed phase enters into the continuous phase and is detached from the dispersed stream by the interfacial tension between the two phases creating droplets (See Fig.2-7A). Co-axial focusing systems can be used to generate complex systems such as multiple emulsions in which dispersed droplets contain smaller droplets inside as shown in Fig.2-7C.⁵¹ This integrated device could control both the size and the number of the inner droplets (Fig.2-7B and C).

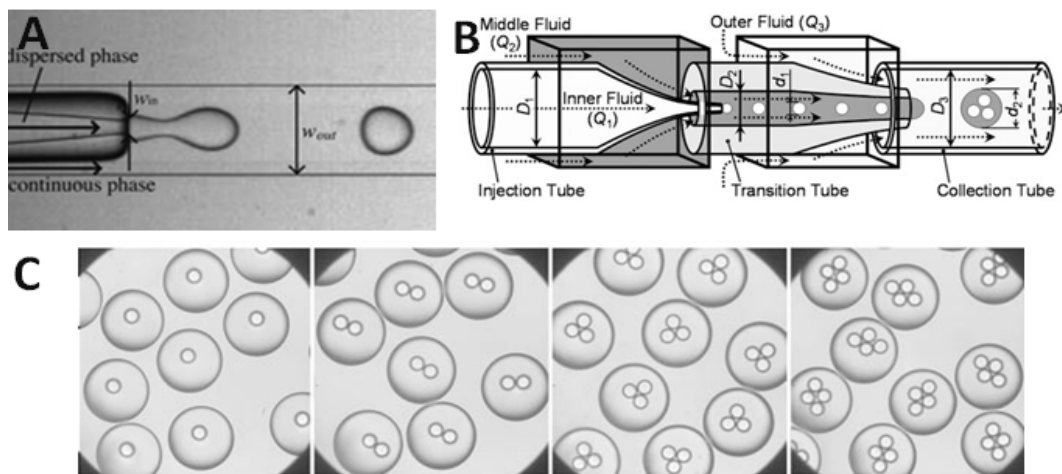


Figure 2-7: (A) Co-axial droplet generators in the microfluidic device by simply inserting the capillary tube into the microchannel [ref.41]. (Reproduced by permission of The Royal Society of Chemistry). Double emulsion can be formed either in water-in-oil-in-water (W/O/W) or oil-in-water-in-oil (O/W/O) modules by inserting the second capillary tube into the first tube (B). The outermost fluid which is the same phase as the inner fluid was injected to flow axially around the second tube and the middle fluid was loaded to flow around the first tube. (C) Optical micrographs of monodisperse double emulsion expressing the controllable size and the number of inner droplets. (Reproduced figure B and C by the permission of Wiley Company, ref. 51)

4. Electrically-induced droplet generating system

Apart from the shear-induced mechanism from the T-junction and the flow-focusing devices and the surface-tension induced mechanism co-axial focusing devices, the droplets can be generated by active control using an electric field in the microfluidic device.⁵²⁻⁵⁴ The electric field can be used for the generation or/and manipulation of droplets which will be discussed in the droplet manipulation section later.

c. Droplet manipulation

Droplet generation can be implemented using different processes as described in the previous section. Generated droplets can be manipulated or arranged by many specific operations such as sorting,^{2, 55-57} coalescing,⁵⁸⁻⁶⁷ mixing,⁶⁸⁻⁷¹ splitting,^{66, 68, 69} rearranging,⁷⁰⁻⁷³ synchronizing,⁷⁴⁻⁷⁶ trapping and guiding droplets,⁷⁶⁻⁸² and so forth. In general, formed droplets can be manipulated either by passive or active approaches. Due to the diverse requirements of specific applications and devices, the approaches to maneuver the droplets

should be considered in particular in view of such requirements. The methods to manipulate droplets have been reviewed below.

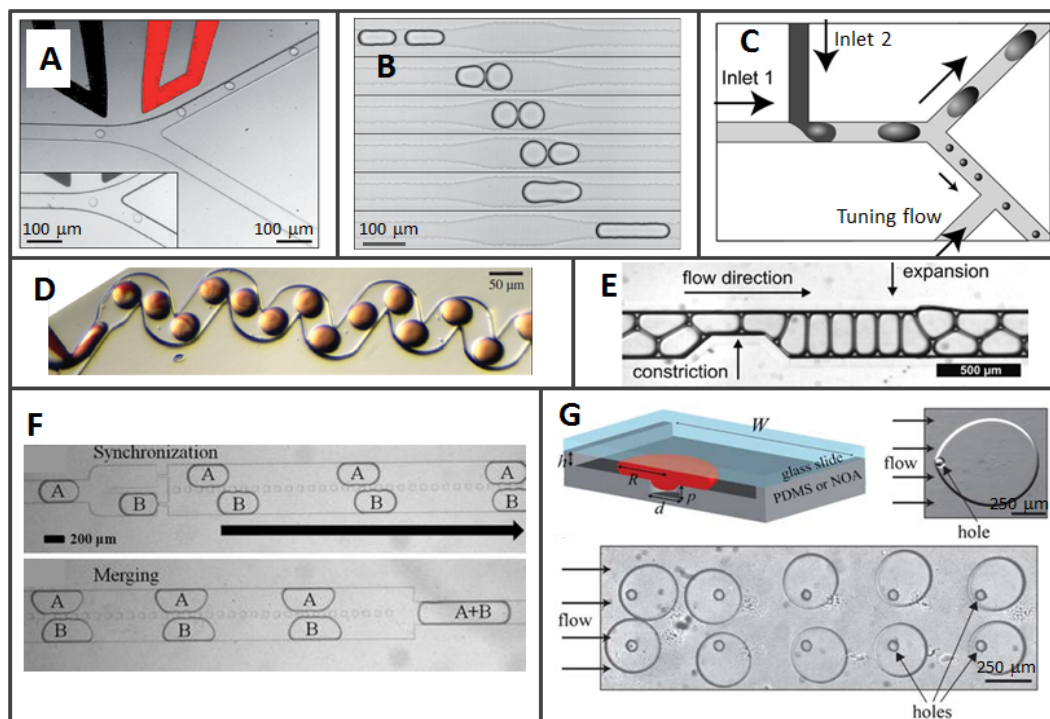


Figure 2-8: Exemplified manipulations of droplets: (A) droplet sorting by electric field [ref.4] (Reprinted figure A with permission from *Anal Chem*, 81, 5840-5845, 2009, American Chemical Society), (B) coalescence of two consecutive droplets in the expansion chamber [ref.55] (Reprinted with permission from *Appl Phys Lett*, 96, Copyright 2010, American Institute of Physics), (C) droplet splitting by hydrodynamic approach [ref.63], (D) mixing inside droplet in the winding channel [ref.31], (Reproduced figure C and D by the permission of Wiley Company), (E) rearrangement of droplets in the constriction and expansion microchannels [ref.71], (F) synchronization of two droplets [ref.76] (Reproduced figure F from *Microfluid Nanofluid*, 11, 685-693, 2011 with kind permission from Springer Science and Business Media) and (G) droplet trapping [ref.79]. (Reproduced figure E and G by permission of The Royal Society of Chemistry).

c.1. Active manipulation

In this method, the additional force from an electric field, magnetic field, optical field, etc. is applied to the fluidic system in order to manipulate the droplets. This method is advantageous due to its precise controllability and specificity, however, its drawbacks might include possible damage to molecules, cells or particles encapsulated inside droplets, more

Chapter: 2

complicated fabrication, etc. Various recent approaches to active manipulation are described below:

Droplet formation and manipulation by electrowetting

Electrowetting (EW) for the formation of droplets was first reported by Washizu *et al.*⁸³ Conceptually, a droplet of water is brought in contact with a hydrophobic surface-coated electrode. When a positive potential is applied to the electrode with respect to an electrode inserted in the droplet, a negative charge is induced on the droplet surface facing the bottom electrode. The system can then be regarded as a variable capacitance system where the droplet deforms its shape to maximize the capacitance between the droplet and the energized electrode to minimize the total energy of the system. The result is the wetting effect as shown in Fig.2-9. When the electrode is switched off, the surface reverts back to a hydrophobic surface which is unfavorable for wetting, resulting in the return of the droplet to its original shape.^{52, 83}

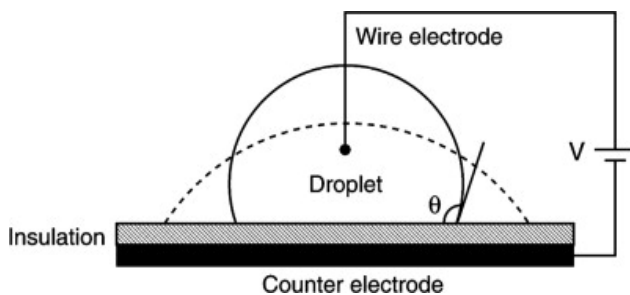


Figure 2-9: Droplet manipulation by electrowetting. A hydrophobic insulating layer is non-wetting for a conducting droplet. In the presence of electric field, the surface becomes wetting due to the reduced liquid-solid interfacial tension resulting in a lower contact angle[ref.83]. (Reproduced figure C from © 2011 IEEE).

This concept was exploited to manipulate droplets by using complex electronic networks, so-called digital microfluidics^{53, 84} which nowadays is a widely-used technique in diverse technologies.^{85, 86} An example of digital microfluidics involving the droplet manipulation is shown in Fig. 2-10.⁵² First, a water droplet was wetting on the left electrode (Fig.2-10A) due to field application, then it expanded to the middle electrode where the electric field was subsequently applied (Fig.2-10B). When the right electrode was switched on and the middle one was switched off, the droplet was split in two droplets (Fig.2-10C-D). Finally, the split droplets were rejoined by switching the voltage back to the middle and left electrodes (Fig.2-10E-F).

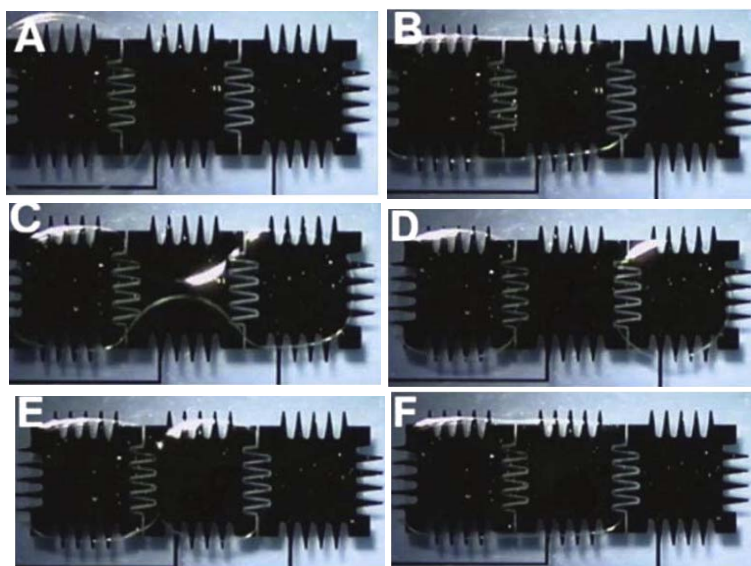


Figure 2-10: Droplet merging and splitting device by electrowetting from three hydrophobic-surface-coated electrodes (A) Firstly, an aqueous droplet was placed on the left electrode. (B) A droplet expanded to the middle electrode where the electric field was applied. (C-D) When the right electrode was switched on and the middle one was switched off, a droplet was split into two droplets on the left and right electrode. (E-F) After switching the voltage back from the right to the middle electrode, the right droplet was reverted to the middle section and coalesced to the left droplet [ref.52]. (Reproduced by permission of The Royal Society of Chemistry).

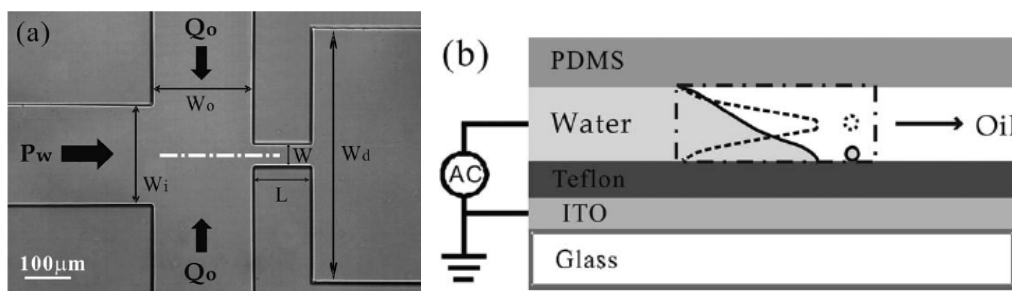


Figure 2-11: Flow-focusing device with electrowetting actuation. (A) Top view of the device ($W_i=W_o=200$, $W= 50$, $L=150$ and $W_d=500 \mu\text{m}$). (B) Cross sectional view of the junction along the dash line in (A). Without voltage, the oil-water interface is in the middle of the channel (dotted curves) and with voltage, the interface is close down to the bottom [ref.53]. (Reprinted with permission from *Appl Phys Lett*, 93, Copyright 2008, American Institute of Physics).

In addition, the electrowetting effect (EW) can be used to perform droplet generation since the applied electric field can reduce the contact angle between the liquid and the surface of the microchannel.⁸³ This method had been investigated by Gu *et al.*^{53, 54} Their flow-focusing

Chapter: 2

device (FFD) with incorporated electrowetting design can generate smaller droplets than those generated by a solely hydrodynamic flow focusing system. (Fig.2-11 and 2-12).

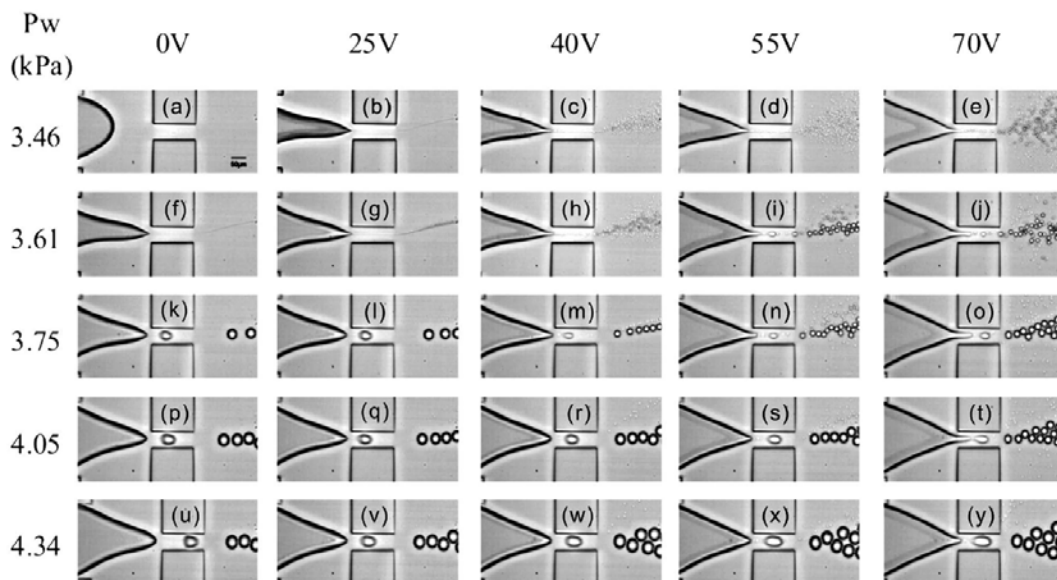


Figure 2-12: Sequence images of droplet generation based on electrowetting actuation at the variation of the pressure of dispersed phase (P_w) and applied voltages [ref.54]. (Reproduced by permission of The Royal Society of Chemistry).

In the device of Gu *et al.*,⁵⁴ the resulting droplet sizes varied with the variation of applied electric field and applied pressures of disperse phase (P_w). At zero voltage (Fig.2-12A), the tip of the water stream was just nearby the center plane of the device and, when applying a voltage, moved toward the bottom substrate (Fig.2-12B). When applying a higher voltage, smaller droplets were generated (Fig.2-12C-E). Due to the electrostatic repulsion of droplets, they moved forward and spread out after formation. At higher applied pressure (Fig.2-12K-Y), the hydrodynamic force became dominant and the mechanism of the droplet generation became similar to the dripping regime in a purely hydrodynamic flow focusing system.

Droplet formation and manipulation by dielectrophoresis

Generally, dielectrophoresis (DEP) is a method to manipulate electrically neutral but polarizable particles or fluid droplets by applying non-uniform electric fields. A DEP device generally comprises two electrodes with different dimension for generating an inhomogeneous electric field through the media or surrounding fluid and the particle or inner fluid (droplet). In case of particles or droplets that are highly polarizable compared to

the medium or surrounding fluid, the particle or droplet moves forward to the region of high electric field intensity. Compared to the EW-based device, the DEP-based system can be used to manipulate dielectric droplets such as oil which are widely used in droplet-based microfluidic applications.

Fan *et al*⁸⁴ proposed a device to manipulate dielectric droplets by dielectrophoresis (DEP) (Fig.2-13). The dielectric droplet of silicone oil can for example be controlled by DEP actuation (Fig.2-13A-G). A 150-nL silicon oil droplet positioned on the center electrode (Fig.2-13B) was split into two drops when high voltage (420V) was applied at the two electrodes indicated by two arrows (Fig.2-13C and D). Subsequently two 75-nL oil droplets were transported to any specific position in the presence of electric fields (Fig.2-13E-F) and finally both were merged at the center electrode (Fig.2-13G). Moreover, they integrated both the dielectrophoresis and electrowetting actuation into the same platform as illustrated in Fig.2-13H. This device can be used to manipulate both aqueous droplets and dielectric oil droplets separately by EWOD and DEP, respectively.

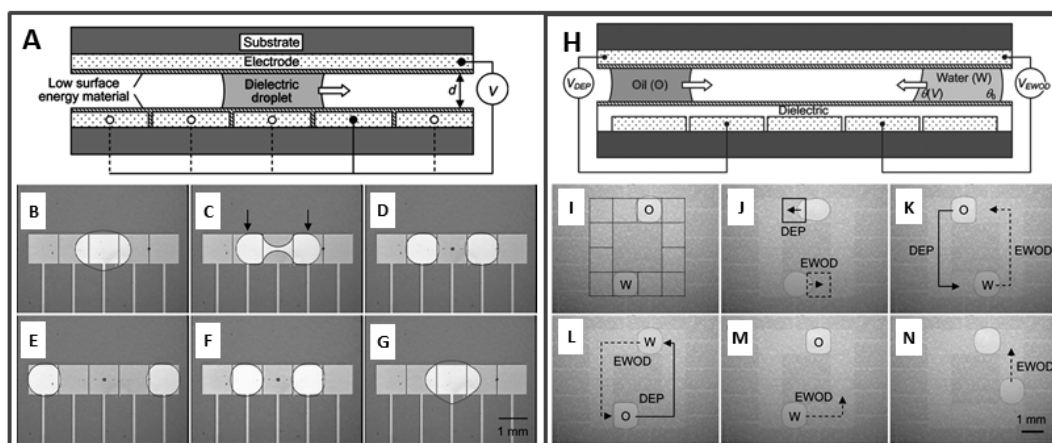


Figure 2-13: (A) A cross-sectional view of the device with DEP actuation of dielectric droplets. (B)-(G) a sequence of images of the manipulation of the silicone oil droplets. (H) A cross-sectional view of the device with DEP and EWOD actuation of dielectric droplet and water droplet, respectively. (I)-(N) a sequence of images of the manipulation of the silicone oil droplets and aqueous droplets on the DEP and EWOD actuated device [ref.84]. (Reproduced by permission of The Royal Society of Chemistry).

Electrostatic actuation for generating and coalescing droplets

Electrostatic actuation can be used to generate a tiny droplet with precisely-controlled timing and also merge two opposite charged droplets generated separately from microfluidic device

Chapter: 2

incorporated with two electrodes (Fig.2-13).⁶³ Via this actuation method, tiny droplets can be formed in large microchannels without the problem from clogging in narrow fluidic channels. When applying an electric field to one electrode in the water stream, the water-oil interface was charged and the charge remained in a droplet after droplet formation. Meanwhile, at another electrode, the tip of the water stream was charged with the opposite charge and then locally formed a droplet containing the opposite charge. Both charged droplets were contacted together at the outlet channel and coalesced by the electrostatic field (Fig.2-13A). In the absence of applied electric field, a slightly different frequency of droplet generation enabled the desynchronization of two charged droplets hindering the droplet fusion (Fig.2-13B). However, upon the application of electric field, two droplets were generated in a synchronized manner and later coalesced due to the electrostatic force between a pair of the oppositely charged droplets generated from two electrodes (Fig.2-13C).

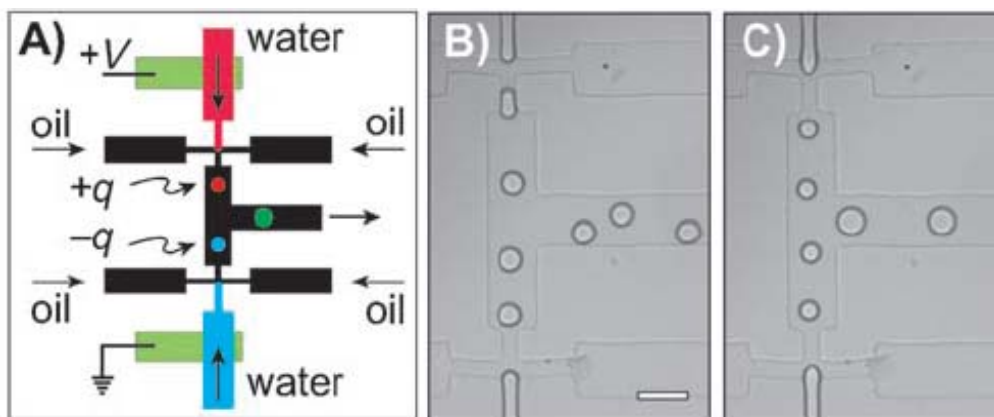


Figure 2-14 (A) Droplet generation and coalescence by using electrostatic charge. Droplets containing opposite charges can be generated by applying a voltage across two aqueous streams. (B) Without applied electric field, the generated droplets from two streams which were different in size and frequency were not fused (Scale bar: 100 μm). (C) With applied electric field of 200V across the 500- μm separation of the nozzles, the simultaneous droplet formation and droplet fusion can be achieved [ref.63]. (Reproduced by the permission of Wiley Company)

Droplet sorting by electrostatic actuation

Oh *et al*⁸⁷ proposed a microfluidic device consisting of three electrodes for electrostatic actuation to sort aqueous droplets in oil phase. The first grounded electrode was placed in the aqueous stream while the other two electrodes for positive or negative pulse were placed under the entrance of each sorting channel (Fig.2-15A). In the absence of the applied electric field (Fig.2-15B), after droplet formation, the formed droplets flowed along the streamline

of laminar flow and then entered the middle channel. Since a water stream behaves as a conductor whilst oil is an insulator, electrostatic actuation charges the water-oil interfaces as a capacitor. In the presence of an applied electric field (Fig.2-15C) either from the left or right electrode, upon droplet formation, the water stream was charged and charged molecules remained at the water-oil interface. After the droplet formation, the charges redistributed on the surface of a conductive droplet due to the repulsion inside a droplet. When travelling to the junction, the precharged droplet was guided to the left or the right sorting channels (Fig.2-15D) corresponding to the charging electrode. Since the electrostatic force impelled the precharged droplet to cross over the streamline of laminar flow, the electric field, the dimension of the droplet, the flow rate and the applied electric field played important roles in the successful droplet sorting (Fig.2-15D).

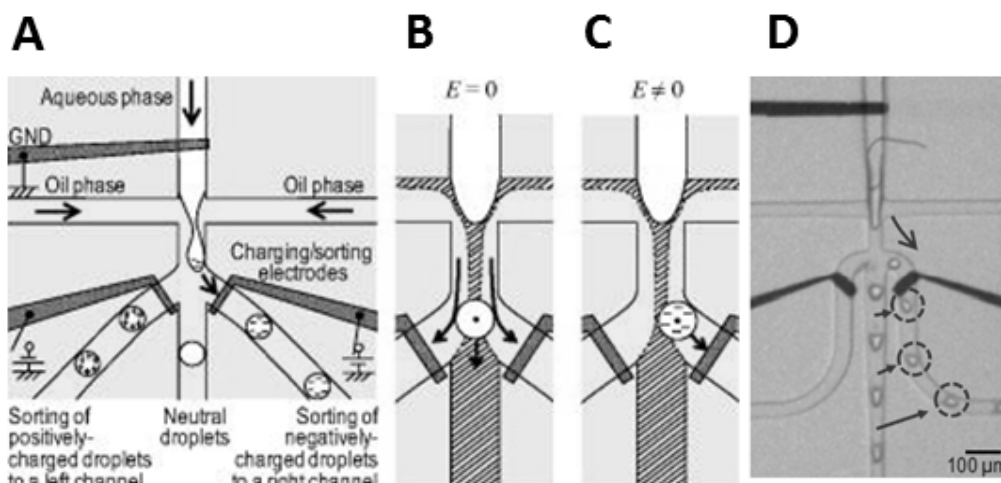


Figure 2-15 (A) Schematic of the concurrent droplet charging and sorting by electrostatic actuation with three electrodes. One electrode was placed inside the aqueous stream, the others were placed either in the left or right sorting channel. Droplets travel along the microchannels with (B) or without (C) the applied electric field. Charging and sorting droplets with the actuation voltage of 120 V, the droplet generation frequency of 200 droplets/s was reached. (aqueous phase : DI water, oil phase : 2% Tween-20 in hexadecane solution [ref.87]). (Reprinted with permission from *Biomicrofluidics*, 3, Copyright 2009, American Institute of Physics).

Manipulation of droplets by magnetic actuation

Recently, many researchers have employed magnetic actuation into microfluidic devices for manipulation of droplets.^{15, 88} One example shown here is a magnetic droplet-manipulation microdevice for polymerase chain reaction (PCR).¹⁵ This device consisted of the reaction chamber in the middle and two magnet handling channels beside the reaction chamber

Chapter: 2

(Fig.2-16A-B). An aqueous droplet containing streptavidin conjugated superparamagnetic beads in mineral oil inside the main chamber was maneuvered by the permanent magnet located in the handling channels. The magnetic beads-containing droplet was transported to merge consequently with single droplets containing different reagents (primer, template DNA and PCR mixture) individually placed in the chamber (Fig.2-16A). After droplet fusion and incubation, DNA was captured on magnetic beads by means of biotin-streptavidin binding, and the reaction could take place. After reaction, amplified DNA on magnetic beads was collected and then magnetically extracted from a droplet by the magnet (Fig.2-16C). Subsequently, the manipulated DNA was merged into the wash buffer droplets to remove non-specifically amplified DNA.

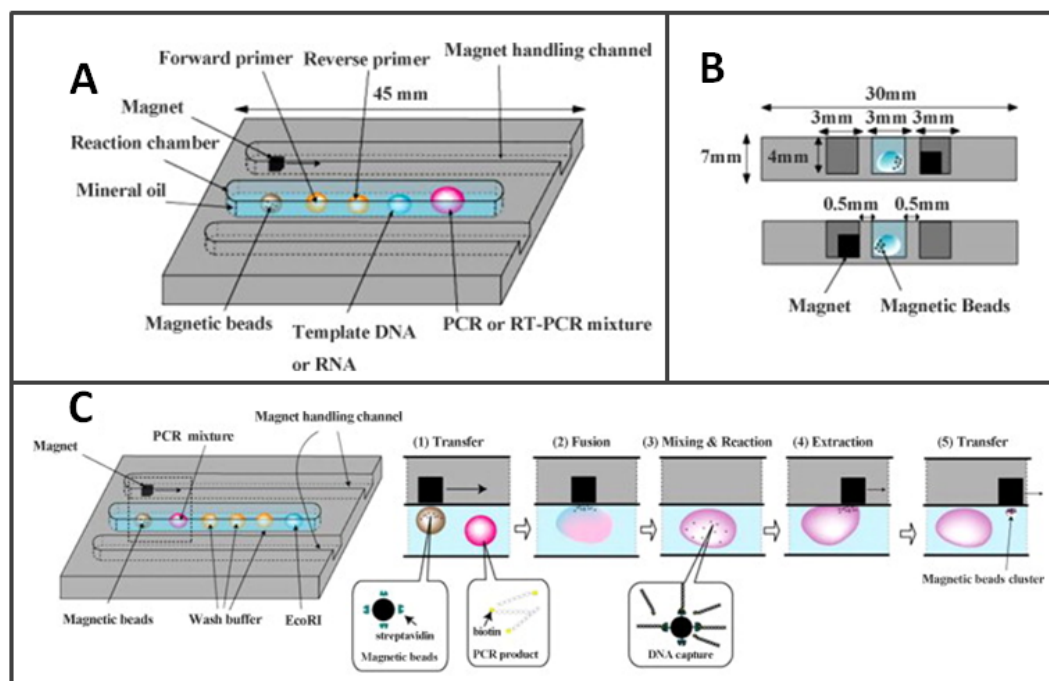


Figure 2-16: Schematic diagram of the microdevice employing a magnetic droplet-manipulation in perspective view (A) and cross-sectional view (B). (C) Capture and purification of amplified DNA using magnetic beads [ref.15]. (Reprinted figure C from *Sensor Actuat B-Chem*, 130, 583-588, 2008 with permission from Elsevier)

Optical manipulation (optical tweezers)

Optical trapping is an alternative method to maneuver droplets by focusing a laser beam onto the droplet.⁸⁹ Due to the different refractive index of droplets and the surrounding solution, a focused laser beam is refracted on the droplet/medium boundary. This refraction

induces a photon momentum change resulting in a force generated at the droplet or particle which is in the order of pN. Unlike many other ways of active manipulation, optical manipulation is contactless, generally non-destructive, and three-dimensional which is advantageous and promising for many biological applications. The principle of optical trapping including its application for chemical analysis has for example recently been reviewed.⁹⁰ Several recent studies⁹¹⁻⁹⁵ utilized an optical approach to manipulate droplets or microparticles. For instance, He *et al*⁹⁵ used optical trapping to transport a single target cell or subcellular structure or particle close to the oil-water interface before droplet formation. When the droplet was formed, the targeted molecule was encapsulated into the formed aqueous droplet (Fig.2-17).

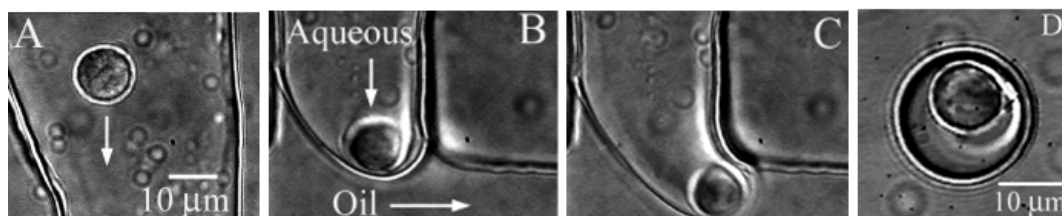


Figure 2-17: Sequences of images showing the encapsulation of a single B lymphocyte into an aqueous droplet in silicone oil with 3wt% Span 85. Optical trapping was used to transport the cell close to the water-oil interface (A-C). After the droplet formation, a cell was entrapped in a droplet as shown in (D) [ref.95]. (Reprinted with permission from *Anal Chem*, 77, 1539-1544, 2005, American Chemical Society).

Droplet manipulation by using microvalves

Microfluidic valves have been employed into microfluidic systems to control the fluidic streams by using external forces to allow or stop the flows. The most commonly used valve is the pneumatic-actuated valve where the valve is switched on and off by air. The concept and applications of microvalves in microfluidic systems have been reviewed before in the literature.⁹⁶ The microvalves-integrated microfluidic system exemplified here was reported by Zeng *et al.*⁹⁷ They utilized pneumatic-based microvalves into a microfluidic device to control precisely the droplet generation as well as droplet fusion (Fig.2-18). The volume of aqueous stream for one droplet is adjusted by varying the opening time of a microvalve (Fig.2-18A). Moreover, the device integrating two microvalves can individually control the generation of two droplets in parallel (Fig.2-18B) enabling synchronization and further fusion of two generated droplets. By synchronously switching on and off microvalves, a pair of droplets can meet each other and fuse in a controlled manner (Fig.2-18C).

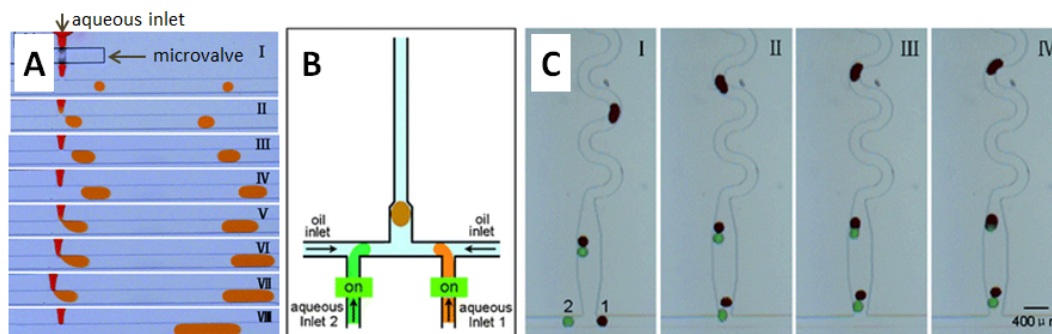


Figure 2-18: Microvalves-integrated microfluidic device for droplet generation and fusion. (A) The opening time of a microvalve regulated the droplet size; the opening times for figure I-VIII were 50, 150, 200, 300, 350, and 450 ms, respectively. (B) Schematic of two microvalves integrated into microfluidic device to control separately two aqueous streams. Droplet pairs can be generated simultaneously by synchronously switching on and off microvalves. (C) The process of the controlled fusion of droplet pairs. Droplets with brown (1) and green (2) ink solutions were generated with opening times of the microvalve of 80 and 60 ms respectively [ref.97]. (Reproduced by permission of The Royal Society of Chemistry).

c.2. *Passive manipulation*

Via this method, generated droplets are handled or manipulated without application of additional external force. The droplet manipulations are now accomplished by hydrodynamic approaches using a modified geometry or by surface energy approaches. It has the advantages that no external forces are applied which might damage the particles or molecules encapsulated in generated droplets. In addition, devices can be simply fabricated without need of additional layers of electrode and insulating layers or the need for an optimized design of electrode.

Geometry-induced manipulation

By-pass channel to alternate droplet traffic

When droplets that are sorted alternatingly at a T-junction enter the outlet channel, the size and number of droplets can increase the hydrodynamic resistance along that channel.⁹⁸ Therefore, the sorting process at the T-junction (Fig.2-19A) becomes nonlinear due to the increasing fluidic resistance which makes it more difficult to achieve the alternation of droplets. By integrating a by-pass channel into a T-junction (Fig.2-19C),⁹⁹ when a first droplet enters the left channel r_1 , the continuous fluid in the by-pass channel flows from right to left, thus the flow rate in a channel r_2 (Q_2) becomes larger than that in a channel r_1

(Q_1). As a consequence, the consecutive droplet flows into the channel r_2 . The accomplished alternation of droplets depends on the position and geometry of the by-pass channel as well as the distance between consecutive droplets.

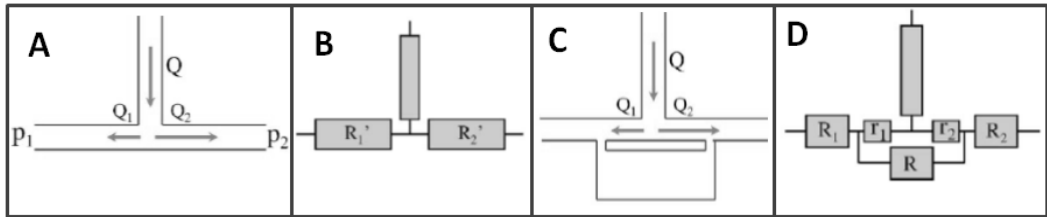


Figure 2-19:(A) A microfluidics droplet generation device with a T- junction; (C) a microfluidic device with a by-pass channel, (B) and (D) are the equivalent circuits of the network (A) and (C), respectively [ref.99]. (Reprinted with permission from Appl Phys Lett, 89, Copyright 2006, American Institute of Physics).

Alternation of droplets by dual nozzles

Frenz *et al*¹⁰⁰ proposed a microfluidic dual nozzle for the production of water-in-oil droplet pairs. In their device, two dispersed streams were pinched off separately by the continuous phase at the double nozzles connected together by a microchannel to generate droplets. Then they flowed along the upper or lower arm channel and eventually entered the confluence channel (Fig.2-20).

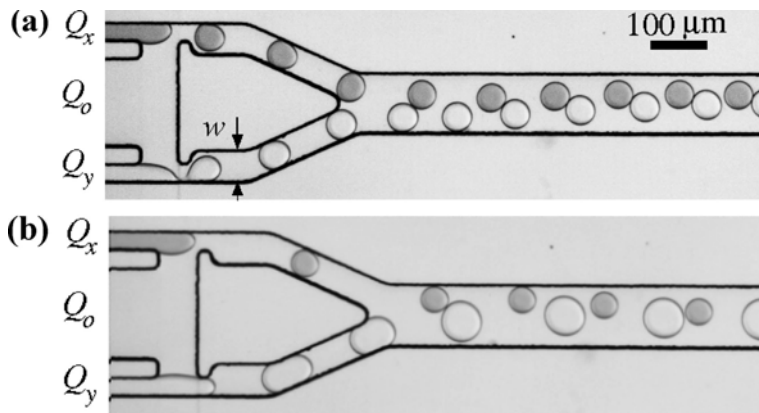


Figure 2-20: Alternating droplet formation from dual nozzles (a) Symmetric module when the flows of two dispersed phases were identical and (b) Asymmetric module when the flows of two dispersed phases were different [ref.100]. (Reprinted with permission from Langmuir, 24, 12073-12076, 2008, American Chemical Society).

Conceptually, when the first generated droplet entered the upper channel, the fluidic resistance in that channel became higher. Therefore, the oil flowed downward to pinch off the tip of the second stream at the lower nozzle to form the second droplet. When the second

Chapter: 2

droplet entered the lower arm channel, the fluidic resistance in the lower channel increased, then the oil flowed upward to the first nozzle again. The switching of oil flow alters the sequence of the droplet generation from the first and second dispersed phases leading to the regular production of the droplet pairs. Their device can alternate two droplets with identical or different size (Fig.2-20). However, this coupling concept was invalid when the size of droplet was smaller than the width of the channel since the droplet was too small to alter the oil flow.

Droplet sorting using geometry-induced hydrodynamics

After droplet formation, generated droplets are transported along the microchannel by the carrier fluid. When the size of generated droplets is larger than the dimension (width or height) of the fluidic channel, the droplet is constrained by the channel walls and is non-spherical. On the other hand, when the droplets are smaller than the channel dimensions, the droplet remains of spherical shape to minimize the surface area. Mazutis *et al*¹⁰¹ employed this concept to sort different-size droplets in a microfluidic system. In their device the larger droplets ($\phi > 24\mu\text{m}$) were squeezed along the vertical axis in the $20\text{-}\mu\text{m}$ -deep microchannel whereas the smaller droplets ($\phi \sim 18\mu\text{m}$) remained of spherical shape.

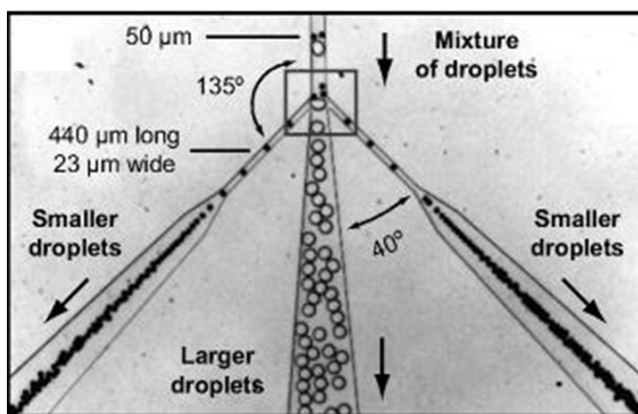


Figure 2-21: A schematic of the passive size-dependent fractionation of droplet mixtures. Larger droplets were 20 pL and smaller droplets were 3 pL [ref.101]. (Reprinted with permission from *Appl Phys Lett*, 95, Copyright 2009, American Institute of Physics.

Due to these size differences, the average velocity of the larger droplets was 1.2-fold lower than that of the smaller ones and the larger droplets thus obstructed the passage of the smaller droplets. However, the wide main channel ($50\mu\text{m}$) allowed the smaller ones to move

in flow paths alongside the walls (Fig.2-21). When arriving at the separation junction where two side narrow channels ($23\ \mu\text{m}$) split off from the main center channel, the hydrodynamic flow dragged the smaller droplets into the narrow channels while the larger droplets stayed in the center of the channel and continued to flow in the main channel (Fig. 2-21).

Bifurcation channel for droplet control

Lee *et al*⁷⁶ demonstrated a new method to precisely control droplets in microchannels by employing microfluidic bifurcation channels with outlet restrictions based on droplet bistability (Fig.2-22). When a droplet reaches the bifurcation channel, it entered either the top or bottom branch channel (Fig.2-22A) and it then encountered a narrow restriction (w_r).

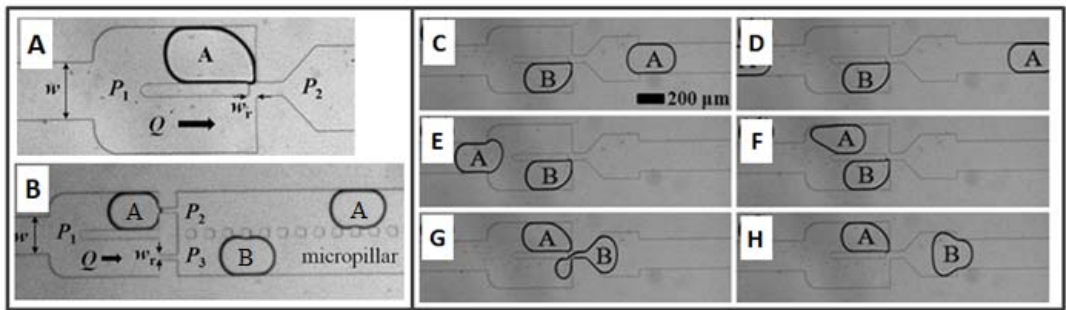


Figure 2-22:(A) A bifurcation channel for a “trap-and-release” scheme of droplets with $w = 200\ \mu\text{m}$ and $w_r = 30\ \mu\text{m}$. P_1 and P_2 were the pressures at two sides of the trapped droplet, Q = the total flow rate of the dispersed and continuous phases. (C)-(J) The “trap-and-release” scheme of droplets with the flow rates of dispersed and continuous phase 30 and 70 $\mu\text{L/h}$, respectively. Time interval between the images was 133ms. (B) The droplet alternation in the bifurcation channel ($w=200\ \mu\text{m}$, $w_r=30\ \mu\text{m}$); the two outlet channels were separated by a micropillar array in between with $50\ \mu\text{m}$ square pillars at intervals of $50\ \mu\text{m}$. (Disperse phase: DI water, Continuous phase: silicone oil) [ref.76]. (Reproduced figure F from *Microfluid Nanofluid*, 11, 685-693, 2011 with kind permission from Springer Science and Business Media).

In general the droplet will minimize its surface energy by deforming its shape to obtain the smallest surface area in the channel. The droplet requires an extra pressure from the flow in main channel to deform its shape to pass through this restriction aperture. The extra pressure should be larger than the Laplace pressure at the restriction side governed by the surface tension between two phases, the height of the channel, the widths of the main channel (w) and the restriction aperture (w_r). When the droplet “B” was trapped at the lower aperture (Fig.2-22C), the consecutive droplet (droplet “A”) flowed to and blocked the upper aperture (Fig.2-22E-F). Subsequently the droplet “B” which had already slightly deformed its shape

Chapter: 2

obtained more pressure until it was released from the restriction aperture as soon as the operating pressure difference was larger than the Laplace pressure (Fig.2-22G-H). The alternation of droplets could be also achieved from the bifurcation channel with two outlet channels which were separated by a micropillar array in between (Fig.2-22B).

Furthermore, a bifurcation channel with two outlet channels which had a single bypass in between them (Fig. 2-23) could switch the droplet pathway from the upper channel to the lower channel. Similar to the concept of the “trap-and-release” scheme, when the first droplet was trapped at the restriction aperture, the succeeding droplet would then flow to another aperture. Then, the excess pressure from the continuous phase exerted on the first trapped droplet would deformed it until it would be released through the restriction aperture. When the continuous phase flowed with a flow rate Q into either the upper or lower branch, it was then divided into two flows in the straight outlet channels (Q_3) and in the bypass way (Q_2). After releasing, a droplet can flow into either the straight channel or into the bypass channel depending on the ratio of the shear force exerted on the droplet by the flows into the straight channel (Q_3), or the bypass channel (Q_2), as well as the widths of both channels.

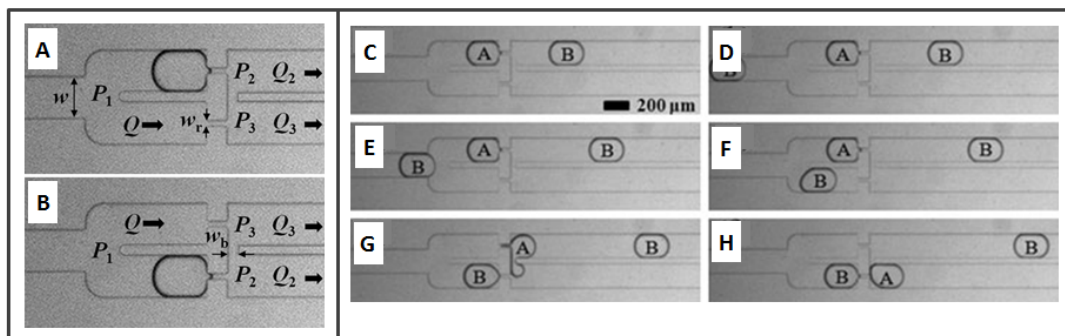


Figure 2-23:(A) A bifurcation channel for an “switching” scheme of droplets ($w = 200 \mu\text{m}$, $w_b = 50 \mu\text{m}$ and $w_r = 30 \mu\text{m}$). P_2 denotes the outlet pressure where a droplet blocks the continuous phase and P_3 denotes the outlet pressure where the continuous phase flows through the restriction. (C)-(H) Sequences of images expressing the switching of the consecutive droplets. (Disperse phase: DI water, Continuous phase: silicone oil) [ref.76]. (Reproduced figure F from *Microfluid Nanofluid*, 11, 685-693, 2011 with kind permission from Springer Science and Business Media).

Guiding and trapping droplets using anchors patterns

In general, the surface tension between two immiscible fluids drives the droplets to their lowest energy shapes. When the energetically-favorable shapes equilibrate with the drag

force acting on the droplets, the droplets can be stationary. Baroud *et al*^{77, 79} used this concept to guide and trap droplets in microfluidic devices by integrating microwells into the bottom of a microchannel (Fig.2-24A). In their device, a microchannel with a high ratio of width to depth was used to squeeze formed droplets. Squeezed droplets with high surface area traveled along the channel until they reached the microwell and then deformed to their lowest energy shapes by penetrating into the well (Fig.2-24A). The droplets were thus trapped onto this well. An external force was therefore required to detach the droplets from the well which depends on the radius of the droplet (R) and the width of the microwell (d). In the presence of the array of microwells, a series of droplets can be trapped for static observation (Fig.2-24C).

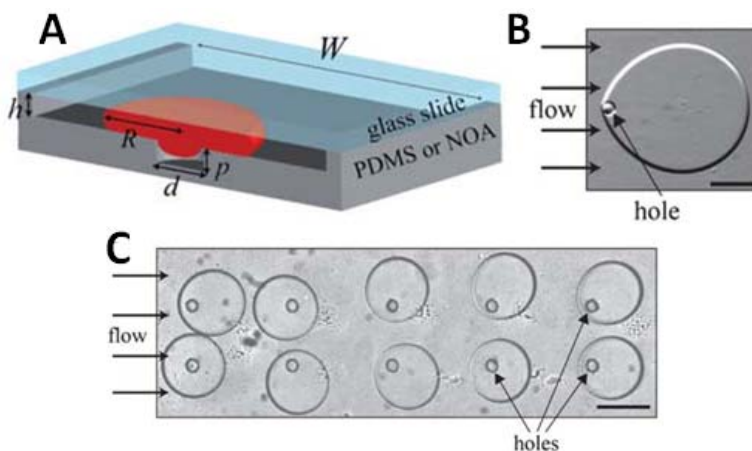


Figure 2-24:(A) Schematic of the microfluidic device with an anchor to trap a droplet. (h and W were the height and width of the microchannel, p and d were the depth and the width of the microwell and R was the radius of the droplet) (B) A water droplet trapped at a hole with oil flowing from left to right. (C) An array of anchored droplets. Scale bar $250\ \mu\text{m}$ [ref.79]. (Reproduced by permission of The Royal Society of Chemistry).

Trapping system for halting droplets

An alternative simple approach to halt the movement of droplets is the integration of a trapping system into a microfluidic device.^{80, 102, 103} A large amount of small-volume droplets can be captured at an array of trapping sites designed specifically for certain dimensions of droplets. Also, the number of the trapped droplets per one trapping site can be adjusted for any specific purpose e.g. a study of the droplet-droplet interface.⁸⁰

Furthermore, Huebner *et al*¹⁰³ proposed a microfluidic device at which the droplets can be trapped and later released by liquid flow from a microfluidic trapping structure which is

Chapter: 2

difficult to achieve by other methods. Their device for the trap-and-release module consisted of the trapping array (Fig.2-25) contained in an expansion chamber. When the continuous phase with the droplets reached the trapping site with the opening in the centre of the site, one single droplet (green droplet in Fig.2-25B) followed the streamline of fluidic flow which passed through the opening aperture of the site. This droplet was eventually trapped on that site and closed the aperture (Fig.2-25C). The opening aperture was used not only as a single-droplet-trapping module but also as a trap-and-release module. After the entrapment of the droplets (Fig.2-30D trap), the liquid flow was stopped. Then the direction of the liquid flow was reversed (from right to left in Fig.2-30D), the liquid stream could then pass through the opening aperture and release the trapped droplets from the trapping sites.

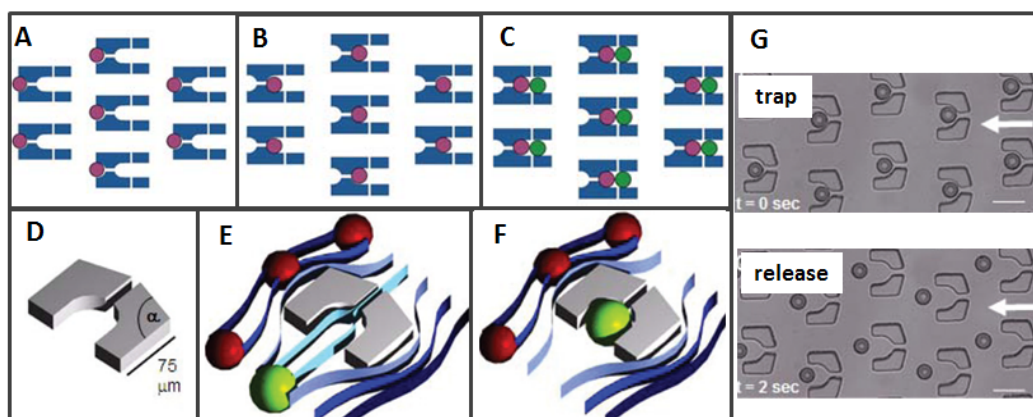


Figure 2-25: (A)-(C) Sequence of images expressing the double droplet trap system. (A) The first droplets (pink) were loaded toward the back-side cup of traps when the liquid flowed from left to right. (B) The direction of the flow was reversed, and the droplets were transferred into the front-side of the downstream traps. (C) The second droplets (green) were loaded from the right and captured in front of the first droplets [ref.80]. (Reproduced by permission of The Royal Society of Chemistry). (D) A design of an individual trap ($\alpha=110^\circ$). (E) Illustration of the flow profile of continuous phase flowing upward. Liquid flowed through the opening aperture of the trap or alongside the traps. (F) A green droplet was trapped at the aperture hindering the fluidic flow through the aperture. (G) The images of the release-and-trap module; trapping mode at $t = 0$ sec when the liquid flowed from left to right and release mode at $t = 2$ sec, the white arrow indicated the liquid flow direction. Scale bars: $75 \mu\text{m}$ [ref.103]. (Reproduced by permission of The Royal Society of Chemistry).

c.3. Droplet Fusion

In the droplet-based microfluidic device, the droplet fusion is another essential manipulation process to merge two (or multi) droplets creating the mixing of two (or multi) discrete liquid

segments. Droplet fusion in microfluidic devices can be achieved when two (or more) droplets are brought in close contact. In general, amphiphilic molecules i.e. surfactant are added to the emulsion to stabilize the formed droplets.¹⁰⁴ As a result an external force might be required to perturb the layer of surfactant molecules at the interface of the two droplets. Some examples of the droplet fusion either by active approach (electric field, laser beam) or passive approach (hydrodynamic approach, surface induction) are demonstrated here.

Electrofusion of droplets

Electric field can be used to merge two droplets by integrating electrode layer onto the microfluidic chip. This approach enhances the efficiency and the controllability of the droplet fusion. Additionally, for the study of (bio-)chemical reactions, the reaction time often needs to be precisely controlled. Therefore, the timing-controllable electrofusion is beneficial for this case. Takeushi *et al*¹⁰⁵ exploited electrofusion to control accurately the fusion time between two droplets used as microreactors inside a microfluidic device. The applied electric field had to be in parallel to the axis of the contacting droplets to initiate the fusion. Two consecutive droplets flowed in the main channel and then moved close together due to hydrodynamic forces in an expansion chamber. In the presence of the electric field, the two droplets then coalesced and the reaction was started. Precise starting times of chemical/biological reactions could be accurately determined in their device (Fig.2.26).

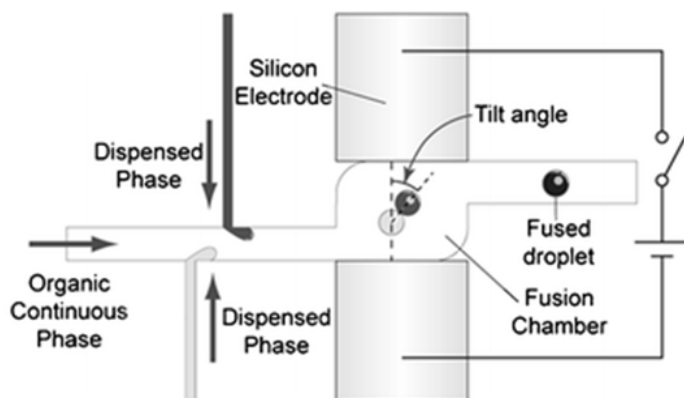


Figure 2-26: Schematic diagram of the electrofusion device. Two consecutive droplets were contacted together in a fusion chamber ($100 \times 750 \mu\text{m}$). The widths of the microchannels for dispersed phase and continuous phase channel were 100 and $250 \mu\text{m}$, respectively, and the depth of all channels was $200 \mu\text{m}$. (dispersed phases : aqueous solutions with blue ink and beta-galactosidase; oil phase: 4 wt% Span 80 in hexadecane solution) [ref.105]. (Reproduced by permission of The Royal Society of Chemistry).

Chapter: 2

Droplet fusion using transient cavitation bubbles

Apart from the manipulation of droplets by the optical tweezer, another usage of optical methods is the droplet fusion by using cavitation bubbles generated from a laser beam. Li *et al*⁶² employed a laser beam to specifically heat a tiny point inside an aqueous droplet resulting in the fusion of two droplets positioned in each other's vicinity (Fig.2-27). When the laser was focused into the upper droplet, a vapor bubble was created and instantaneously grown (Fig.2-27B). Due to the rapid expansion in volume of the bubble, the internal pressure was reduced and in turn the bubble began to shrink creating a thin oil film between the two droplets (Fig.2-27C). Eventually, the fusion occurred during the retraction of the interfaces (Fig.2-27D-F). In their work, the growth of the bubble is anisotropic and more directed downward to the other droplet due to the higher viscosity of the oil as compared to that of the dispersed phase which was placed downward. Moreover, they successfully fused two droplets both in static (stationary droplets) and dynamic (flowing droplets) scenario via this method.

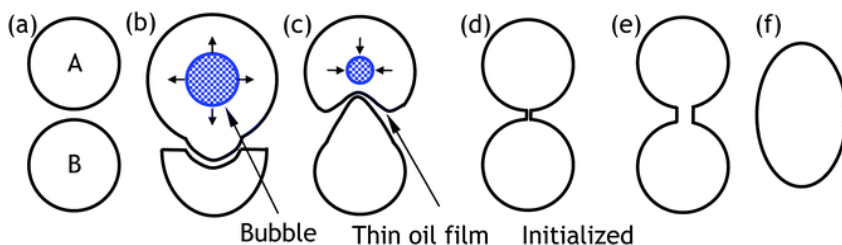


Figure 2-27: Schematic mechanism of the two equal-sized droplets fusion using a laser-induced cavitation bubble. The dispersed phase was an aqueous solution with ink (viscosity ~ 2 cSt), the continuous phase was Cargille oil with 2 wt% Span 80 (viscosity ~ 1250 cSt) [ref.62]. (Reproduced by permission of The Royal Society of Chemistry).

Droplet fusion by pillar structures

Recently, a novel method for controllably merging droplets by exploiting a pillar array in a microfluidic system was proposed.⁶⁴ This approach employed the difference in hydrodynamic resistance of the continuous phase and the surface tension of the dispersed phase to stop or de-accelerate a droplet. Then consecutive droplets can flow to meet and merge with the first droplet (Fig.2-28). In this design, the pillars divided the fusion chamber to be the middle branch of width W_2 , and two side branches of width W_1 and W_3 which were interconnected via side channels of width W_s as depicted in Fig.2-28A. Conceptually, the first droplet slowed down at the pillar array due to the expansion of the channel and reached

the pillar array. In the pillar array, as W_2 was larger than W_s , the droplet remained and deformed in the middle branch (Fig.2-28A and B). Subsequently, the asymmetry deformation of the droplet generating a differential pressure between the head and the tail of the droplet from the different Laplace pressures between the head and tail of the droplet due to the different radii of curvature (Fig.2-28B). This pressure difference, balanced with the total hydrodynamic pressure drop (ΔP) between the tail and the head of a droplet, enabled the quasi-stationary state of droplet in the pillar array leading to the trapping of the droplet.

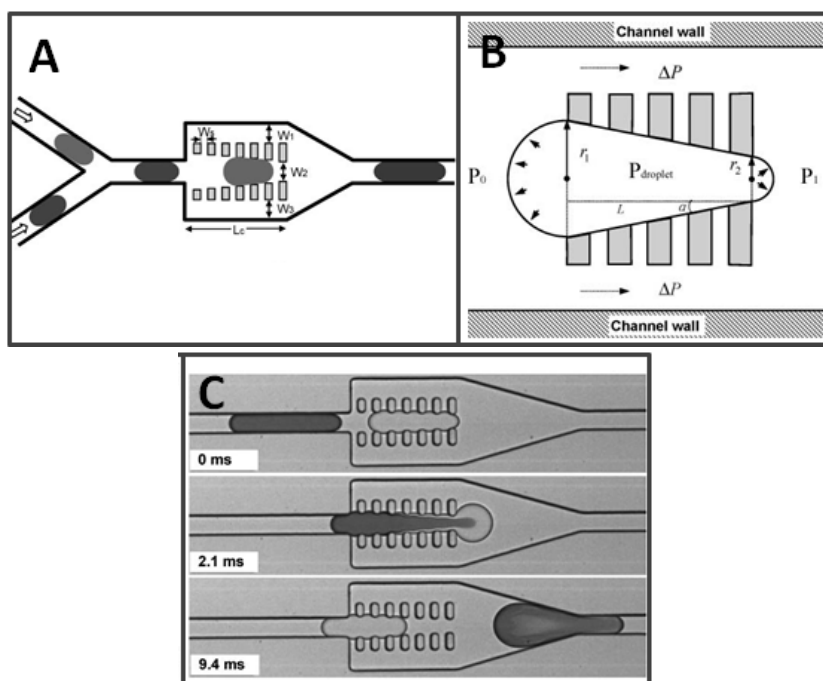


Figure 2-28:(A) Droplet fusion device with pillar array consisting of two channels connected at a Y-junction and a fusion chamber containing a pillar array. (B) Schematic illustration of droplet trapped at the pillar array. (C) Sequence of images showing the fusion of two adjacent droplets [ref.64]. (Reproduced by permission of The Royal Society of Chemistry).

Droplet fusion by surface patterning

Fidalgo *et al*⁶⁰ proposed a new method of droplet fusion based on surface energy patterning inside microfluidic channels. The hydrophilic polyacrylic acid (PAA) was patterned by using UV photopolymerization on a planar benzophenone-containing PDMS substrate. Then, the patterned substrate was bonded to a PDMS microfluidic chip by using oxygen plasma activation. The covalent bonding of the pattern to the PDMS substrate was strong enough to withstand the plasma activation. In this device, alternating aqueous droplets were generated

Chapter: 2

from a double T-junction channel (Fig.2-29). When passing through a hydrophilic pattern, the droplets were trapped or slowed down due to the lower surface energy between aqueous droplets and the hydrophilic surface and subsequently two droplets merged together. The trapped or mixed droplet was subsequently released when the viscous drag force overcame the surface energy stabilization.

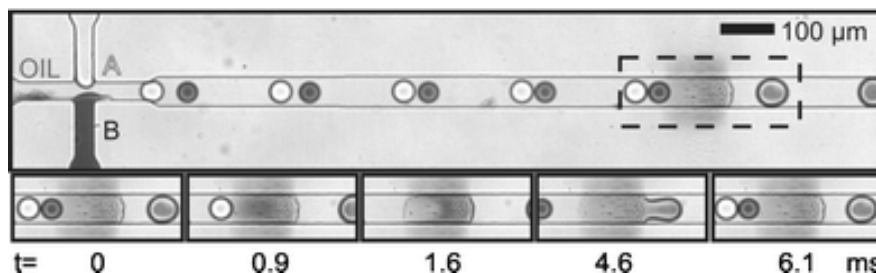


Figure 2-29: Sequence of images expressing the surface induced droplet fusion. The pair of droplets were generated at two T-junctions (A and B) then passed through a hydrophilic pattern (the shadow section in the dot rectangle) ($t=0\text{ms}$). They were subsequently trapped and fused ($t=0.9, 1.6\text{ms}$). Finally, the fused droplet was released ($t=4.6\text{ms}$). The channel was $50\ \mu\text{m}$ wide, and $25\ \mu\text{m}$ deep. The length of the hydrophilic pattern was around $100\ \mu\text{m}$ [ref.60]. (Reproduced by permission of The Royal Society of Chemistry).

d. Conclusion of droplet-based microfluidics

Multisteps and constriction structures are still required ?

From this review, when the droplets are used as microreactors, most research works has been done by loading each reagent into droplets separately in a T-junction or flow-focusing configuration. A pair of the reagent-encapsulated droplets are subsequently synchronized and finally coalesced either by active or passive approach to mix two (or more) reagents resulting in the reaction occurring. Furthermore, the droplet fusion by a passive scheme mostly requires a constriction structure to confine and manipulate the generated droplets. Generally, the dimension of this constriction structure is smaller than the droplet size. This requirement might be problematic for the case of droplets of μm dimensions.

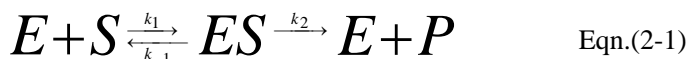
II. Enzymes

Enzymes and enzymatic kinetics

Enzymes are biological macromolecules yielding the conversion of one or more substrate molecules into one or more different product molecules in biochemical reactions. Enzymes

have remarkable properties such as catalytic power, specificity, and regulation.¹⁰⁶ They can increase the reaction rate as high as 10^{19} fold¹⁰⁷ by decreasing the activation energy towards the transition state of the substrate. The study of enzyme kinetics enables the understanding of the enzymatic mechanism and the efficient usage of enzymes to selectively enhance or inhibit the rate of specific enzyme-catalyzed processes.

The fundamental reaction mechanism in enzymology, known as the Michaelis-Menton mechanism, is written as;



Where;

E	=	Free enzyme,
S	=	Substrate,
ES	=	Enzyme-substrate complex,
P	=	Product,
k_1	=	Rate constant for formation of ES ,
k_{-1}	=	Rate constant for conversion of ES to $E+S$,
k_2	=	Rate constant for product formation.

The rate of consumption and formation of ES is expressed as

$$\frac{d[ES]}{dt} = k_1[E][S] - k_{-1}[ES] - k_2[ES] \quad \text{Eqn.(2-2)}$$

At the steady-state, the rate of production of ES is equal to zero,

$$k_1[E][S] = k_{-1}[ES] + k_2[ES] \quad \text{Eqn.(2-3)}$$

$$[ES] = \frac{k_1[E][S]}{k_{-1} + k_2} \quad \text{Eqn.(2-4)}$$

While $K = \frac{k_{-1} + k_2}{k_1}$ and $[E]_t = [E] + [ES]$, thus

$$[ES] = \frac{[E]_t[S]}{K + [S]} + \frac{[ES][S]}{K + [S]} \quad \text{Eqn.(2-5)}$$

$$[ES] = \frac{[E]_t[S]}{K + [S]} \quad \text{Eqn.(2-6)}$$

The rate of product formation, v , is given by $v = k_2[ES]$, thus

$$v = \frac{k_2[E]_t[S]}{K + [S]} \quad \text{Eqn.(2-7)}$$

The turnover number (k_{cat}) is defined as the maximum number of substrate molecules converted to product per one enzyme molecule per unit of time which is a first-order rate constant equal to k_2 , thus

Chapter: 2

$$v = \frac{k_{cat}[E]_t[S]}{K + [S]} \quad \text{Eqn.(2-8)}$$

At high concentration of substrate ($[S] \gg K$) the formation rate tends to reach a maximum value ($v = V_{max}$), therefore $V_{max} = k_{cat} * [E]_t$. Hence Eqn.(2-8) can then be rewritten as:

$$v = \frac{V_{max}[S]}{K + [S]} \quad \text{Eqn.(2-9)}$$

When $v = V_{max}/2$, $[S] = K$. Thus K corresponds to the concentration of substrate when the velocity is half-maximal and it is known as the *Michaelis constant* (K_m).

Therefore, Eqn.(2-9) can be rewritten to “*Michaelis-Menten Equation*” as shown below

$$v = \frac{V_{max}[S]}{K_m + [S]} \quad \text{Eqn.(2-10)}$$

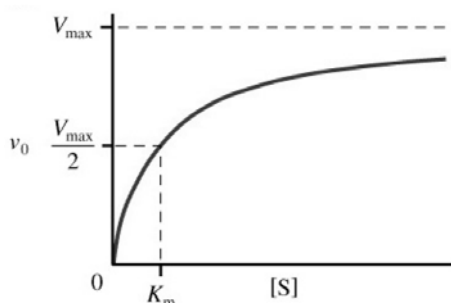


Figure 2-30: An illustration showing the dependence of the production rate (v) on substrate concentration ($[S]$). K_m is the concentration of substrate at $v = V_{max}/2$.

From Eqn.(2-10), at low concentration of substrate, the reaction is first order in $[S]$, but at high concentration of substrate, the reaction is zero order in $[S]$. At intermediate values of $[S]$, the reaction is of a fractional order in $[S]$.

References

1. L. L. Shui, A. van den Berg and J. C. T. Eijkel, *Microfluid Nanofluid*, 2011, **11**, 87-92.
2. J. C. Baret, O. J. Miller, V. Taly, M. Ryckelynck, A. El-Harrak, L. Frenz, C. Rick, M. L. Samuels, J. B. Hutchison, J. J. Agresti, D. R. Link, D. A. Weitz and A. D. Griffiths, *Lab Chip*, 2009, **9**, 1850-1858.
3. T. Endo, A. Okuyama, Y. Matsubara, K. Nishi, M. Kobayashi, S. Yamamura, Y. Morita, Y. Takamura, H. Mizukami and E. Tamiya, *Anal Chim Acta*, 2005, **531**, 7-13.
4. Z. Y. Han, W. T. Li, Y. Y. Huang and B. Zheng, *Anal Chem*, 2009, **81**, 5840-5845.
5. E. Hardiman, M. Gibbs, R. Reeves and P. Bergquist, *Appl Biochem Biotech*, 2010, **161**, 301-312.
6. P. R. Marcoux, M. Dupoy, R. Mathey, A. Novelli-Rousseau, V. Heran, S. Morales, F. Rivera, P. L. Joly, J. P. Moy and F. Mallard, *Colloid Surface A*, 2011, **377**, 54-62.
7. G. Ocvirik, H. Salimi-Moosavi, R. J. Szarka, E. A. Arriaga, P. E. Andersson, R. Smith, N. J. Dovichi and D. J. Harrison, *P Ieee*, 2004, **92**, 115-125.

8. J. U. Shim, L. F. Olguin, G. Whyte, D. Scott, A. Babbie, C. Abell, W. T. S. Huck and F. Hollfelder, *J Am Chem Soc*, 2009, **131**, 15251-15256.
9. N. Wu, F. Courtois, R. Surjadi, J. Oakeshott, T. S. Peat, C. J. Easton, C. Abell and Y. G. Zhu, *Eng Life Sci*, 2011, **11**, 157-164.
10. N. Wu, F. Courtois, Y. G. Zhu, J. Oakeshott, C. Easton and C. Abell, *Electrophoresis*, 2010, **31**, 3121-3128.
11. W. H. Tan and S. Takeuchi, *Lab Chip*, 2006, **6**, 757-763.
12. H. Song and R. F. Ismagilov, *J Am Chem Soc*, 2003, **125**, 14613-14619.
13. M. Srisa-Art, A. J. deMello and J. B. Edel, *Anal Chem*, 2007, **79**, 6682-6689.
14. V. Taly, B. T. Kelly and A. D. Griffiths, *Chembiochem*, 2007, **8**, 263-272.
15. H. Tsuchiya, M. Okochi, N. Nagao, M. Shikida and H. Honda, *Sensor Actuat B-Chem*, 2008, **130**, 583-588.
16. J. J. Agresti, E. Antipov, A. R. Abate, K. Ahn, A. C. Rowat, J. C. Baret, M. Marquez, A. M. Klibanov, A. D. Griffiths and D. A. Weitz, *P Natl Acad Sci USA*, 2010, **107**, 4004-4009.
17. M. Chabert and J. L. Viovy, *P Natl Acad Sci USA*, 2008, **105**, 3191-3196.
18. J. F. Edd, D. Di Carlo, K. J. Humphry, S. Koster, D. Irimia, D. A. Weitz and M. Toner, *Lab Chip*, 2008, **8**, 1262-1264.
19. L. Granieri, J. C. Baret, A. D. Griffiths and C. A. Merten, *Chem Biol*, 2010, **17**, 229-235.
20. S. Koster, F. E. Angile, H. Duan, J. J. Agresti, A. Wintner, C. Schmitz, A. C. Rowat, C. A. Merten, D. Pisignano, A. D. Griffiths and D. A. Weitz, *Lab Chip*, 2008, **8**, 1110-1115.
21. J. Hong, A. J. deMello and S. N. Jayasinghe, *Biomed Mater*, 2010, **5**.
22. J. Clausell-Tormos, D. Lieber, J. C. Baret, A. El-Harrak, O. J. Miller, L. Frenz, J. Blouwolff, K. J. Humphry, S. Koster, H. Duan, C. Holtze, D. A. Weitz, A. D. Griffiths and C. A. Merten, *Chem. Biol.*, 2008, **15**, 427-437.
23. J. W. Kim, D. Lee, H. C. Shum and D. A. Weitz, *Adv Mater*, 2008, **20**, 3239-+.
24. D. Lee and D. A. Weitz, *Adv Mater*, 2008, **20**, 3498-+.
25. K. S. Huang, K. Lu, C. S. Yeh, S. R. Chung, C. H. Lin, C. H. Yang and Y. S. Dong, *J Control Release*, 2009, **137**, 15-19.
26. F. Malloggi, N. Pannacci, R. Attia, F. Monti, P. Mary, H. Willaime, P. Tabeling, B. Cabane and P. Poncet, *Langmuir*, 2010, **26**, 2369-2373.
27. S. Seiffert, J. Thiele, A. R. Abate and D. A. Weitz, *J Am Chem Soc*, 2010, **132**, 6606-6609.
28. R. K. Shah, J. W. Kim and D. A. Weitz, *Langmuir*, 2010, **26**, 1561-1565.
29. H. Hwang, S. H. Kim and S. M. Yang, *Lab Chip*, 2011, **11**, 87-92.
30. A. J. C. Kuehne and D. A. Weitz, *Chem Commun*, 2011, **47**, 12379-12381.
31. H. Song, J. D. Tice and R. F. Ismagilov, *Angew Chem Int Edit*, 2003, **42**, 768-772.
32. H. Song, D. L. Chen and R. F. Ismagilov, *Angew Chem Int Edit*, 2006, **45**, 7336-7356.
33. J. Atencia and D. J. Beebe, *Nature*, 2005, **437**, 648-655.
34. T. T. Fu, Y. G. Ma, D. Funfschilling, C. Y. Zhu and H. Z. Li, *Chem Eng Sci*, 2010, **65**, 3739-3748.
35. P. Garstecki, M. J. Fuerstman, H. A. Stone and G. M. Whitesides, *Lab Chip*, 2006, **6**, 437-446.
36. P. Garstecki, I. Gitlin, W. DiLuzio, G. M. Whitesides, E. Kumacheva and H. A. Stone, *Appl Phys Lett*, 2004, **85**, 2649-2651.
37. D. Pekin, Y. Skhiri, J. C. Baret, D. Le Corre, L. Mazutis, C. Ben Salem, F. Millot, A. El Harrak, J. B. Hutchison, J. W. Larson, D. R. Link, P. Laurent-Puig, A. D. Griffiths and V. Taly, *Lab Chip*, 2011, **11**, 2156-2166.

Chapter: 2

38. J. C. Baret, F. Kleinschmidt, A. El Harrak and A. D. Griffiths, *Langmuir*, 2009, **25**, 6088-6093.
39. A. B. Theberge, F. Courtois, Y. Schaerli, M. Fischlechner, C. Abell, F. Hollfelder and W. T. S. Huck, *Angew Chem Int Edit*, 2010, **49**, 5846-5868.
40. T. Thorsen, R. W. Roberts, F. H. Arnold and S. R. Quake, *Phys Rev Lett*, 2001, **86**, 4163-4166.
41. C. N. Baroud, F. Gallaire and R. Dangla, *Lab Chip*, 2010, **10**, 2032-2045.
42. A. Gupta and R. Kumar, *Microfluid Nanofluid*, 2010, **8**, 799-812.
43. R. M. Lorenz, G. S. Fiorini, G. D. M. Jeffries, D. S. W. Lim, M. Y. He and D. T. Chiu, *Anal Chim Acta*, 2008, **630**, 124-130.
44. S. L. Anna, N. Bontoux and H. A. Stone, *Appl Phys Lett*, 2003, **82**, 364-366.
45. A. R. Abate, A. Poitzsch, Y. Hwang, J. Lee, J. Czerwinska and D. A. Weitz, *Phys Rev E*, 2009, **80**.
46. P. Garstecki, H. A. Stone and G. M. Whitesides, *Phys Rev Lett*, 2005, **94**.
47. M. Hashimoto and G. M. Whitesides, *Small*, 2010, **6**, 1051-1059.
48. W. Lee, L. M. Walker and S. L. Anna, *Phys Fluids*, 2009, **21**.
49. L. Zhao, Q. Zeng, Z. Guo, J. Liu and X. Zhao, presented in part at the Bioinformatics and Biomedical Engineering, 2007, Wuhan, 2007.
50. P. B. Umbanhowar, V. Prasad and D. A. Weitz, *Langmuir*, 2000, **16**, 347-351.
51. L. Y. Chu, A. S. Utada, R. K. Shah, J. W. Kim and D. A. Weitz, *Angew Chem Int Edit*, 2007, **46**, 8970-8974.
52. M. G. Pollack, A. D. Shenderov and R. B. Fair, *Lab Chip*, 2002, **2**, 96-101.
53. H. Gu, F. Malloggi, S. A. Vanapalli and F. Mugele, *Appl Phys Lett*, 2008, **93**.
54. H. Gu, M. H. G. Duits and F. Mugele, *Lab Chip*, 2010, **10**, 1550-1556.
55. F. Guo, X. H. Ji, K. Liu, R. X. He, L. B. Zhao, Z. X. Guo, W. Liu, S. S. Guo and X. Z. Zhao, *Appl Phys Lett*, 2010, **96**.
56. A. R. Abate, J. J. Agresti and D. A. Weitz, *Appl Phys Lett*, 2010, **96**.
57. Y. C. Tan, Y. L. Ho and A. P. Lee, *Microfluid Nanofluid*, 2008, **4**, 343-348.
58. N. Bremond, A. R. Thiam and J. Bibette, *Phys Rev Lett*, 2008, **100**.
59. V. Chokkalingam, B. Weidenhof, M. Kramer, W. F. Maier, S. Herminghaus and R. Seemann, *Lab Chip*, 2010, **10**, 1700-1705.
60. L. M. Fidalgo, C. Abell and W. T. S. Huck, *Lab Chip*, 2007, **7**, 984-986.
61. L. Li, J. Q. Boedicker and R. F. Ismagilov, *Anal Chem*, 2007, **79**, 2756-2761.
62. Z. G. Li, K. Ando, J. Q. Yu, A. Q. Liu, J. B. Zhang and C. D. Ohl, *Lab Chip*, 2011, **11**, 1879-1885.
63. D. R. Link, E. Grasland-Mongrain, A. Duri, F. Sarrazin, Z. D. Cheng, G. Cristobal, M. Marquez and D. A. Weitz, *Angew Chem Int Edit*, 2006, **45**, 2556-2560.
64. X. Niu, S. Gulati, J. B. Edel and A. J. deMello, *Lab Chip*, 2008, **8**, 1837-1841.
65. J. Sivasamy, Y. C. Chim, T. N. Wong, N. T. Nguyen and L. Yobas, *Microfluid Nanofluid*, 2010, **8**, 409-416.
66. M. Yamada, S. Doi, H. Maenaka, M. Yasuda and M. Seki, *J Colloid Interf Sci*, 2008, **321**, 401-407.
67. S. J. Zeng, X. Y. Pan, Q. Q. Zhang, B. C. Lin and J. H. Qin, *Anal Chem*, 2011, **83**, 2083-2089.
68. G. F. Christopher, J. Bergstein, N. B. End, M. Poon, C. Nguyen and S. L. Anna, *Lab Chip*, 2009, **9**, 1102-1109.
69. D. R. Link, S. L. Anna, D. A. Weitz and H. A. Stone, *Phys Rev Lett*, 2004, **92**.
70. M. Zagnoni and J. M. Cooper, *Lab Chip*, 2010, **10**, 3069-3073.
71. E. Surenjav, C. Priest, S. Herminghaus and R. Seemann, *Lab Chip*, 2009, **9**, 325-330.

72. E. Surenjav, S. Herminghaus, C. Priest and R. Seemann, *Appl Phys Lett*, 2009, **95**.
73. P. Garstecki and G. M. Whitesides, *Phys Rev Lett*, 2006, **97**.
74. J. Hong, M. Choi, J. B. Edel and A. J. deMello, *Lab Chip*, 2010, **10**, 2702-2709.
75. S. J. Zeng, B. W. Li, X. O. Su, J. H. Qin and B. C. Lin, *Lab Chip*, 2009, **9**, 1340-1343.
76. B. Lee and J. Y. Yoo, *Microfluid Nanofluid*, 2011, **11**, 685-693.
77. R. Dangla, S. Lee and C. N. Baroud, *Phys Rev Lett*, 2011, **107**.
78. B. Ahn, K. Lee, H. Lee, R. Panchapakesan, L. F. Xu, J. Xu and K. W. Oh, *Lab Chip*, 2011, **11**, 3915-3918.
79. P. Abbyad, R. Dangla, A. Alexandrou and C. N. Baroud, *Lab Chip*, 2011, **11**, 813-821.
80. Y. P. Bai, X. M. He, D. S. Liu, S. N. Patil, D. Bratton, A. Huebner, F. Hollfelder, C. Abell and W. T. S. Huck, *Lab Chip*, 2010, **10**, 1281-1285.
81. E. Um and J. K. Park, *Lab Chip*, 2009, **9**, 207-212.
82. R. Aoki, M. Yamada, M. Yasuda and M. Seki, *Microfluid Nanofluid*, 2009, **6**, 571-576.
83. M. Washizu, *Ieee T Ind Appl*, 1998, **34**, 732-737.
84. S. K. Fan, T. H. Hsieh and D. Y. Lin, *Lab Chip*, 2009, **9**, 1236-1242.
85. M. Cho and D. Z. Pan, *Ispd'08: Proceedings of the 2008 Acm International Symposium on Physical Design*, 2008, 200-206.
86. R. B. Fair, *Microfluid Nanofluid*, 2007, **3**, 245-281.
87. K. W. Oh, B. Ahn, K. Lee and R. Louge, *Biomicrofluidics*, 2009, **3**.
88. Z. C. Long, A. M. Shetty, M. J. Solomon and R. G. Larson, *Lab Chip*, 2009, **9**, 1567-1575.
89. A. Ashkin, *P Natl Acad Sci USA*, 1997, **94**, 4853-4860.
90. N. Kitamura and F. Kitagawa, *J Photoch Photobio C*, 2003, **4**, 227-247.
91. D. A. Woods, C. D. Mellor, J. M. Taylor, C. D. Bain and A. D. Ward, *Soft Matter*, 2011, **7**, 2517-2520.
92. J. Y. Tang, A. M. Jofre, R. B. Kishore, J. E. Reiner, M. E. Greene, G. M. Lowman, J. S. Denker, C. C. C. Willis, K. Helmersen and L. S. Goldner, *Anal Chem*, 2009, **81**, 8041-8047.
93. M. L. Cordero, D. R. Burnham, C. N. Baroud and D. McGloin, *Appl Phys Lett*, 2008, **93**.
94. J. E. Reiner, A. M. Crawford, R. B. Kishore, L. S. Goldner, K. Helmersen and M. K. Gilson, *Appl Phys Lett*, 2006, **89**.
95. M. Y. He, J. S. Edgar, G. D. M. Jeffries, R. M. Lorenz, J. P. Shelby and D. T. Chiu, *Anal Chem*, 2005, **77**, 1539-1544.
96. K. W. Oh and C. H. Ahn, *J Micromech Microeng*, 2006, **16**, R13-R39.
97. J. H. Qin, S. J. Zeng, B. W. Li, X. O. Su and B. C. Lin, *Lab Chip*, 2009, **9**, 1340-1343.
98. W. Engl, M. Roche, A. Colin, P. Panizza and A. Ajdari, *Phys Rev Lett*, 2005, **95**.
99. G. Cristobal, J. P. Benoit, M. Joanicot and A. Ajdari, *Appl Phys Lett*, 2006, **89**.
100. L. Frenz, J. Blouwolf, A. D. Griffiths and J. C. Baret, *Langmuir*, 2008, **24**, 12073-12076.
101. L. Mazutis and A. D. Griffiths, *Appl Phys Lett*, 2009, **95**.
102. J. Nilsson, M. Evander, B. Hammarstrom and T. Laurell, *Anal Chim Acta*, 2009, **649**, 141-157.
103. A. Huebner, D. Bratton, G. Whyte, M. Yang, A. J. deMello, C. Abell and F. Hollfelder, *Lab Chip*, 2009, **9**, 692-698.
104. J. C. Baret, *Lab Chip*, 2012, **12**, 422-433.
105. S. Takeuchi and W. H. Tan, *Lab Chip*, 2006, **6**, 757-763.
106. C. J. Suckling, *Chem Brit*, 1983, **19**, 423-423.
107. R. Wolfenden and M. J. Snider, *Accounts Chem Res*, 2001, **34**, 938-945.

CHAPTER 3:

Design, Material and Realization

In this chapter, the design of our fluidic system will be described in aspects of the concept of fluidic network and fluidic manipulation. Then, the selection of materials for fabrication of the device is discussed in relation to properties and fabrication procedures. Next the preliminary tests performed to choose the material for our device are illustrated. Then the experimental (fluidic and optical) setups are detailed. Lastly the fluidic flow rates in each channel network are determined by a circuit simulation program in order to estimate the necessary length of the detection line and to verify the ratio of fluidic flows of dispersed and continuous phases at the splitting T-junction.

Design and Realization

I. Conceptual Design

The droplet-based microfluidic platform had been designed and fabricated to encapsulate single (or more) molecules for bio and chemical analysis. The fabricated platform was utilized to generate and facilitate the water-in-oil (W/O) emulsion at which the aqueous droplets were used to encapsulate molecules. The characteristics of this fluidic system such as the size of carrier, the regulation of fluidic flow, droplet coalescence and the detection of the targeted molecules are described below.

Miniaturization of the carriers

In general, the single-molecule encapsulation can be implemented either by compartmentalization or dilution. In the water-in-oil (W/O) emulsion, the size of the water droplets can be modulated by adjusting the flow rates and the viscosities of water and oil as well as the geometry of fluidic channel.¹⁻³ By adjusting the size of droplets, the amount of encapsulated molecules in droplets can be simply adjusted. For instance, when 1.6-nM enzyme solution is compartmented into an array of 1- μ L aqueous droplets, one generated droplet contains $[1.6 \times 10^{-9} \times 10^{-6} \times 6.02 \times 10^{23}] \approx 10^9$ enzyme molecules. The single-molecule encapsulation by dilution can become problematic due to the abundant amount of solvent molecules compared to that of enzyme molecules creating high background noise. By compartmentalization, the confined tiny droplets can encapsulate one single enzyme with a small amount of solvent. To achieve the single-molecule encapsulation, the enzyme solution is, for example, compartmented into 1-fL droplets resulting in an average of one molecule $[1.6 \times 10^{-9} \times 10^{-15} \times 6.02 \times 10^{23} \approx 1]$ per 1-fL droplet. Moreover, when the volume of solvent is reduced from 10^{-6} L to 10^{-15} L, the background signal from the solvent diminishes 10^9 fold resulting in a high signal to noise ratio in the measurement. In addition, as mentioned in the previous chapter, the W/O emulsion used as carriers for any reactions would be beneficial for low contamination, precisely-controlled reaction with high-throughput results since each droplet is isolated in the continuous phase, the reaction in each droplet can take place

independently in parallel providing plentiful results at the same time and the generated droplets can be simply manipulated in the microfluidic device.

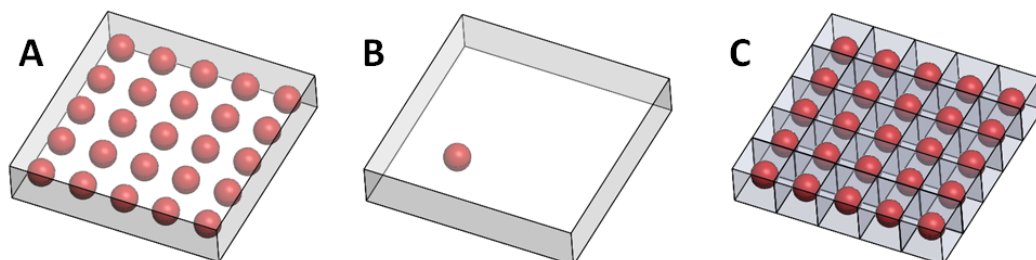


Figure 3-1: (A) An illustration of the enzyme solution dissolved in 1- μL carrier (enzyme: red and water: grey). (B) By dilution, single-molecule encapsulation can be achieved but the excess amount of solvent provides high background noise. (C) By compartmentalization, the enzyme solution is confined as tiny droplets containing single enzymes.

Regulation of a small flow rate

In our design, a T-junction had been utilized to generate droplets. The dimension (width and height) of this junction as well as the channel for facilitating the flow of generated droplets should be scaled down to be of comparable size to the droplet dimensions. Conventionally, small fluidic flow rates can be obtained from pressure-driven systems such as a pressure-driven pump or a hydrostatic adjustment. However, it is difficult and time consuming to precisely control the flow rate to transport the liquid from a reservoir to the fluidic channel. At the minimal flow rates of classical syringe pumps very high pressures will be generated due to the high resistance of the nanochannel network, creating leakage problems. Furthermore, when very high flow velocity is generated in nanochannels, the droplets are more difficult to be maneuvered and observed. To enable the regulation of very small flow rates, we designed a splitting junction to split a tiny portion from the fluidic flow (generated by a classical syringe pump) in a main microchannel (Q_m) to flow in a nanochannel (Q_n).⁴ The splitting ratio (Q_n/Q_m) is thereby governed by the geometry (width, length and height) of nano- and microfluidic networks downstream from this junction to the outlet and given by;

$$\frac{Q_n}{Q_m} = \frac{Lwh^3}{lWH^3} \quad \text{Eqn.(3-1)}$$

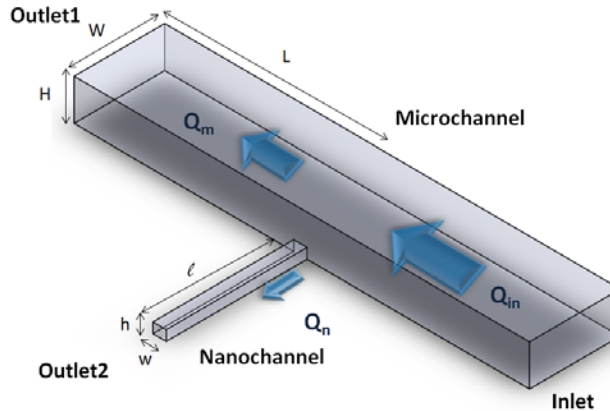


Figure 3-2: Schematic of a splitting junction to distribute a flow from a main microchannel to a nanochannel governed by the geometry of channels downstream of this junction.

For instance, when the width, height, and length of microchannel from a splitting junction to the outlet1 were 20, 5 and 1000 μm and those of a nanochannel to outlet2 were 5, 0.5, 500 μm respectively, then the splitting ratio (Q_n/Q_m) was equal to $(1000 \times 5 \times 0.5^3)/(500 \times 50 \times 5^3) = 1/5000$ implying that when $Q_{in} = 5001 \mu\text{L}/\text{min}$, Q_n and Q_m were 1 and 5000 $\mu\text{L}/\text{min}$, respectively (split ratio 1:5000).

Droplet Fusion Concept

A tremendous amount of work on droplet manipulation and fusion in microfluidic systems has recently been reported in the literature as discussed in the previous chapter. Briefly, the droplets can be generated from the microfluidic system with T-junction, flow-focusing or co-axial focusing systems or with the electrical induction.^{1, 2, 5} Generated droplets are then manipulated and/or coalesced either by passive or active approaches. Generally, the W/O emulsions are generated and droplets are collected from one microfluidic device and subsequently loaded into another device for manipulation and coalescence.⁶ However, in case of the generation of sub-fL droplets, when loading generated droplets into the second device, it is difficult to manipulate tiny droplets inside a microchannel, since the dimension of the channel should be comparable hence very narrow and/or shallow. In view of this, we think it is more convenient to integrate both droplet generation and droplet coalescence schemes into one chip by implementing the droplet fusion immediately (or within a short period of time) after generating droplets.

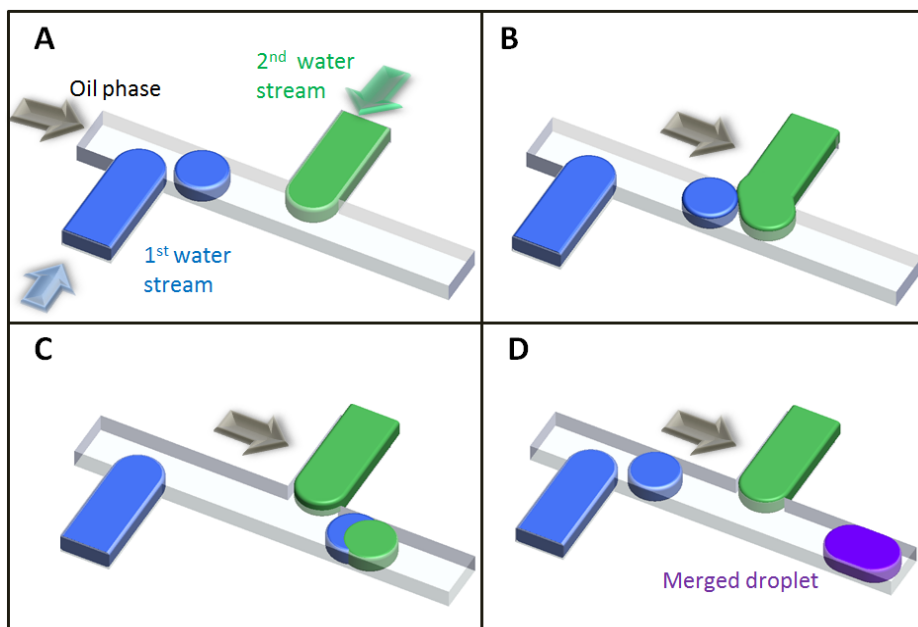


Figure 3-3: Schematic of a nanofluidic network consisting of two T-junctions; A: at the first junction, the first aqueous droplet (blue) is created in the oil phase. B: First droplet flows to contact the tip of a second aqueous stream (green). C and D: Two aqueous solutions merged creating the product droplet (purple). The arrows express the fluidic direction.

In our design, the simple approach to fuse droplets is by using the shear stress from a first aqueous droplet formed upstream and the continuous oil phase (see Fig 3-3).^{7,8} In addition, Baret *et al*⁹ reported that after droplet generation at the time-scale of \sim ms, the surfactant does not fully cover the water/oil interface and the coverage of surfactant is asymmetric between the front and rear of the droplet. It is expected that droplet fusion can more easily occur directly after the droplet generation if full coverage of the surfactant onto the interface is not yet reached. In general, droplets can be formed and stabilized in continuous phase by adding amphiphilic molecules such as surfactants. Surfactants play essential roles in the droplet-based microfluidic technology by reducing the interfacial tension between two immiscible fluids and hindering droplet coalescence.^{9,10} After the generation of droplet, the surfactant molecules diffuse on the interface and rearrange to form the layer covering the interface of the two fluids. In our system, inside a nanochannel the shear force from a first droplet with the continuous phase should however be large enough to rearrange the surfactant layer. After rearrangement of this layer, two aqueous droplets merge and their contents diffuse simultaneously while the surfactant molecules rearrange again at the

interface of the two phases and form a layer surrounding the merged droplet. In the absence of surfactant, the required shear force might be less than in the case with surfactant, however, the merged droplets might not be stable or might merge with consecutive droplets.

Concept of Detection Channel

After fusion of the two aqueous droplets, a merged droplet as described above will contain the enzyme molecules and the substrate, and subsequently the enzymatic reaction takes place generating a product. An enzymatic reaction creating a fluorescent product is the model reaction for our first study (more details on the fluorescent product and the detection will be given in chapter 7). In the outlet channel, the merged droplets have to be retarded or even trapped for the measurement of the increasing fluorescent intensity of the product as a function of time. Therefore, an expanding outlet channel was designed to slow down these droplets. Due to the high surface energy of the longitudinally deformed droplets in a narrow nanochannel, when arriving at an expanding nanochannel, the droplets deform to a pancake-like shape which is more stable, and further flow in the outlet nanochannel (Fig.3-4). Subsequently, the time-resolved measurement of fluorescence can be performed in many droplets simultaneously. Also, the droplets can be halted just by simply stopping all the flow from the pumps.

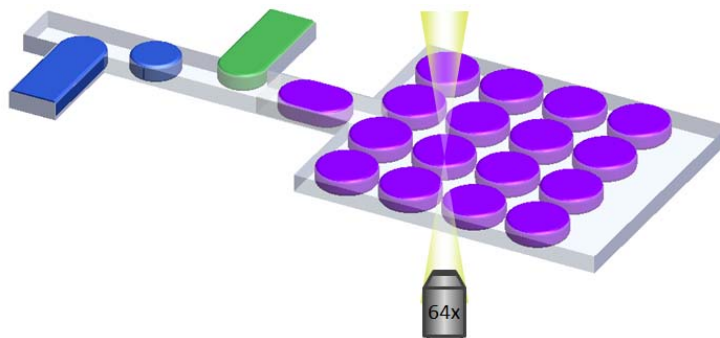


Figure 3-4: Schematic of merged droplets flowing into the outlet channel at which the increasing amount of product is detected by a fluorescence microscope and a high-sensitivity camera.

Alternative ideas are an outlet channel expanding in the z-axis (gravitational axis) or an outlet channel with a change in the depth from nanometer to micrometer range. The changing depth will reduce Laplace pressure around the droplets which is governed by the interfacial tension between two immiscible liquids as well as the depth of the channel.

Therefore, entering the deeper channel section droplets will take on a spherical shape to reduce surface energy. However, the detection of spherical droplets might be problematic since droplets can become located on top of each other leading to misinterpretations of the fluorescence at the intersecting areas.

II. Material Selection

In the micro- and nano-fabrication technology, there are several materials available for the fabrication of microfluidic devices, i.e. silicon, glass, polymers. However, some properties of these materials are of high concern regarding the specific requirements of our device, for instance, light transmission for optical measurement, low autofluorescence, suitable surface energy with the liquids used (hydrophilicity/hydrophobicity), the possibility to obtain a high aspect ratio of the patterns and so on. After patterning, two (or more) substrates are assembled together and the quality of bonding is also crucial in the case that high pressure must be applied to a device, for example for the nanofluidic devices with high fluidic resistance. Hence, the types of material for device fabrication were preliminarily considered in these different aspects as depicted in a table 3.01.

In practice, several materials are commonly used for fabrication of microfluidic devices in our laboratory, namely, glass, polydimethylsiloxane (PDMS), SU-8, polyimide and parylene. Firstly discussing glass, there are several categories of glass materials considering their composition but the most commonly used glasses for fabrication of fluidic devices are borofloat (borosilicate glass substrate) and fused silica. Borofloat is preferable for microfabrication due to its better mechanical properties. Glass material is rigid and two glass substrates can be bonded by thermal bonding technique at high temperature (650°C) creating high bonding strength from siloxane (Si-O-Si) bonds.¹¹ Glass surfaces are hydrophilic with a contact angle (C.A.) of around 25°. Fluidic channels can be patterned by wet or dry etching processes. However, the etching process can create rough surfaces and can also undercut structures which makes it difficult to pattern channels whose depth is much larger than the width. Most significantly, the glass surface must be hydrophobized to enable the generation of the required water in oil emulsion.

Table 3-01: List of materials commonly-used in our laboratory including their fabrication methods, advantage and disadvantages

Material	Fabrication method	Contact Angle	Bonding	Pros	Cons	Ref.
Glass	Wet or Dry Etching	25	Thermal bonding	<ul style="list-style-type: none"> Simple fabrication method Rigid material High bonding strength 	<ul style="list-style-type: none"> Surface modification required Rough surface from etching Undercut structure Difficult to pattern channel with the depth much larger than width 	[4], [11], [34], [35], [36]
PDMS	Photolithography and Casting	105	Oxygen Plasma	<ul style="list-style-type: none"> Rapid and cheap fabrication Smooth surface High aspect ratio (width to height) pattern 	<ul style="list-style-type: none"> Low bonding strength Roof collapse Permeability to gaseous and small molecules 	[12], [13], [14], [15], [16], [17], [25], [26], [27], [28], [29], [30], [32]
SU-8	Photolithography	70	Adhesive layer or thermal bonding	<ul style="list-style-type: none"> Smooth surface High aspect ratio pattern 	<ul style="list-style-type: none"> Auto-fluorescence 	[18], [20], [23]
Polyimide	Photolithography	75	Adhesive layer or thermal bonding	<ul style="list-style-type: none"> Smooth surface High aspect ratio pattern 	<ul style="list-style-type: none"> Auto-fluorescence 	[19], [24]
Parylene	Deposition	90	Thermal bonding	<ul style="list-style-type: none"> Smooth surface 	<ul style="list-style-type: none"> Auto-fluorescence 	[21], [22], [23], [24]

Chapter: 3

Secondly, PDMS is a flexible polymer commonly used in many laboratories, but its intrinsic properties should be well considered for every individual application. PDMS is fabricated from a casting technique against the master.¹² If the surface of the master is smooth, then the casted PDMS device is also smooth. Due to low Young's Modulus of PDMS, in fluidic channels with a small depth or a high width-to-depth ratio, the top wall (roof) can collapse to the bottom wall¹³⁻¹⁷ making it more difficult to construct such devices from this material. Due to the hydrophobic surface of PDMS (C.A.~105°), the PDMS-based device can be immediately used for the generation of water-in-oil emulsion without surface modification, which is an advantage of the material. A disadvantage is, that solid PDMS is permeable to gaseous or small molecules which might be absorbed onto the surface or penetrate inside the bulk of the PDMS.

SU-8 and polyimide can be fabricated by standard photolithography.^{18, 19} High-aspect ratio patterns can be formed with a smooth surface using these polymers. Patterned substrates made from these materials have to be bonded by using an adhesive layer such as the polymer itself or another gluing layer.²⁰ The contact angle of these materials is around 70-90°. Next, parylene (C.A.~80-90°) can be deposited onto silicon or glass substrates with fluidic channels as a thin layer by vaporized deposition. The parylene-coated substrate is then bonded to another parylene-coated surface or another substrate by thermal bonding at the glass transition temperature of parylene (90°C).^{21, 22}

For single enzyme detection, the signal of the detected substrate molecules is very weak compared to that from the surroundings i.e. solution and substrates. Hence, one of the most significant issues for detection of low amounts of substance is the autofluorescence from the substrate and solution. Consequently, these polymers (SU-8, polyimide, parylene) are discarded from our selection due to their auto-fluorescence.^{23, 24} Eventually only two materials have been deemed appropriate for the fabrication of our device, namely, borosilicate glass and PDMS. The details of these materials will be discussed here.

III. Polydimethylsiloxane (PDMS)-based Microfluidic Device

Polydimethylsiloxane (PDMS) is an elastomeric polymer widely used in microfluidic device fabrication. Due to its excellent properties such as optical transparency, non-toxicity and non-flammability, bio- and chemical compatibility as well as its simple fabrication protocol, PDMS is one of the most commonly used materials for cellular and biological studies in the laboratory. Thus, also in view of its hydrophobicity and relatively low autofluorescence, PDMS was the first material to be considered for the fabrication of the devices for our experiments. The fabrication procedure comprises two main steps, namely, (i) producing the master with an inverted pattern made from SU-8 on the silicon substrate and, (ii) casting of the PDMS polymer (Fig. 3-5).

(i) The master with an inverted pattern

- 1) Silicon wafer was oxidized at 1050°C by thermal oxidation (Amtech Tempress, USA) to generate a thin layer (250 nm or 500 nm) of silicon dioxide on the silicon substrate. Positive photoresist (OIR907-17) was spin-coated on the SiO₂/Si substrate, patterned using a mask aligner (EVG-620, using 4 s exposure at 12 mW/cm²) and developed in the developer (OPD4262, Fujifilm, Japan).
- 2) SiO₂ was etched by immersion into buffer hydrofluoric acid solution (BHF) (VLSI Selectipur, BASF) to form the inverted nanochannel.
- 3) The negative photoresist SU-8 (Microchem, Germany) was spin-coated onto the patterned SiO₂/Si substrate, photolithographed using a mask aligner, and developed in RER600 (Fujifilm) to form the inverted microchannel.
- 4) The SU-8 patterned Si master was hard-baked at 150° C for 1 hour to crosslink the polymer and eliminate remaining acidic photoinitiator inside the polymer.
- 5) Fluorosilane molecules (1H, 1H, 2H, 2H-perfluorodecyltrichlorosilane: FDTS) bought from Sigma Aldrich were deposited onto the SU8-based silicon master by vaporized deposition to enhance the quality and resolution of the pattern from a subsequent casting step. *

* Due to the fact that FDTS is highly reactive to water and air, FDTS is prepared under nitrogen flow and then placed together with the Si master in the desiccator and stored under vacuum for a few hours.

Chapter: 3

(ii) The replica of patterns from PDMS polymer

- 1) Sylgard 184 PDMS base (a pre-polymer) and PDMS curing agent (a cross linker) were mixed together in the standard ratio of 10:1 w/w. Both were bought from Dow Corning, USA.
- 2) The mixture was poured on top of the patterned silicon wafers, degassed and cured at 60°C for 10 hours.
- 3) PDMS cast was peeled off from the master, cut into individual chips and punched to create the access holes by a punching cutter (Harris Uni-core, USA) for fluidic inlet and outlets.
- 4) A PDMS chip was bonded to an glass substrate after oxygen plasma treatment of the PDMS (Harrick Plasma Cleaner, USA).

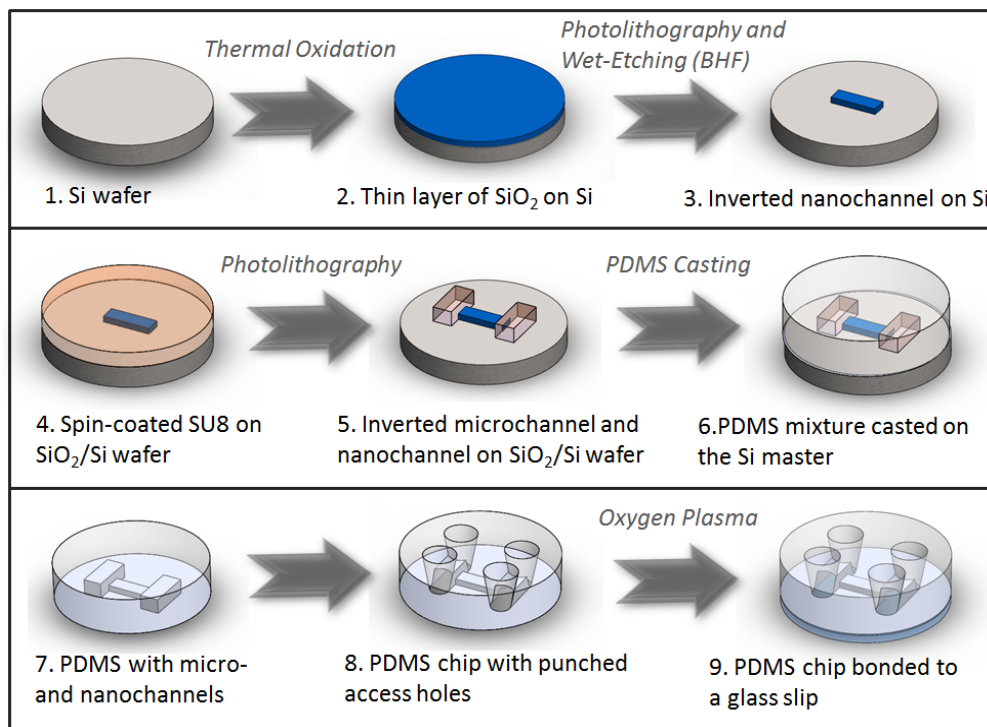


Figure 3-5: Schematic diagram showing the fabrication protocol of PDMS chips

One single PDMS master can be used to produce numerous PDMS replica for several times. This replication as well as the cost of material itself make PDMS-based devices promising in aspect of rapid production and low expense in the laboratories.

Experimental results

We encountered problems during the fabrication procedure of the PDMS-based chips due to the flexibility of PDMS. Flexible PDMS layers can cause some problems when the aspect ratio (width to height of the channel) is too high, causing the top wall of the channel to collapse and stick to the bottom wall, as shown in Fig. 3-6.



Figure 3-6: PDMS-based fluidic chip (Left), and the roof collapse in the fluidic channels (Right).

In general, the roof collapse results from the intrinsic properties, low Young's Modulus, of PDMS. Some parameters upon fabrication procedure as shown earlier can fine tune these elastic properties of the polymer, such as the curing conditions (time and temperature) and the mixing ratio of PDMS base and curing agent.²⁵⁻²⁹ Briefly, with a lower mixing ratio (1:5), the Young's Modulus of PDMS increases compared to a higher mixing ratio (1:10) at the same other parameters. In addition, the PDMS mixture can be cured longer to obtain a higher Young's Modulus.

In our design, one of the most critical geometries among several dimensions was the nanochannel with a width of 10 μm and height of 250 or 500 nm. With the standard PDMS fabrication protocol (mixing ratio of 1:10, curing condition at 80°C for a few hours) both nanochannels collapsed. Subsequently, the fabrication protocol was adapted to using PDMS mixtures at the ratio of 1:5 and curing in the oven at 60°C overnight. Using this protocol, the 500-nm-deep nanochannel could be successfully constructed, but the roof collapse still occurred in 250-nm-deep nanochannels.

Solid PDMS is hydrophobic with a contact angle of around 105° and is permeable to gaseous or small molecules.^{30,31} In addition, minute amounts of non-polar liquids such as oil might be able to penetrate through PDMS surface. Therefore, preliminary swelling tests were performed by immersing PDMS slabs into different solutions for four days. The dimensions and mass of the samples were measured before and after immersion.

Chapter: 3

Table 3-02: Preliminary Swelling Test.

	Water				Oil		
	H ₂ O	Fluo ^b	H ₂ O+Surf ^c	Fluo+Surf ^d	HD ^e	SO ^f	SO+Surf ^g
Swelling Ratio: S (S=D/D ₀) ^a	1.00	1.00	1.00	1.00	1.20	1.28	1.30
Mass Change (%)	0.1	0.1	0.1	0.1	55.4	76.7	83.8

Note: a) *D* and *D*₀ are the length of PDMS slabs in the solvent and in air, respectively
b) 0.5 mM fluorescein solution c) 2% Tween20 in water
d) 2% Tween20 in 0.5 mM fluorescein solution e) Hexadecane
f) Silicone Oil 1 cSt g) 5% Span80 in Silicone Oil 1 cSt

From these preliminary tests we found some evidence that PDMS absorbs negligible amounts of aqueous solution. However, we do have evidence that quite large amounts of non-polar liquid were absorbed into PDMS samples also in the presence of surfactant. The resulting swelling ratio for the hexadecane was corresponding to those found in the literature for other hydrocarbon oils ($S \sim 1.2-1.44$).³² This property will be highly problematic in our experiments, since we will use an oil as the continuous phase.

Furthermore, PDMS might not be the best choice for single molecular studies since it expresses autofluorescence.³³ Even though this autofluorescence is less than that of other polymers, it is still worse than that of glass substrate.

Another significant disadvantage of PDMS-based device is their low bonding strength. As shown before, PDMS can be bonded to PDMS or glass slides by first using oxygen plasma, however, the bonding strength reported in the literature is quite low, compared to whole-glass devices. For our design, the fluidic chip contains a long nanofluidic network creating a high fluidic resistance and consequently high pressure is required to introduce solution into the chip (approximately at least a few bar). This high pressure can create leakage in the PDMS-based device either at the interface PDMS and the substrate or at the fluidic connection. The bonding method for a whole-glass device e.g. borosilicate is thermal bonding whereby siloxane bonds (Si-O-Si) are formed at the glass transition temperature of borofloat (650°C)¹¹ and the thermally bonded device can withstand the high applied pressure which is up to 20 bar.³⁴

In addition, PDMS-based fluidic devices were tested by generating aqueous droplets containing fluorescein solution in the oil phase by a nanofluidic network. During transportation of tiny aqueous droplets ($\phi \sim 2\text{-}5\ \mu\text{m}$) to the 500-nm-deep nanochannel, the fluorescence intensity inside the droplets decreased rapidly and they eventually became dark. We ascribe this phenomenon to mass transport of water from the droplet to the continuous phase and the PDMS, driven by an energy gradient. The movement of water molecules changes the aqueous droplet pH and dimension causing the observed dramatic change in fluorescent intensity. Also fluorescein and oil can be absorbed into the PDMS. This changing intensity will be highly complicating in case of time-resolved measurements of the fluorescence intensity to investigate enzymatic reactions. Eventually, we therefore decided to use an alternative material (glass) for fabrication of our device.

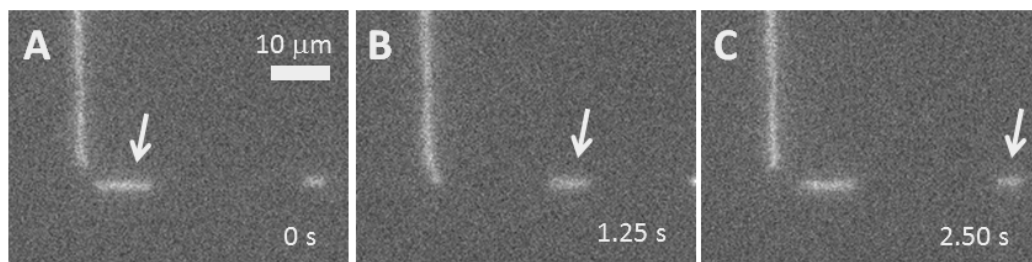


Figure 3-7: An illustration showing the changing size of generated water droplets in the oil phase when droplets are transported through a nanofluidic channel in the PDMS-based fluidic device; water phase: 0.01 mM fluorescein solution, oil phase: 1% Span 80 in hexadecane; the width and depth of the nanochannel are 2 and 0.5 μm , respectively. The arrow indicates one generated droplet, which changes its dimension when travelling through the nanochannel.

IV. Glass-based Microfluidic Device

Due primarily to the intrinsic properties of PDMS (permeability to small molecules, low Young's Modulus) and the quality of bonding, PDMS would not be the best material to create the tiny aqueous droplets in oil for our experiments. Glass-based devices represent the second most promising approach for us due to the rigidity of glass and the bonding strength resulting from the thermal bonding process. The fabrication process is shown in Fig. 3-8.

- 1) Borofloat wafer (Schott Technical Glasses, Germany) was photolithographed and wet-etched by BHF mixture solution to create nanochannels.

Chapter: 3

- 2) A thin layer gold/chromium (Cr/Au) was sputtered onto the nano-patterned substrate with a thickness of 15/150 nm (Cr is used as an adhesive layer for Au onto the glass substrate).
- 3) The Au/Cr layer was patterned by photolithography and wet-etched in Au and Cr etchants (Merck), consecutively.
- 4) The patterned glass substrate was wet-etched in 25% HF solution to create microchannels prior to Cr/Au removal.
- 5) Access holes were made by powderblasting and subsequently the patterned wafer was pre-bonded to the glass plate.
- 6) Pre-bonded glass wafers were thermally bonded in the oven at 650°C for 1 hour with heating and cooling ramping steps.
- 7) Thermally bonded glass wafers were diced to obtain individual glass chips which were then connected to the in-house manufactured chip holder for fluidic connection.

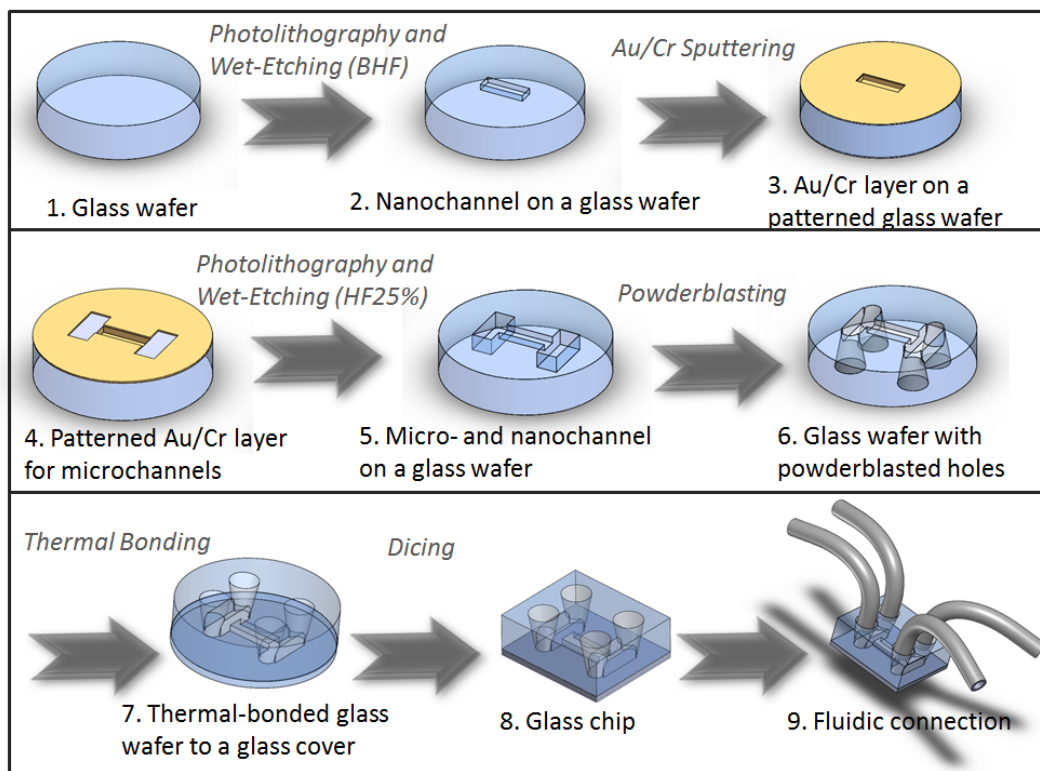


Figure 3-8: Schematic diagram of the fabrication of the glass-based fluidic device.

In general, patterning micro- and nanochannels on glass wafers can be accomplished either by wet etching (shown here) or dry etching. By dry etching, a sharp profile of the channel wall can be obtained but the surface roughness also becomes larger. Rough surfaces can create some problems, for example, debris can become stuck to the surface especially inside the nanochannels. Therefore wet etching was used for our fabrication approach.

For the wet etching, we used a HF mixture solution containing HF and hydrochloric acid (HCl) in a ratio of 9 to 1 to obtain a smoother etched surface as will now be explained.³⁵ The borofloat glass substrate consists of SiO₂ and metal oxide molecules i.e. CaO, MgO, Al₂O₃. HF molecules can react with these metal oxides forming insoluble products onto the surface of substrate which prevent HF molecules etching the underneath substrate causing a nonuniform etched surface. Added HCl can transform these insoluble products to soluble molecules improving the uniformity of the etched surface.

After the fabrication procedures detailed here, the glass chip presents a hydrophilic surface (C.A.~25°) which is not appropriate to facilitate the generation of W/O emulsions which requires a hydrophobic surface. Our subsequent hydrophobization approach as well as conventional hydrophobization methods will be discussed in chapter 5 of this thesis.

V. Fluidic and optical setups

Fluidic Connection

After hydrophobization (detailed in chapter 5), the glass-based chip was mounted into an in-house manufactured chip holder and connected to a neMESYS syringe pump (Cetoni, Korbussen, Germany) with fused silica tubing ($\phi=360\mu\text{m}$), and fluidic connectors bought from Upchurch Scientific (WA, USA). The neMESYS syringe pump is a flow rate-driven pump with three modules enabling to individually manipulate three different solutions into the fluidic chip.

Optical Setup

The chip holder incorporating a fluidic chip was placed on top of an epifluorescence microscope (DMI 5000M, Leica) equipped with a specific filter cube (L5) for the excitation

Chapter: 3

and emission wavelengths of 480 and 520 nm, respectively. A mercury lamp was used to direct a UV-containing light beam to the filter which allowed light with only specific wavelength (480 nm) pass through. Then, this light reaches the fluidic channel and excites the fluorescein molecules. Subsequently fluorescent molecules emit photons at 520-nm wavelength which can pass through the filter and are collected by a photodetector. To enable detecting very tiny amounts of fluorescent molecules, a highly sensitive camera is required. In our experiment, an electron multiplying CCD camera (EMCCD, Andor Ixon, UK) was therefore attached to the microscope. The EMCCD camera uses photodetectors that multiply collected photons up to a few hundred folds, and thereby it is very sensitive to any weak signal sources including thermal noise.³⁶ Hence, it is required to cool the camera down to low temperature (-65°C) by an interior cooling system. The fluid flow and emulsion were visualized and recorded by the Andor Solis program.

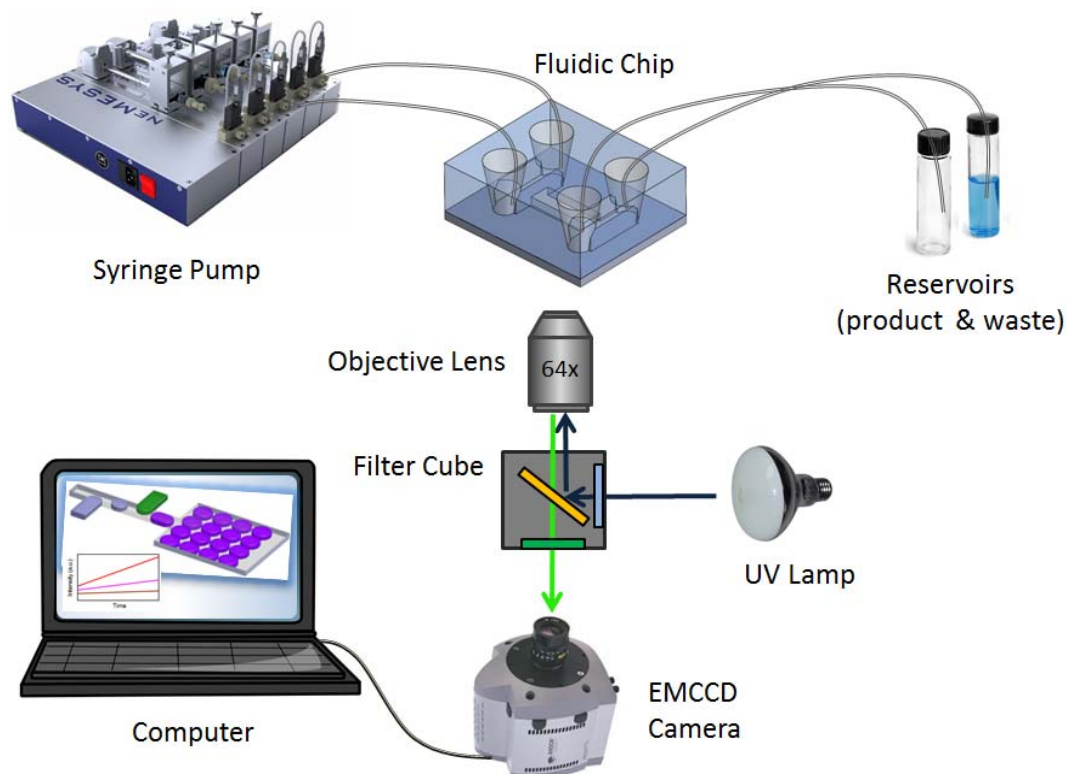


Figure 3-9: Illustration of the microfluidic chip mounted on the epifluorescence microscope and connected to the fluidic setup.

VI. PSPICE simulations

In order to determine the direction and the quantity of fluid flow in the complex fluidic system, the fluidic network was simulated in a program designed to model electronic networks, namely PSpice. To simplify this determination, only three electrical parameters, electrical potential (V), current (I) and resistance (R), were considered in this simulation. In case of a device fabricated from polymers whose surfaces are flexible, the electrical capacity representing the flexibility should be included into a simulation which would make it more complicated than the case of rigid material such as glass. In our case, the device was fabricated from glass and capacity was discarded. The representation of each electrical parameter of the fluidic system is shown in the table below:

Table03-3: Fluidic parameters and equivalent electrical parameters

Fluidic Parameter (Unit)	Electrical Parameter (Unit)
Pressure (Pa)	Potential (V)
Flow rate ($\mu\text{m}^3/\text{s}$)	Current (A)
Fluidic Resistance ($\text{Pa}\cdot\text{s}/\mu\text{m}^3$)	Electrical Resistance ($\text{V}/\text{A}=\Omega$)

- Basis data:
1. Glass-based device
 2. Flow-rate driven pump (fixed flow rate)
 3. Contact angle of hydrophobized surface inside a chip $\approx 105^\circ$
 4. DI water as aqueous phase; Silicone oil 1 cSt as continuous phase
 5. No surfactant added in oil phase
 6. Interfacial tension between water and silicone oil $\approx 30 \text{ mPa}\cdot\text{s}$ at 25°C
 7. Viscosity of W/O emulsion \approx viscosity of oil
 8. Fluidic resistance from the tubing and the access holes are negligible

The conversion of fluidic parameters to electrical parameters was performed by comparing two equations that relate effort variables (V , ΔP) to flow variables in the two domains, namely Ohm's Law (Eqn.3-2) and the Hagen-Poiseuille equation (Eqn.3-3), shown below

$$V = IR \quad \text{Eqn.(3-2)}$$

where

V = Electrical potential (V)

I = Electrical current (A)

R = Electrical resistance (Ω)

Chapter: 3

$$\Delta P = \frac{12\eta LQ}{wh^3} \quad \text{Eqn.(3-3)}$$

where ΔP = Pressure Drop (Pa) η = Fluidic viscosity (Pa.s)
 L = Length of fluidic channel (μm) Q = Volumetric Flow rate ($\mu\text{m}^3/\text{s}$)
 w = Width of fluidic channel (μm) h = Height of fluidic channel (μm)

Since V is equated to ΔP and I to Q , therefore,

$$R = \frac{12\eta L}{wh^3} \quad \text{Eqn.(3-4)}$$

Our microfluidic device consisted of four fluidic networks for three fluidic streams, oil phase, 1st water stream and 2nd water stream and the outlet network for emulsion whereas each fluidic network comprised the microfluidic and nanofluidic channels (Fig. 3-10A).

The conversion of a fluidic resistance into an electrical resistance is exemplified here. The dimensions of the inlet microchannel of the 1st water stream were 100 μm width, 3900 μm length and 5 μm height and the viscosity of water ≈ 1 mPa.s. Hence, the fluidic resistance along this channel was equal to $12 \times (1 \times 10^{-3}) \times 3900 / [100 \times (5)^3] \approx 0.00374$ Pa.s/ μm^3 . In the equivalent circuit the relation between ΔP and Q can now be modeled as the relation between V and I using the R given in Eqn.(3-4).

In addition, since streams of fluids were applied into the network by three constant flow-rate pumps, current sources were used to represent these pumps. Furthermore, to generate the aqueous droplets in oil, the water stream needed extra pressure to overcome the Laplace pressure present at the interface between water and oil. The Laplace pressure is related to the interfacial tension between two immiscible fluids, and the radius of curvature of the meniscus (half the height of the nanochannel in this case) as shown in Eqn.3-5.

$$\Delta P = \frac{2\gamma \cos \theta}{h} \quad \text{Eqn.(3-5)}$$

The contact angle of water on the hydrophobic surface of our device was approximately 105° and the interfacial tension between water and silicone oil (1cSt) ≈ 30 mPa.s (in case of the absence of surfactant) while the height of the junction (nanochannel) was 0.5 μm . Therefore, the Laplace pressure was equal to $(2 \times (30 \times 10^{-3}) \times (\cos 105^\circ)) / (0.5 \times 10^{-6}) = -31,058$ Pa. This extra constant pressure can be represented by a voltage source providing a potential in the opposite direction of the current source in the simulation.

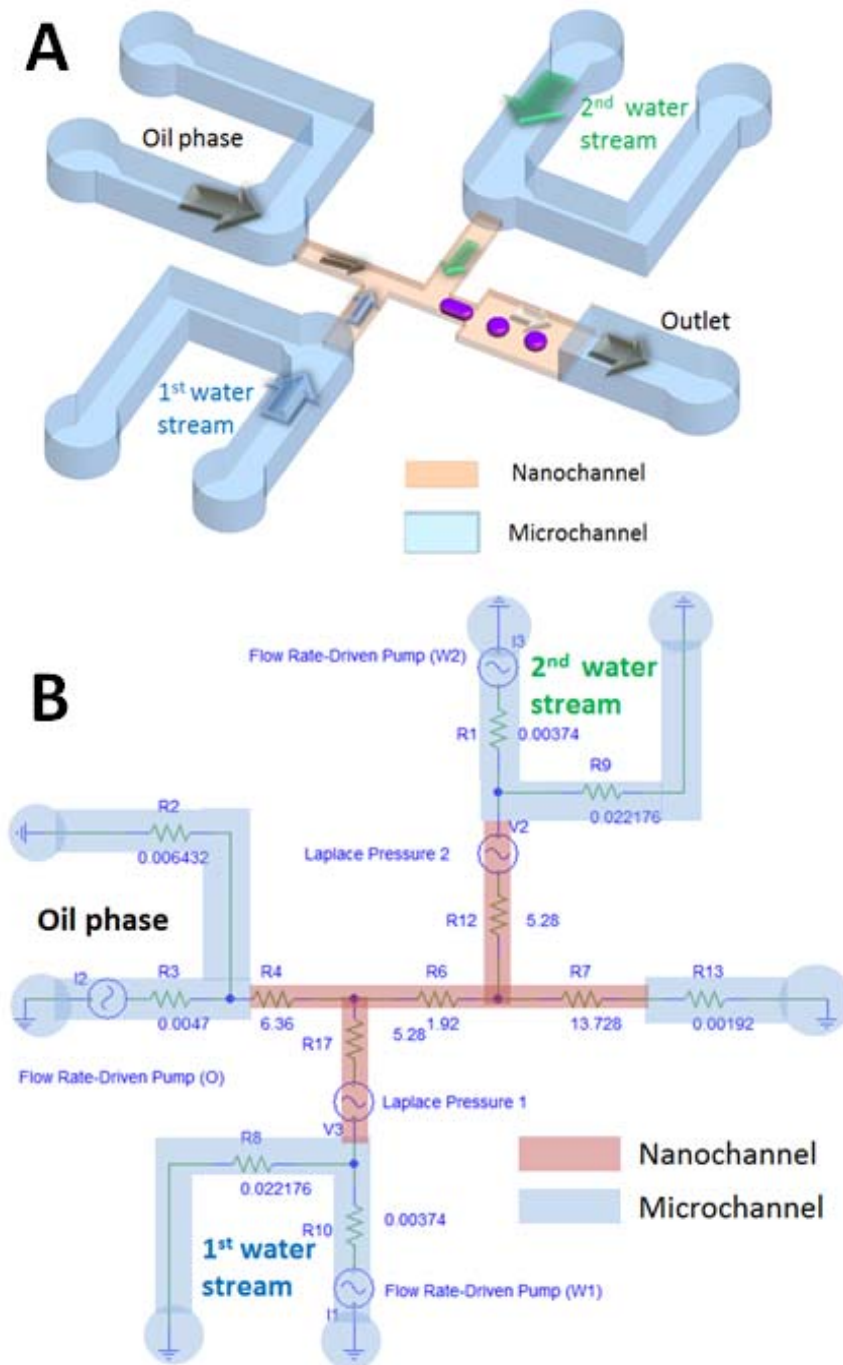


Figure 3-10: (A) An illustration of the fluidic system containing microchannels (blue) and nanochannels (pink) superimposed onto the equivalent electrical network modeled in the PSpice program (B). The arrows indicate the direction of fluidic flows in each channel.

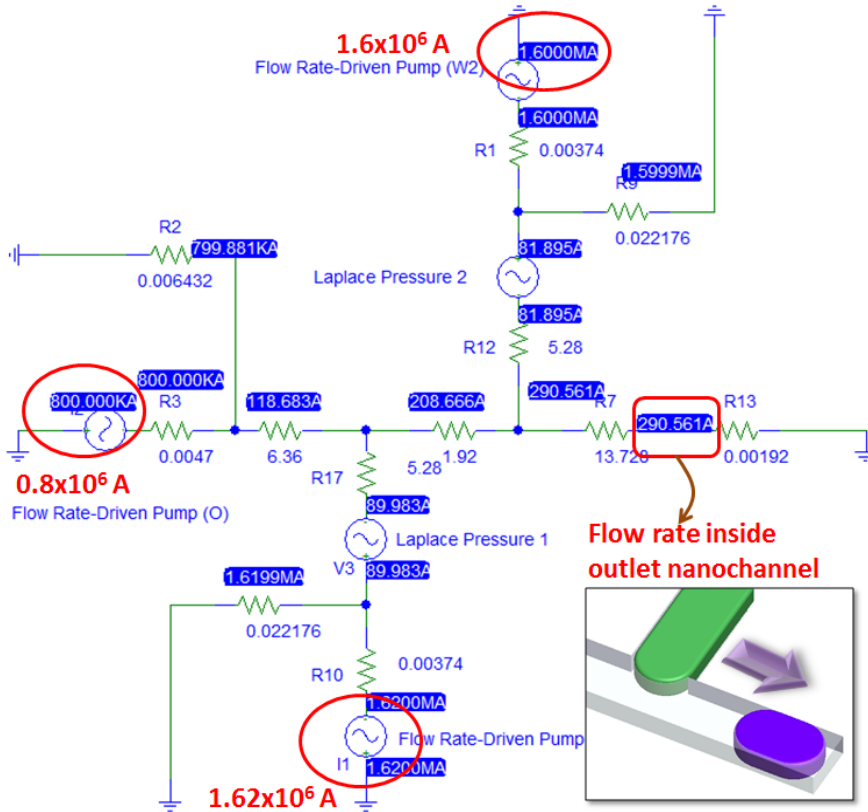


Figure 3-11: Simulated fluidic circuit when the flow rates in the inlet of 1st water stream, 2nd water stream and oil are 1.6×10^6 , 1.6×10^6 , and 0.8×10^6 A, respectively. Potential (in Volt) represents pressure (in Pa) and current (in A) represents flow rate (in $\mu\text{m}^3/\text{s}$).

From this simulation we calculated that when the applied fluidic flow rates for 1st and 2nd water streams and oil stream were 1.6×10^6 , 1.6×10^6 and $0.8 \times 10^6 \mu\text{m}^3/\text{s}$ or 0.0972, 0.09 and 0.045 $\mu\text{L}/\text{min}$, respectively, the resulting flow rate in the detection channel was around $300 \mu\text{m}^3/\text{s}$. Using this resulting flow rate, and assuming the detection time needed for the enzyme reaction was around 600 s, the total volume of fluid in the detection line must be $(300 \mu\text{m}^3/\text{s}) \times (600 \text{ s}) = 180,000 \mu\text{m}^3$. Since the height and the width of the detection line were 0.5 and 100 μm , respectively, the total length of the detection line must be at least $180,000 / (0.5 \times 100) = 3600 \mu\text{m}$. Considering the ratio of oil and water phases at the T-junction which facilitated the droplet formation, the $Q_{\text{water}1}$, Q_{oil} $Q_{\text{water}2}$ were 90, 120 and 80 $\mu\text{m}^3/\text{s}$, respectively. The flow rate for each stream should be regulated in such a way as to create droplets.

The conceptual design of our micro- and nano-fluidic platform to generate water-in-oil emulsions was discussed in detail in this chapter. To achieve the single-molecule encapsulation, the solution is required to be compartmented into femtolitre droplets. These tiny droplets were maneuvered in the nanofluidic networks. The materials used for fabrication of this platform were considered in many aspects and further validated for our applied device.

References

1. P. Garstecki, M. J. Fuerstman, H. A. Stone and G. M. Whitesides, *Lab Chip*, 2006, **6**, 437-446.
2. P. Garstecki, I. Gitlin, W. DiLuzio, G. M. Whitesides, E. Kumacheva and H. A. Stone, *Appl Phys Lett*, 2004, **85**, 2649-2651.
3. T. T. Fu, D. Funfschilling, Y. Ma and H. Z. Li, *Microfluid Nanofluid*, 2010, **8**, 467-475.
4. L. L. Shui, E. S. Kooij, D. Wijnperle, A. van den Berg and J. C. T. Eijkel, *Soft Matter*, 2009, **5**, 2708-2712.
5. A. S. Utada, A. Fernandez-Nieves, H. A. Stone and D. A. Weitz, *Phys Rev Lett*, 2007, **99**.
6. D. Pekin, Y. Skhiri, J. C. Baret, D. Le Corre, L. Mazutis, C. Ben Salem, F. Millot, A. El Harrak, J. B. Hutchison, J. W. Larson, D. R. Link, P. Laurent-Puig, A. D. Griffiths and V. Taly, *Lab Chip*, 2011, **11**, 2156-2166.
7. B. Zheng, C. J. Gerdtts and R. F. Ismagilov, *Curr Opin Struc Biol*, 2005, **15**, 548-555.
8. B. Zheng and R. F. Ismagilov, *Angew Chem Int Edit*, 2005, **44**, 2520-2523.
9. J. C. Baret, F. Kleinschmidt, A. El Harrak and A. D. Griffiths, *Langmuir*, 2009, **25**, 6088-6093.
10. A. B. Theberge, F. Courtois, Y. Schaerli, M. Fischlechner, C. Abell, F. Hollfelder and W. T. S. Huck, *Angew Chem Int Edit*, 2010, **49**, 5846-5868.
11. Petersen D., Mogensen K. B. and K. H., *Glass Micromachining*, Wiley-VCH Verlag GmbH & Co., KGaA, Weinheim, 2004.
12. Y. N. Xia and G. M. Whitesides, *Annu Rev Mater Sci*, 1998, **28**, 153-184.
13. K. J. Hsia, Y. Huang, E. Menard, J. U. Park, W. Zhou, J. Rogers and J. M. Fulton, *Appl Phys Lett*, 2005, **86**.
14. Y. G. Y. Huang, W. X. Zhou, K. J. Hsia, E. Menard, J. U. Park, J. A. Rogers and A. G. Alleyne, *Langmuir*, 2005, **21**, 8058-8068.
15. J. Lee, Y. K. Yun, Y. Kim and K. Jo, *B Korean Chem Soc*, 2009, **30**, 1793-1797.
16. S. M. Park, Y. S. Huh, H. G. Craighead and D. Erickson, *P Natl Acad Sci USA*, 2009, **106**, 15549-15554.
17. W. Zhou, Y. Huang, E. Menard, N. R. Aluru, J. A. Rogers and A. G. Alleyne, *Appl Phys Lett*, 2005, **87**.
18. S. Metz, C. Trautmann, A. Bertsch and P. Renaud, *J Micromech Microeng*, 2004, **14**, 324-331.
19. K. P. Nichols, J. C. T. Eijkel and H. J. G. E. Gardeniers, *Lab Chip*, 2008, **8**, 173-175.
20. R. Arayanarakool, S. Le Gac and A. van den Berg, *Lab Chip*, 2010, **10**, 2115-2121.

Chapter: 3

21. H. S. Noh, Y. Huang and P. J. Hesketh, *Sensor Actuat B-Chem*, 2004, **102**, 78-85.
22. A. T. Ciftlik and M. A. M. Gijs, *J Micromech Microeng*, 2011, **21**.
23. R. Marie, S. Schmid, A. Johansson, L. E. Ejsing, M. Nordstrom, D. Hafliger, C. B. V. Christensen, A. Boisen and M. Dufva, *Biosens Bioelectron*, 2006, **21**, 1327-1332.
24. B. Lu, S. Y. Zheng, B. Q. Quach and Y. C. Tai, *Lab Chip*, 2010, **10**, 1826-1834.
25. D. Armani, C. Liu and N. Aluru, *Proc Ieee Micr Elect*, 1999, 222-227.
26. X. Q. Brown, K. Ookawa and J. Y. Wong, *Biomaterials*, 2005, **26**, 3123-3129.
27. D. Fuard, T. Tzvetkova-Chevolleau, S. Decossas, P. Tracqui and P. Schiavone, *Microelectron Eng*, 2008, **85**, 1289-1293.
28. H. C. Hong, C. M. Chen, Y. C. Chou and C. H. Lin, *Microsyst Technol*, 2010, **16**, 423-430.
29. M. Liu, J. R. Sun and Q. F. Chen, *Sensor Actuat a-Phys*, 2009, **151**, 42-45.
30. M. W. Toepke and D. J. Beebe, *Lab Chip*, 2006, **6**, 1484-1486.
31. P. Tremblay, M. M. Savard, J. Vermette and R. Paquin, *J Membrane Sci*, 2006, **282**, 245-256.
32. J. N. Lee, C. Park and G. M. Whitesides, *Anal Chem*, 2003, **75**, 6544-6554.
33. A. Piruska, I. Nikcevic, S. H. Lee, C. Ahn, W. R. Heineman, P. A. Limbach and C. J. Seliskar, *Lab Chip*, 2005, **5**, 1348-1354.
34. Y. Akiyama, K. Morishima, A. Kogi, Y. Kikutani, M. Tokeshi and T. Kitamori, *Electrophoresis*, 2007, **28**, 994-1001.
35. C. Iliescu, J. Jing, F. E. H. Tay, J. M. Miao and T. T. Sun, *Surf Coat Tech*, 2005, **198**, 314-318.
36. O. Castillo-Fernandez, G. B. Salieb-Beugelaar, J. W. van Nieuwkastele, J. G. Bomer, M. Arundell, J. Samitier, A. van den Berg and J. C. T. Eijkel, *Electrophoresis*, 2011, **32**, 2402-2409.

CHAPTER 4:

Low-temperature, Simple and Fast Integration Technique of Microfluidic Chips by using a UV-curable Adhesive

*In the fields of MicroElectroMechanical Systems (MEMS) and Lab On a Chip (LOC), a device is often fabricated using diverse substrates which are processed separately and finally assembled together using a bonding process to yield the final device. Here we describe and demonstrate a novel straightforward, rapid and low-temperature bonding technique for the assembly of complete microfluidic devices, at the chip level, by employing an intermediate layer of gluing material. This technique is applicable to a great variety of materials (e.g., glass, SU-8, parylene, UV-curable adhesive) as demonstrated here when using NOA 81 as gluing material. Bonding is firstly characterized in terms of homogeneity and thickness of the gluing layer. Following this, we verify the resistance of the adhesive layer to various organic solvents, acids, bases and conventional buffers. Finally, the assembled devices are successfully utilized for fluidic experiments.**

* This chapter had been published as “*Low-temperature, simple and fast integration technique of microfluidic chips by using a UV-curable adhesive, **Lab on a chip***”, R. Arayanarakool, S. Le Gac, and A. van den Berg, **2010**,10 (16). pp. 2115-2121.

Introduction

In MEMS or microfluidic technologies, the structured components of devices are often separately fabricated from different substrates and subsequently assembled to obtain a final device. This assembly step can be done either at the wafer-scale or at the chip level. In general, the assembly is broadly categorized into two major groups, direct bonding and bonding with an intermediate layer.

The direct bonding generally utilizes harsh conditions such as a high temperature, a high electric field or plasma to promote bonding between two substrates i.e. fusion bonding, anodic bonding, and plasma-based bonding. For fusion bonding a temperature higher than 800°C is employed e.g. for bonding of silicon wafers.¹ With anodic bonding, a high voltage (few hundred volt DC) is applied between the two substrates to assist the bonding and to enable to decrease the bonding temperature to 300-450°C.^{2, 3} Plasma activation⁴ is widely used for bonding a polydimethylsiloxane (PDMS) to a great variety of materials (PDMS, glass, silicon). Milder conditions have been reported for direct bonding with a pre-treatment step prior to bonding, for instance, using plasma⁵ or UV exposure⁶ before direct bonding. Direct bonding techniques present several main drawbacks. Firstly, they require harsh conditions (high temperature, oxidative plasma, high voltage) or a pre-treatment step which may damage delicate structures in the devices or surface-immobilized molecules. Secondly, the surfaces must be extremely clean, flat and smooth to form a strong bond. Thirdly, this bonding process is time-consuming and labor-intensive and requires the access to dedicate equipment such as clean-room facilities.⁸⁻¹⁰

On the contrary, bonding with an intermediate layer can be done at a low temperature or even in the case of substrates with high surface roughness or the presence of micron-sized contamination.¹¹ Moreover, polymers which provide a great variety of properties to individual application can be used as intermediate layers, for instance, epoxy-glue,²¹ Hysol,²² parylene,^{23, 24} or PDMS.²⁵ These materials are cured with a thermal process which usually requires long curing times especially when a high bonding strength is needed. In addition, some of the thermo-curable materials have shown some practical difficulties for bonding. PDMS, for example, expresses a high thermal expansion and therefore shrinks at

low temperature after thermal curing, notably leading to misalignment²⁶ or detachment of the bonded substrates. In addition, several thermo-curable materials need to be mixed with a solvent to obtain the thin layer needed for bonding, solvent then evaporates from the gluing layer after bonding.^{13, 27, 28} In some cases, the polymerization of the gluing materials can create gaseous by-products. The gaseous by-products or evaporating solvent can form gas bubbles between two substrates after the curing step. These gas bubbles can remain in the glue and subsequently decrease the bonding strength of the integrated substrates.

Alternatively, UV-curable adhesives can be used as an intermediate layer and cured by UV irradiation for a short time (a few minutes or even seconds) at ambient conditions. This approach using UV-curable materials has recently gained in popularity and has been adapted for the assembly of capillary electrophoresis (CE) chips,^{27, 28} Surface Plasmon Resonance (SPR) sensor chips,²⁹ immunoassay platforms,³⁰ and integrated microfluidic devices for genetic analysis.³¹ Also, the applicable choices of the adhesive material can be selected for bonding a great variety of substrates such as glass, silicon or polymers.

In this work, we propose a bonding technique to enable the assembly of two patterned substrates by applying a thin layer of gluing material to the first structured substrate. Then it is aligned and bonded to another substrate prior to the final curing step. Our technique is derived from the Stamp and Stick technique³² with enhanced control on the application of the gluing layer. In our methodology, the UV-curable adhesive is first prepared as a thin layer on a transfer wafer using spin-coating technique and subsequently pre-cured by UV light, while being covered by a PDMS slab (See Fig.4-1). During this pre-curing step, as the polymerization is inhibited in presence of oxygen,³³ the thin layer of glue in contact with oxygen in the PDMS slab still remains uncured, and is subsequently transferred to the structured substrates before assembly to the cover substrates. Finally, the glue is fully cured by UV irradiation. Microfluidic structures were made from glass, SU-8, and assembled with glass cover slips or parylene-coated silicon substrates. Glass substrates are standard in the field of LOC, while parylene is widely used as an insulating layer for electrical measurements.³⁴ Bonding was demonstrated here at the chip level. We characterized the quality of the bonding in terms of uniformity and thickness of the gluing layer and the leakage test of the integrated chip.

Chapter: 4

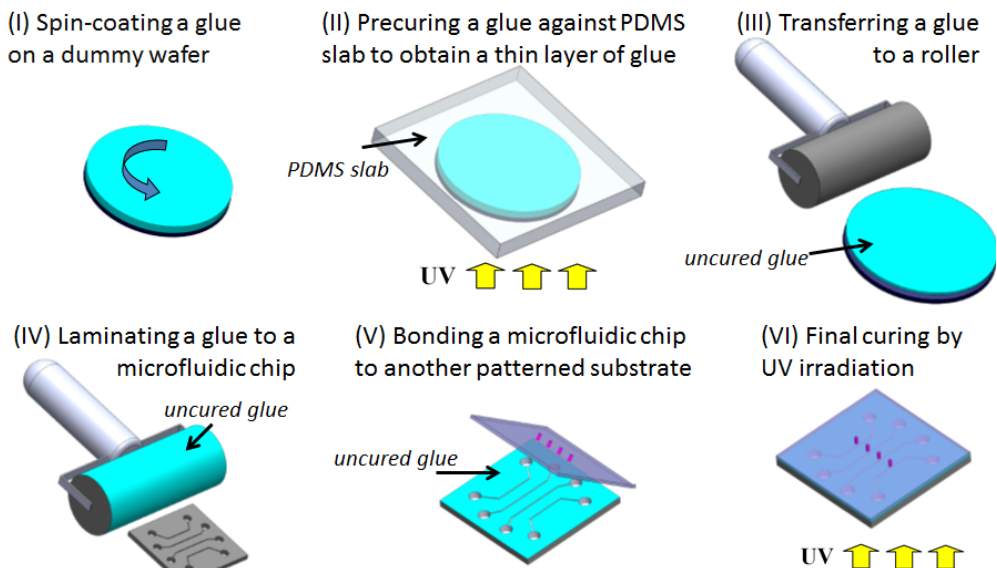


Figure 4-1: Illustration of the bonding procedure with the aid of a roller. The process starts with the formation of a thin layer of glue on a transfer wafer by spin-coating (I), and subsequent UV pre-curing of the glue (II). Following this, the glue is partly cured (shown in purple) and the top of the gluing layer remains uncured (light blue). Uncured glue is transferred to a roller (III) before being laminated onto the microfluidic chip (IV). Finally, the chip with a thin layer of glue is assembled to a cover substrate (V) and finally cured by UV irradiation (VI).

Experimental Details

Chip Bonding

Bonding of the chips was demonstrated at the chip level (8 mm x 8 mm). UV-curable adhesive (NOA 81, Norland Product), used as gluing material, was firstly spin-coated (500 rpm for 5 s followed by 4000 rpm for 20 s) on a transfer wafer, then pressed by a flat PDMS slab and pre-cured by UV irradiation (365 nm) for a few seconds. After peeling off the PDMS slab, a thin layer of gluing material was transferred to the microfluidic chips either using the stamp and stick technique³² or with the help of a roller (See Fig. 4-1). Subsequently, the microfluidic chip with a thin layer of glue was aligned and pre-assembled with the cover substrate. To promote homogeneous spreading of the glue between the two substrates; the pre-assembled chips were placed in an oven (60°C) for a few hours. Finally, integrated chips were exposed to UV irradiation (365 nm, 5 min) for curing the gluing material, and ultrasonically cleaned in ethanol for 15 min and dried before use.

Characterization

Homogeneity of the gluing layer

To examine the homogeneity of the gluing layer between two substrates, a 0.04 wt% fluorescent dye (Rhodamine B, Sigma, Zwijndrecht, The Netherlands) was first added to the glue. After bonding, chips were imaged using a microscope (Olympus IX71 Inverted Microscope, Germany) equipped with a mercury lamp together with appropriate filters, and a camera connected to a computer. The intensity patterns of the dye-supplemented glue were measured using Analysis Docu Software (Olympus Soft Imaging Solutions).

Thickness of the gluing layer

The thickness of the gluing material after bonding was characterized by SEM techniques and fluorescence microscopy. After bonding, the integrated sample was first diced using a dicing machine (Disco DAD-321), coated with a thin layer of gold and then imaged by Scanning Electron Microscope (SEM, JEOL 5610, Tokyo, Japan). Alternatively, a fluorescent dye was mixed with a glue prior to the bonding of two chips. After bonding, the integrated chip was diced and imaged by using an inverted fluorescence microscope. Furthermore, to assess the reproducibility of this bonding technique, the thickness of the gluing layer was measured (Veeco Dektak 8, USA) after each step of the procedure.

Chemical Test

Chemical tests were performed to verify the resistance of the UV-curable adhesive used for bonding two substrates to a variety of solvents and solutions, namely, isopropanol, ethanol, acetone, hydrochloric acid (1% vol) solution, sodium hydroxide (1% wt) solution, water and PBS buffer (pH 7.4). The integrated chips were immersed in these solutions for several hours, rinsed using DI water and dried. Afterward, we observed whether integrated chips were still bonded and whether the glue between two substrates disappeared.

Fluidic Test

To check the quality of bonding from integrated chips, an aqueous solution of 0.625 mM fluorescein solution (Sigma, Zwijndrecht, The Netherlands) was introduced by capillary force from the side of the chip. The behavior of the liquid was observed using fluorescence microscopy. Movies and pictures were recorded using Analysis Docu Software.

Results and Discussion

Optimization of the bonding method

In the beginning, we employed SU-8 precursor diluted in its developer (RER600) as a bonding agent, we however encountered a number of problems. Firstly, air gaps were observed between the two substrates due either to poor spreading of the SU-8 glue or resulting from the formation of gaseous by-products of polymerization or evaporation of the solvent during the thermal curing step. At the same time, SU-8 glue appeared in the microfluidic channels resulting in clogging after curing of the glue. With the optimized protocol, most of these problems could be solved but a large number of curing steps had to be implemented to promote evaporation of any solvents present in the resin as well as the application of a high pressure to enhance spreading of the glue.

In a second phase, NOA 81 was used as a gluing material. The thickness of the adhesive layer on the transfer wafer had to be dramatically decreased and optimized to alleviate clogging of the microfluidic channels. Alternatively, the adhesive had to be partially cured by a short UV exposure, so-called pre-curing step, to reduce the thickness of uncured glue. One unsolved problem was the homogeneity of the gluing layer since the glue was prone to aggregate and became inhomogeneous when detaching the chip from transfer wafer.

Therefore, we further modified the method for transferring a thin layer of the glue from a transfer wafer onto the microfluidic structures by using a roller as illustrated in Fig. 4-1. Thereby, the homogeneity of the gluing layer was greatly improved, and a thinner layer of glue could easily be transferred onto the microfluidic chip. Still the process of transfer had to be fast to prevent the glue from aggregating prior to bonding.

This improved procedure was finally successfully applied for bonding various materials, such as glass, SU8 together with glass cover slips or parylene-coated substrates. We subsequently assessed the capability of the technique in terms of dimensions of the microchannels. We successfully bonded channels of 15 μm height and down to 20 μm width without any problems. Only channels narrower than 20 μm still gave problems and would require another level of optimization to be bonded using this technique.

Bonding characterization

Homogeneity of the layer of adhesive

We characterized the homogeneity of the adhesive layer with fluorescence measurements by mixing a fluorescent dye (Rhodamine B) with the glue before bonding. The fluorescence intensity profile of the dye was measured after assembling and final curing. Fig. 4-2 shows channels fabricated from glass and SU-8 after bonding to glass cover slips or parylene-coated silicon substrates using a dye-supplemented adhesive, as well as the intensity profiles measured across the channels along the dashed line added on the pictures (insets in Fig.4-2). The pictures and graphs both show a uniform layer of glue between the two substrates for the different devices, without any adhesive inside the channels. It should be noted that the SU-8 channels (Fig. 4-2 C and D) give an overall higher intensity than glass channels; we believe this is due to the auto-fluorescence of the SU-8 resin. On other aspects, a peak in the fluorescent intensity is detected at the edge of the microchannel. A first reason for this could be the accumulation of adhesive at the edge of the channel. However, this is not likely to happen as we do not detect any glue aggregate on the channel walls when imaging a cross-section of a channel (See next section, Fig 4-3). A second and most plausible explanation is the reflection of light at the channel walls.

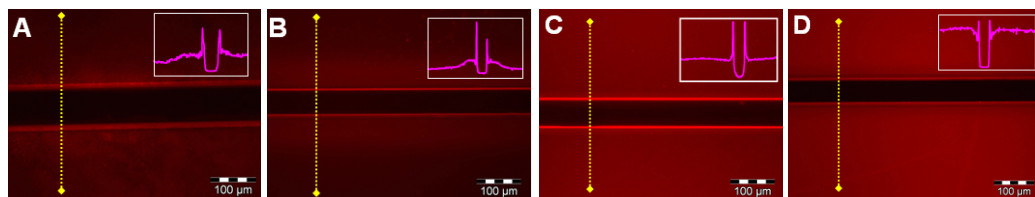


Figure 4-2: Homogeneity of the gluing layer of UV-curable adhesive applied between a microfluidic substrate and a cover lid, for different materials. For visualization purpose, the glue was mixed with Rhodamine B (0.04%wt). Glass-based microchannels (depth: 20 μm) bonded to a parylene-coated silicon substrate (A) or bonded to a glass cover lid (B); SU-8-based microchannels (depth: 15 μm) bonded to a parylene-coated silicon substrate (C) or bonded to a glass cover lid (D). Inset: Fluorescence intensity profiles measured across the microchannel along the dashed lines shown.

Thickness of the adhesive layer

After bonding, the chips were diced perpendicularly to the channel and the resulting cross-section imaged using SEM technique and fluorescent microscopy. Fig. 4-3 represents the results for both visualization techniques for a glass channel bonded to a glass cover lid. From this, the thickness of the adhesive layer is determined to be $1.15 \pm 0.44 \mu\text{m}$ –using

Chapter: 4

thirty chips- for a channel height of 14-18 μm . The obtained fluorescence image in Fig4-3B shows that no glue appears inside the channel, confirming that the higher fluorescence intensity observed previously at the channel edge must be due to the reflection of light.

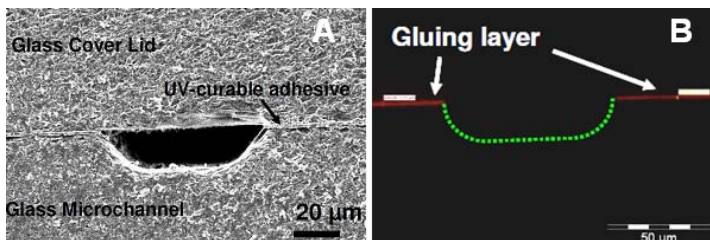


Figure 4-3: Thickness of gluing layer in a cross section view of a glass-based microfluidic chip bonded to a glass cover lid using UV-curable adhesive and our bonding technique are visualized by (A) SEM and (B) Fluorescent Microscopy. (B) Fluorescent image shows the gluing layer (in red) between two bonded substrates after supplementation of the glue with a fluorescent dye (Rhodamine B). The dashed line in Fig. 4 B is the profile of the microchannel. The thickness of gluing material was measured to be $1.15 \pm 0.44 \mu\text{m}$.

Moreover, after dicing the integrated chips, the cover lid was not detached from the substrate with the microchannels, showing the good bonding strength obtained with our technique.

The thickness of the gluing layer was measured after each step of the bonding process to assess the reproducibility of the bonding method. Table 1 summarizes the results for the spin-coating, pre-curing, laminating, and transfer steps. After spin-coating, the thickness of the gluing layer was found to be 7.4 μm , which was relatively thick for bonding shallow or narrow microchannels. After the UV pre-curing step, the thickness of uncured glue was reduced to 2.9 μm due to the polymerization of the glue. Afterward, a 1.3 μm -thick layer of glue was attached to the roller during the transfer step. Finally, only a 1.2 μm -thick layer of gluing material was laminated onto a microfluidic chip.

Table 4-1: Thickness of the gluing layer at each step of the bonding procedure when using a roller to transfer the glue (Bonding procedure scheme shown in Fig.4-1) from seven samples.

Step	Thickness of the gluing layer (μm)
Spin-coated glue (4000 rpm, 30 sec)	7.4 ± 0.68
UV pre-curing (Uncured glue)	2.9 ± 0.22
Rolling (Transferred glue on a roller)	1.3 ± 0.34
Glue actually transferred on the microfluidic chip (without cover lid)	1.2 ± 0.31

Chemical Tests

Chemical tests were performed to examine the resistance of the gluing layer to a number of chemicals and solutions, namely, ethanol, isopropanol, acetone, and water, hydrochloric acid (1% vol), sodium hydroxide (1% wt) and PBS buffer. After immersing integrated chips into these solutions for several hours, no detachment of the substrate was observed. These tests confirmed the good chemical resistance of NOA 81 to these solvents and solutions, as expected from the information given by the supplier (Norland Product).

Fluidic tests

An aqueous solution of fluorescein was introduced in the channels by capillary action, and the behavior of the liquid was followed with a fluorescence microscopy. We did not detect any leakage of the dye solution outside the channels and between the two bonded substrates, illustrating the good quality of the bonding and correct curing of the glue.

Conclusion

We report here a novel technique to assemble microsystems using an intermediate layer of UV-curable material. The layer of glue was uniform and was shown to be reproducibly prepared with a thickness of 1.15 μm . Assembled devices were successfully diced without detachment of each substrate and were leakage-free when liquid was introduced into the channels by capillary force. Though this work focuses on one particular adhesive material, NOA 81, the bonding methodology described here is more universal and can be employed for other gluing materials as well. Our bonding technique is also suitable for assembling two structured substrates, which is not the case for most of the bonding techniques using an intermediate gluing layer which are limited to one structured wafer.

References

1. M. A. Schmidt, *Proc. IEEE*, 1998, **86**, 1575-1585.
2. G. Wallis and Pomerant.Di, *Journal of Applied Physics*, 1969, **40**, 3946-&.
3. J. Wei, H. Xie, M. L. Nai, C. K. Wong and L. C. Lee, *Journal of Micromechanics and Microengineering*, 2003, **13**, 217-222.
4. D. C. Duffy, J. C. McDonald, O. J. A. Schueller and G. M. Whitesides, *Analytical Chemistry*, 1998, **70**, 4974-4984.

Chapter: 4

5. M. Eichler, B. Michel, M. Thomas, M. Gabriel and C. P. Klages, *Surface & Coatings Technology*, 2008, **203**, 826-829.
6. X. H. Lin, G. L. Liao, Z. R. Tang and T. L. Shi, *Microsystem Technologies-Micro-and Nanosystems-Information Storage and Processing Systems*, 2009, **15**, 317-321.
7. P. B. Allen and D. T. Chiu, *Analytical Chemistry*, 2008, **80**, 7153-7157.
8. B. Ilic, P. Neuzil, T. Stanczyk, D. Czaplowski and G. J. Maclay, *Electrochem. Solid State Lett.*, 1999, **2**, 86-87.
9. K. W. Oh, A. Han, S. Bhansali and C. H. Ahn, *Journal of Micromechanics and Microengineering*, 2002, **12**, 187-191.
10. J. Bart, R. Tiggelaar, M. L. Yang, S. Schlautmann, H. Zuilhof and H. Gardeniers, *Lab on a Chip*, 2009, **9**, 3481-3488.
11. F. Niklaus, G. Stemme, J. Q. Lu and R. J. Gutmann, *Journal of Applied Physics*, 2006, **99**.
12. F. Niklaus, H. Andersson, P. Enoksson and G. Stemme, *Sens. Actuator A-Phys.*, 2001, **92**, 235-241.
13. F. Niklaus, P. Enoksson, E. Kalvesten and G. Stemme, *Journal of Micromechanics and Microengineering*, 2001, **11**, 100-107.
14. Y. S. Choi, J. S. Park, H. D. Park, Y. H. Song, J. S. Jung and S. G. Kang, *Sens. Actuator A-Phys.*, 2003, **108**, 201-205.
15. X. D. Zhou, S. Virasawmy and C. G. Quan, *Microsystem Technologies-Micro-and Nanosystems-Information Storage and Processing Systems*, 2009, **15**, 573-580.
16. B. Ilic, D. Czaplowski, M. Zalalutdinov, B. Schmidt and H. G. Craighead, *Journal of Vacuum Science & Technology B*, 2002, **20**, 2459-2465.
17. J. Xie, J. Shih, Q. A. Lin, B. Z. Yang and Y. C. Tai, *Lab on a Chip*, 2004, **4**, 495-501.
18. S. Takeuchi, D. Ziegler, Y. Yoshida, K. Mabuchi and T. Suzuki, *Lab on a Chip*, 2005, **5**, 519-523.
19. E. Meng, P. Y. Li and Y. C. Tai, *Sens. Actuator A-Phys.*, 2008, **144**, 18-28.
20. S. W. Youn, H. Goto, M. Takahashi, S. Oyama, Y. Oshinomi, K. Matsutani and R. Maeda, *Microelectronic Engineering*, 2008, **85**, 161-167.
21. J. W. Kwon, H. Y. Yu and E. S. Kim, *Journal of Microelectromechanical Systems*, 2005, **14**, 1399-1408.
22. C. Lee, E. H. Yang, S. M. Saeidi and J. M. Khodadadi, *Journal of Microelectromechanical systems*, 2006, **15**, 686-696.
23. K. N. H.S. Kim, Wafer bonding using parylene and wafer-level transfer of free-standing parylene membranes, Boston, 2003.
24. H. S. Noh, K. S. Moon, A. Cannon, P. J. Hesketh and C. P. Wong, *Journal of Micromechanics and Microengineering*, 2004, **14**, 625-631.
25. H. K. Wu, B. Huang and R. N. Zare, *Lab on a Chip*, 2005, **5**, 1393-1398.
26. S. W. Lee and S. S. Lee, *Microsystem Technologies-Micro-and Nanosystems-Information Storage and Processing Systems*, 2008, **14**, 205-208.
27. Z. L. Huang, J. C. Sanders, C. Dunsamor, H. Ahmadzadeh and J. P. Landers, *Electrophoresis*, 2001, **22**, 3924-3929.
28. S. Carroll, M. M. Crain, J. F. Naber, R. S. Keynton, K. M. Walsh and R. P. Baldwin, *Lab on a Chip*, 2008, **8**, 1564-1569.
29. S. Schlautmann, G. A. J. Besselink, R. Prabhu and R. B. M. Schasfoort, *Journal of Micromechanics and Microengineering*, 2003, **13**, S81-S84.
30. S. H. Kim, Y. Yang, M. Kim, S. W. Nam, K. M. Lee, N. Y. Lee, Y. S. Kim and S. Park, *Advanced Functional Materials*, 2007, **17**, 3493-3498.

31. R. Pal, M. Yang, R. Lin, B. N. Johnson, N. Srivastava, S. Z. Razzacki, K. J. Chomistek, D. C. Heldsinger, R. M. Haque, V. M. Ugaz, P. K. Thwar, Z. Chen, K. Alfano, M. B. Yim, M. Krishnan, A. O. Fuller, R. G. Larson, D. T. Burke and M. A. Burns, *Lab on a Chip*, 2005, **5**, 1024-1032.
32. S. Satyanarayana, R. N. Karnik and A. Majumdar, *Journal of Microelectromechanical Systems*, 2005, **14**, 392-399.
33. H. E. Jeong and K. Y. Suh, *Lab on a Chip*, 2008, **8**, 1787-1792.
34. J. I. Kroschwitz, *Kirk-Othmer Encyclopedia of Chemical technology*, Wiley, New York, 1998.
35. K. G. H. Janssen, H. T. Hoang, J. Floris, J. de Vries, N. R. Tas, J. C. T. Eijkel and T. Hankemeier, *Analytical Chemistry*, 2008, **80**, 8095-8101.

CHAPTER 5:

In-channel UV-patternable Hydrophobization of Micro- and Nanofluidic Networks

*In this chapter, a new method to hydrophobize glass-based micro- and nanofluidic networks is proposed. Conventional methods of hydrophobizing glass surfaces often create particulate debris causing clogging especially in shallow nanochannels or require skilful handling. Our novel method employs oxygen plasma, silicone oil and ultraviolet (UV) light. The contact angle of the modified bare glass surface can reach 100° whilst the inner channels after treatment facilitate stable and durable water-in-oil droplet generation. This modified surface was found to be stable for more than three weeks. The use of UV in principle enables in-channel hydrophobic patterning.**

* This chapter had been published as “A new method of UV-patternable hydrophobization of micro- and nanofluidic networks, R. Arayanarakool, L. Shui, A. van den Berg, and J.C.T. Eijkel, *Lab on a chip*, 2011, 11 (24). pp. 4260-4266”

Introduction

In a droplet-based microfluidic system, the emulsion can be formed either as water-in-oil (W/O) or oil-in-water (O/W) depending on the surface properties of the material of a chip, facilitating different usages¹ such as, the encapsulation of cells in water droplets in the oil phase²⁻⁶ or the polymerization of microparticles from the emulsion of non-polar droplets with dissolved monomers in the water phase.⁷⁻¹² In general, polydimethylsiloxane (PDMS)-based microfluidic devices are used to generate W/O emulsions.¹³⁻²² However, its intrinsic properties i.e. oil adsorption,²³⁻²⁵ gas and small-molecule permeability,^{26, 27} roof collapse,²⁸⁻³¹ and low bonding strength inhibit its usages especially in nanofluidic devices, as shown in chapter 3 of this thesis. Alternatively, glass-based microfluidic devices can be used after chemical hydrophobization by silanization using e.g. perfluorodecyltrichlorosilane (FDTS),³²⁻³⁵ or octadecyltrichlorosilane (ODS).³⁶⁻³⁹ However, these chemicals are quite reactive to oxygen or water in air causing the formation of particulate debris in the shallow channels. The modification operation must therefore be skillfully handled under nitrogen atmosphere or water-free conditions and even then particle formation often occurs. Especially the intersections of micro- and nanochannels are critical areas for particulate clogging.

Apart from its use in chips to create w/o emulsions, hydrophobic patterning is a promising technique applicable to various lab-on-a-chip devices for example to create hydrophobic valves,⁴⁰⁻⁴² cellular or biomolecular attachment^{43, 44} and so on. However, almost all the modification approaches are successfully performed on a plane wafer before bonding but not in the enclosed system, and rarely approaches enabling in-channel hydrophobic patterning have been reported. Zhao *et al*⁴⁰ proposed two approaches to pattern hydrophobic surfaces in the enclosed microfluidic system. In the first approach, they utilized multistream laminar flows of silane solution and solvent to pattern a hydrophobic area in a glass-based microchannel network. However, this method was limited by the preformed channel networks. Alternatively, in the second approach, the hydrophobic surface was initially formed by photocleavable self-assembly monolayers with a 2-nitrobenzyl group prior to UV irradiation through a photomask to pattern the hydrophilic regions. However, the method

Chapter: 5

still required several steps to perform the photolithography. Additionally, Vong *et al*⁴⁴ proposed an alternative approach to pattern hydrophobic sites inside a fused silica capillary tube using trifluoroethyl undec-10-enoate (TFEE) with a 10-hour UV exposure. The TFEE molecule was used to create a hydrophobic surface with high surface coverage due to less steric hindrance and could also be used as a linker for further surface coupling with primary amines. Even though this method provided patterned hydrophobization with high surface coverage and the opportunities for further surface coupling, it took quite a long time (10 hours) to achieve the whole procedure.

The authors found that simple microchannels of down to 2 μm depth and 60 μm width could be hydrophobized using conventional methods both liquid based hydrophobization (ODS or FDTS) and vapour-based hydrophobization (hexamethylsilazane, HMDS), as reported both by the authors and in many literature reports.^{33, 45, 46} Problems however arose when these methods were tried in micro- and nanochannels networks, where at the interface of micro- and nanochannels and also inside nanochannels clogging occurred. Even though clogging could possibly be removed by flushing, it will be difficult to perform this method in the complex microfluidic network or nanochannels.

Here we propose a novel approach to hydrophobize glass surfaces inside closed channels which is suitable for micro- and nanochannel networks in which the intersections of micro- and nanochannels are critical areas for particulate clogging. Furthermore, this method allows easy patterning of the surface. The method is based on the use of silicone oil, which has a low toxicity, unlike other chemicals generally used in the surface modification by other methods. Also, it is widely used in droplet-based microfluidic experimentations, and available in a variety of viscosities. Via this method that does not produce particulate debris, the hydrophobization is more conveniently obtained than by the conventional methods especially in sub-micron fluidic channels and the complicated fluidic networks.

Experimental Details

Surface Modification

The micro- and nanofluidic chips have been fabricated from borosilicate glass substrates and thermally bonded as earlier described in chapter 3. Prior to the modification process, the glass chip was cleaned and dehydrated in the oven at 120°C for 2 hours. Subsequently, the chip was activated by oxygen plasma (Harrick Plasma Cleaner, NY, USA), at a pressure of 400 mTorr and a power of 30W for 10 min. Then, silicone oil (Sigma-Aldrich, The Netherlands) was applied into the fluidic chips using a syringe pump. All types of silicone oil (silicone oil 1, 5, 20 and 50 cSt) were purchased from Sigma-Aldrich, the Netherlands. (The optical and fluidic setups have been earlier detailed in chapter 3.) After filling with silicone oil, the chip was exposed to UV light (680 mW cm^{-2} , Konrad Benda UV-lamp short and long wave UV-8S/L, Germany) with a wavelength of 254 nm. The lamp was placed at a fixed distance ($\sim 0.5 \text{ cm}$) from the samples. During UV exposure, the glass chip was immersed into silicone oil to prevent the evaporation of oil. Finally, the glass chip was cleaned by octane, acetone and isopropanol. Alternatively, a stainless-steel mask was used to confine hydrophobic patterns on the glass chip upon UV exposure. The procedure of the modification is illustrated in Fig. 5-1.

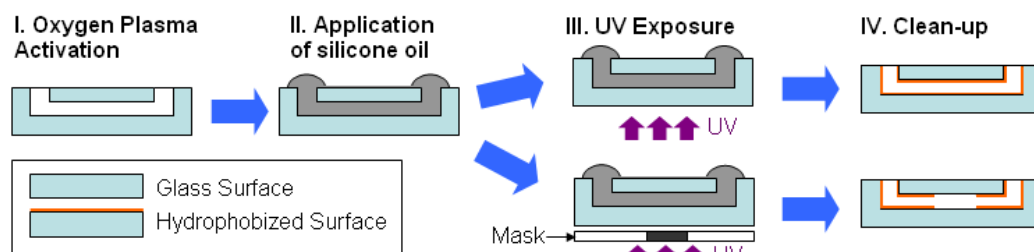


Figure 5-1: Schematic diagram of the procedure of the surface modification by using UV-light and silicone oil.

Characterization

Contact Angle Measurement

Static contact angle measurement of the outer surface of a glass chip was performed using a Dataphysics System (Dataphysics, OCA20, Germany) in the sessile drop mode using DI

Chapter: 5

water before and after hydrophobization using various modification parameters such as UV-treatment time, and oil type as shown in Fig. 5-2 and Table 5-1. In the first approach, the samples were treated by oxygen plasma and then exposed to UV light. In the second approach samples were irradiated by UV light directly without oxygen plasma treatment. The third samples were activated by oxygen plasma, immersed into the oil and then stored in the dark for two hours instead of being irradiated by UV light. Furthermore, the stability of the modified surfaces was investigated by immersing the modified samples into different-polarity solvents (Water, Ethanol, Acetone, Silicone Oil, Octane) for 24 hours as well as by keeping the modified samples in atmospheric circumstances for 3 weeks. All solvents used in this stability test were purchased from Sigma-Aldrich (The Netherlands).

X-Ray Photoelectron Spectroscopy (XPS)

XPS characterization had been conducted with a monochromatic X-ray beam (Al KR, 1486.6 eV, 100W, Quantera, Physical Electronics). Mapping was done at 3×10^{-9} Torr and detector angles of 70 and 45°. XPS spectra were taken from a bare glass substrate and a modified glass sample.

W/O Emulsion Generation

The micro- and nanochannel network modified by this approach was used to generate a W/O emulsion. The homogeneity of the surface modification inside the nanochannel sections was judged by observing the undisturbed flow of water droplets in the oil phase, since any unmodified glass surface would present a hydrophilic area on which water droplets would be trapped. The aqueous phase in these experiments was DI water and the oil phase was 0.5 wt % Span80 in hexadecane. The viscosity of water and oil phases ≈ 1 and 3 mPa.s, respectively. All chemicals used in this test were bought from Sigma-Aldrich Chemie GmbH (Germany).

Hydrophobic Patterning

Hydrophobic areas were patterned both on the plane glass sample and in an enclosed microchannel system using the above-mentioned procedure in combination with an in-house produced stainless steel mask. The UV-exposed area became hydrophobic whereas the

unexposed area remained hydrophilic. After modification, on the plane substrate, vaporized water was condensed onto the hydrophobic patterned surface. Difference in dimensions of condensed droplets then expressed the diverse hydrophobicity on the patterned surface.⁴⁷ In the enclosed microchannel device, DI water would flow into hydrophilic microchannels by capillary force, but would cease to flow when reaching the hydrophobic area. The magnitude of the additionally applied pressure that would make the water resume its flow through the hydrophobic sector was used to determine the contact angle inside the hydrophobic section.

Results and Discussion

Contact Angle

The effects of oxygen plasma and UV exposure on the surface modification were determined from the change in the contact angle of the outer surface of a glass chip. A table 5-1 gives a comparison of the contact angle of surface hydrophobized by the different processes (with or without O₂ plasma activation and UV exposure steps) when applying silicone oil 50 cSt in combination with two-hour UV exposure. It was shown that only one step of either oxygen plasma or UV exposure does enhance the contact angle but to a lesser extent than the combination of both steps (see Table 5-1). The effect of oxygen plasma and UV exposure is discussed in the next section.

Table 5-1: Contact angle measurements of glass surfaces before and after modification using different modification approaches.

Before Modification	After Modification		
	O ₂ (+), UV (+)	O ₂ (-), UV (+)	O ₂ (+), UV (-)
31.9±3.9	100.9±2.8	68.2±0.2	89.0±4.0

Note: Three different approaches of surface modification were carried out

- (1) With oxygen plasma [O₂(+)] and with UV exposure [UV(+)]
- (2) Without oxygen plasma [O₂(-)] and with UV exposure [UV(+)]
- (3) With oxygen plasma [O₂(+)] and without UV exposure [UV(-)]

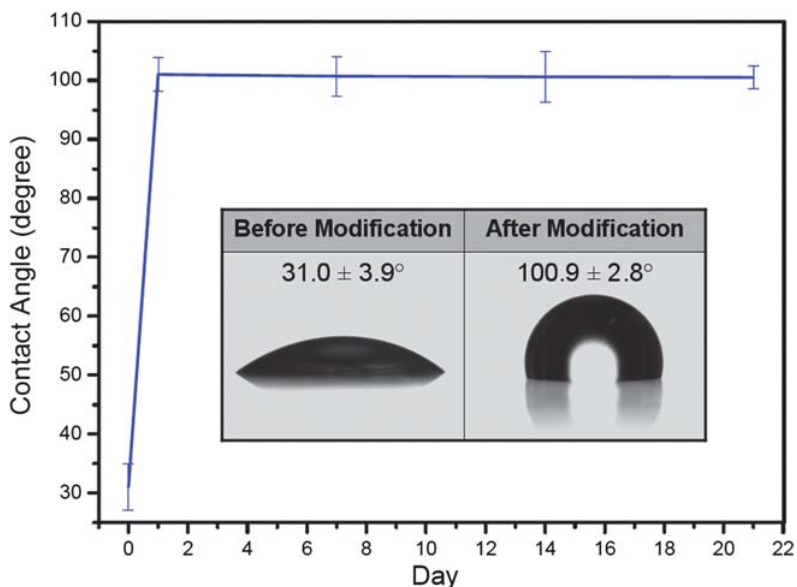


Figure 5-2: Contact angle measurement of the outer glass surface before (date 0th) and after modification (until three weeks). Inset: images of water droplet (2 μ L) onto the glass surface before and after surface modification.

In addition, as can be seen from Fig.5-2, modification of the glass surfaces by silicone oil 50 cSt in combination with 2-hour UV exposure results in a contact angle of 100° measured from several samples. Additionally, the UV treatment times were varied from 10 min to 6 hours to investigate the optimal time for modification. Three-hour curing time proved the optimal condition for silicone oil 50 cSt since the obtained contact angle then reached a maximum (105.9°). When the sample was treated by UV irradiation for a longer time, the resultant contact angle decreased and showed higher deviation. Other types of silicone oil (Silicone Oil 1, 5 and 20 cSt) were also tested (Fig. 5-3) showing the same trend of resultant contact angle as a function of treatment time. The optimal curing times were found to be dependent on the type of oils, and the hydrophobic surface modified by silicone oil 50 cSt provided the highest contact angle among these oils. Overexposure was found to heat the oil (temperature increase to 45°C after 2 hours) causing the evaporation of oil or the formation of tiny air bubbles in the oil phase.

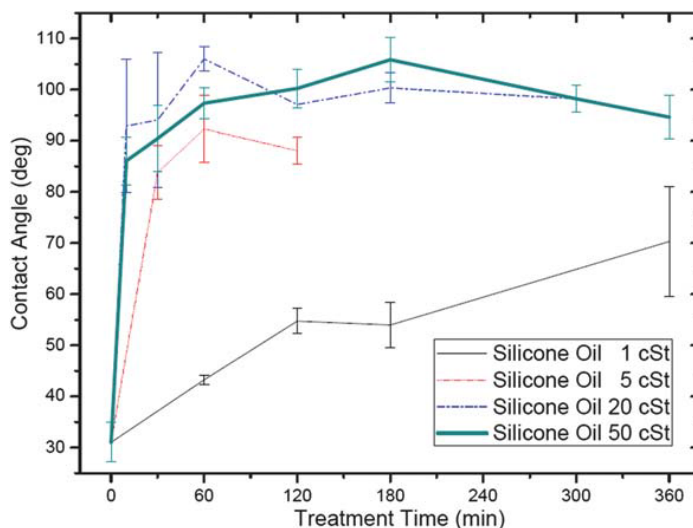


Figure 5-3: Contact angle measurement of the outer glass surface at different UV-treatment time (min) and types of silicone oil.

X-Ray Photoelectron Spectroscopy (XPS)

XPS data of unmodified and modified samples are shown in Fig. 5-4 (A-D). A survey spectrum of both samples (Fig. 5-4A) shows the changes in the atomic ratio of each element especially for carbon (C1s), oxygen (O1s) and silicon (Si2p). High-resolution spectra of C1s, O1s and Si2p are individually illustrated in Fig. 5-4 (B-D). An obvious increase in carbon atom content from 11% to 34% (Fig. 5-4B and Table 5-2) was attributed mainly to the formation of fragments of silicone oil molecules. The peak of C1s from the unmodified glass surface might be assigned to the contamination of organic compounds on the surface. In general, the binding energy of O1s in SiO₂ and in hydroxyl groups is 533 and 532 eV, respectively.⁴⁸ The shift of binding energy for O1s after modification (Fig. 5-4C and Table 5-2) was mainly due to the absence of OH groups resulting from the formation of a silicone oil layer onto the glass surface. The binding energy of Si2p in the silicone oil molecule (Si-C or Si-O bond) and in SiO₂ is 102 and 103 eV, respectively.⁴⁸ After hydrophobization, more silicon atoms with a binding energy of 102 eV were observed in the Si2p XPS data as opposed to an unmodified sample, verifying that silicon oil molecules were attached onto the glass surface (Fig. 5-4D and Table 5-2). The atomic ratio of each element (C1s, O1s, Si2p) and of the shifted binding energy (O1s, Si2p) after modification are shown in Table 5-2.

Chapter: 5

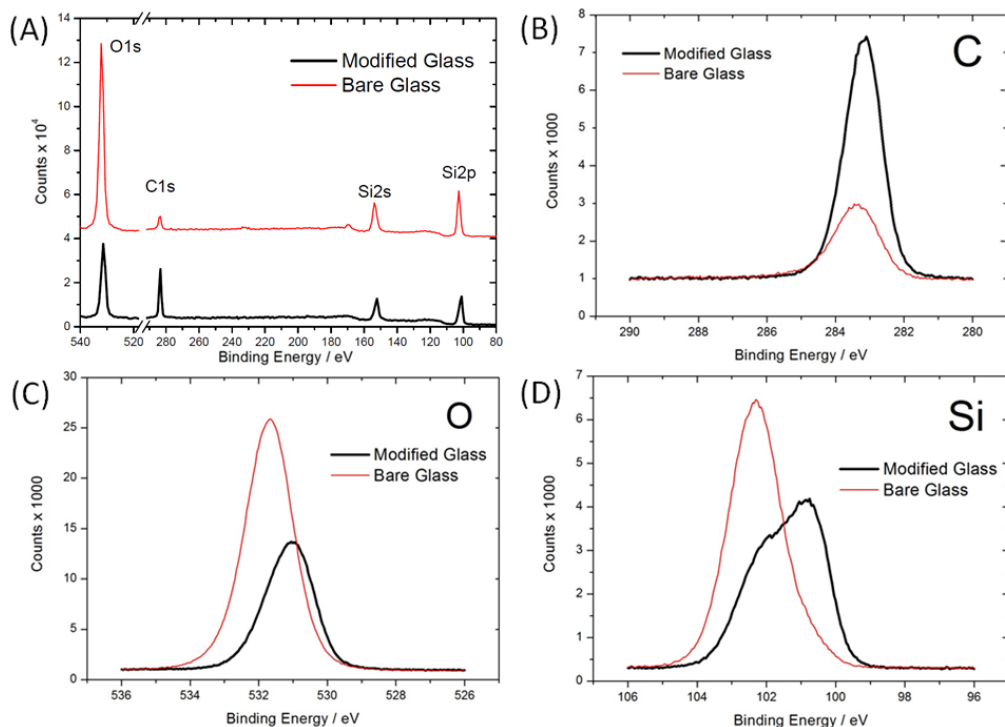


Figure 5-4: XPS results of bare glass and modified glass substrate; (A) Survey spectrum, (B) C1s spectrum, (C), Si2p spectrum and (D) O1s spectrum. The enhancement of carbon atom content in modified substrate was attributed to the formation of fragments of silicone oil.

Table 5-2: Atomic ratio of C1s, O1s and Si2p from the XPS results.

Sample \ Element	Atomic Ratio (%)						
	C	O		Si			
Bare Glass	11.1	60.5	532eV	533eV	27.9	102eV	103eV
			96	4		4	96
Modified Glass	34.3	36.7	532eV	533eV	27.4	102eV	103eV
			75	25		40	60

Stability

Contact angles of the hydrophobized surfaces measured before and after immersion into various solutions with different polarities (water, ethanol, acetone, octane, and silicone oil) until 24 hours are shown in Fig. 5-5. Also, the contact angles of the samples stored in atmospheric circumstances were measured until three weeks after modification as illustrated

in Fig.5-2. After 24-hour immersion into different solutions, the contact angles slightly decreased with maximally around 5° (Fig. 5-5) and almost remained constant for three weeks in case of the samples stored in the atmosphere (see Fig.5-2). These data indicate the good stability of the hydrophobized surface modified with this approach in different-polarity solvents. We interpret the results as showing that the solvents applied can remove a physisorbed layer of silicone oil or organic compounds on the glass surface, but not break covalent bonds of the hydrophobic layer formed at the surface.

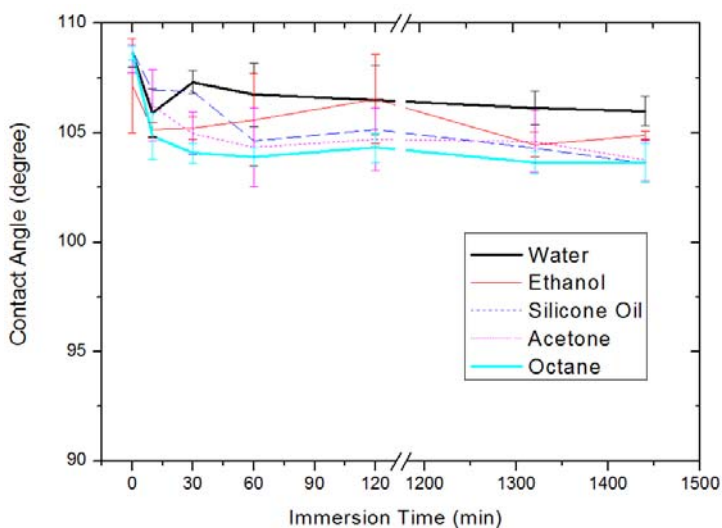


Figure 5-5: Stability of the hydrophobized glass surface in several solutions with different polarities until 24 hours.

In-channel Modified Surface

After hydrophobization, neither particulate debris nor clogging was found in the glass-based micro- and nanofluidic networks, which is especially remarkable inside the nanochannel network (Fig.5-6 *Left*) and the intersection of micro- and nanochannels (Fig.5-6 *Middle*), where standard hydrophobization methods tended to cause particle deposition. When water was applied in the microfluidic channel, the contact angle deduced from the meniscus shape was above 90° as shown in Fig. 5-6 (*Right*).

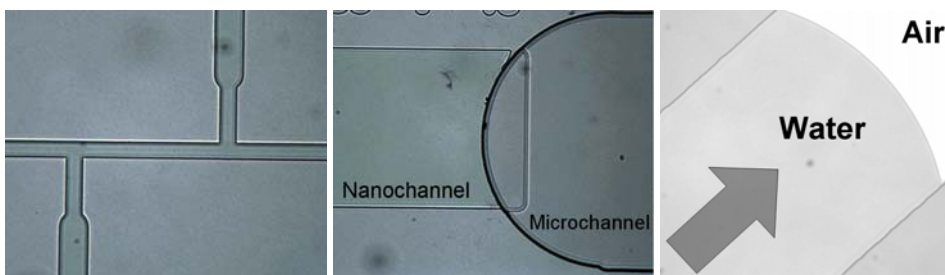


Figure 5-6: Micro- and nanofluidic networks after modification. No clogging or formation of particulate debris occurred. (Left) Nanochannel network (width: 6 and 8 μm). (Middle) Intersection of nano- and microchannel. The width of nanochannel and microchannel were 100 and 150 μm , respectively. (Right) Meniscus of water phase against air in microchannel after surface modification (arrow indicates the flow direction of fluid); the width of the channel was 100 μm . The depth of all nanochannels and microchannels was 500 nm and 5 μm , respectively.

Homogeneity of hydrophobization (W/O Emulsion)

After modification, the modified glass-based chip was used for generation of water-in-oil droplets. The fluidic chip consists of micro- and nanochannel networks with a T-junction of the nanochannels where the tip of the water stream was detached by shear force from the oil stream forming water droplets flowing in a continuous oil phase. Fig.5-7 (Left) shows the successful generation of 50-fL water droplets at the nanochannel T-junction (width: 10 μm , depth: 0.5 μm). When performing this fluidic experiment for a few hours, the formed droplets continuously homogeneously flowed in the nanochannel outlet (width: 100 μm , depth: 0.5 μm) without droplets sticking on the channel wall as illustrated in Fig.5-7 (Right). This stands in contrast to cases of inhomogeneous coating, where water droplets would become stuck on hydrophilic surface patches.

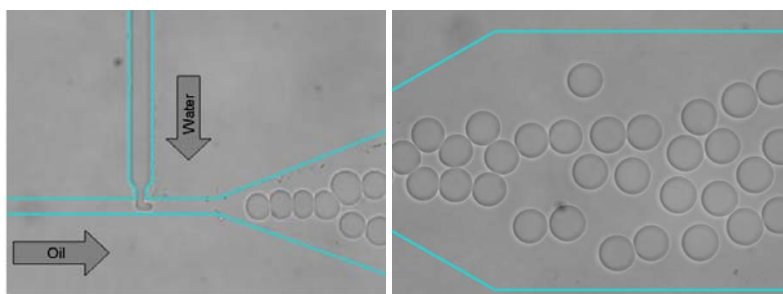


Figure 5-7: (Left) Water-in-oil droplet formation in a hydrophobized glass chip (water phase : DI water and oil phase : hexadecane with 0.5wt% Span80), (Right) generated aqueous droplets flowing in outlet channel without sticking shows the homogeneous coating obtained by this method; (all channels were 1 μm deep and the width of the inlet and outlet channels was 10 and 100 μm , respectively. The blue lines visualize the confinement of the nanofluidic network.

Hydrophobic Patterning

After illumination incorporated with a metal mask and clean-up, the hydrophobic pattern on a plane glass surface was characterized by exposing the surface to vaporized DI water. The difference in hydrophobicity on the surface then caused different dimensions of condensed droplets on the glass surface.⁴⁷ Due to the larger surface energy on the hydrophilic area (the wetting effect of water on a hydrophilic surface), condensed droplets were larger and flatter than those on the hydrophobic area. Flatter droplets on the hydrophilic surface also showed a brighter image than those on the hydrophobic surface as illustrated in Fig. 5-8.

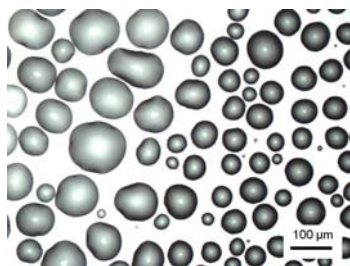


Figure 5-8: *Patterned hydrophobic surface on a bare glass substrate illustrating the hydrophobized area on the right side and unmodified area on the left side. Vaporized water condensed onto the patterned hydrophobic surface creating smaller droplets due to lower surface energy; on the contrary, larger and flatter droplets condensed onto a hydrophilic glass surface because of better wetting.*

For the micro- and nanofluidic chip, the hydrophobic patterning was tested by using the principle of hydrophobic valving as described earlier in the literature.^{40, 41} The water phase is wetting on hydrophilic sectors and non-wetting on hydrophobic sectors. In our chip, the sections that are exposed to only oxygen plasma and silicone oil in the experiments on free glass surfaces are expected to be hydrophilic ($\theta < 90^\circ$) while the sections exposed to oxygen plasma, silicone oil and UV light will be hydrophobic ($\theta > 90^\circ$). We indeed observed that after treatment of the channels the water spontaneously but slowly advanced through the section treated with oxygen plasma and silicone oil while it ceased to advance when reaching the border of the sectors treated with oxygen plasma, silicone oil and UV. The pressure needed to resume the flow through the non-wetting sector can be described by a model of capillary filling. This given pressure is ruled by the water/gas interfacial tension (γ_{wg}), the radius of curvature of the aqueous phase which is related to the height (h) and the

Chapter: 5

width (w) of the fluidic channel, and the contact angle of the hydrophobic surface (θ_{phob}) as shown in the following equation:

$$P = -2\gamma_{wg} \frac{h+w}{hw} \cos \theta_{phob} \quad \text{Eqn. (1)}$$

The hydrostatic pressure ($P_{hydrostatic}$) of water as adjusted by the positions of a water reservoir and the microchannel system (ΔH) was used to provide a relatively low pressure to the water as shown in eqn. (2) where ρ is the density of water and g is the gravitational acceleration.

$$P_{hydrostatic} = \rho g (\Delta H) \quad \text{Eqn. (2)}$$

In our experiment, the height and the width of the fluidic channel were 5 and 100 μm , respectively, and the surface tension between water and air (γ_{wg}) $\sim 70 \text{ mN m}^{-1}$. A height difference (ΔH) of around 35 cm was needed to introduce water into the hydrophobic sector. The applied pressure was therefore approximately 34 mbar or $3,418 \text{ N m}^{-2}$ according to eqn.(1) yielding a contact angle of the in-channel hydrophobic surface of about 96.4° .[†]

Discussion: Possible Mechanism

The glass surface is first activated by oxygen plasma enabling removal of contaminants such as dust, grease, and organic compounds from the glass surface. Plasma can also enhance the number of hydroxyl terminated groups (OH) on the surface of SiO_2 as shown in Fig. 5-8, causing a higher surface energy and decreasing water contact angle.⁴⁹ In general, when silicone oil is applied to the glass surface, the oil would physically adsorb onto terminal OH groups on the glass surface due to Van der Waals attraction and hydrogen bonding between the oxygen atoms in the polymeric backbone and the silanol groups on the glass surface.⁵⁰ With oxygen plasma activation, oil was seen to spread out faster than without plasma activation which we interpret as the result of an increasing number of hydroxyl surface groups.

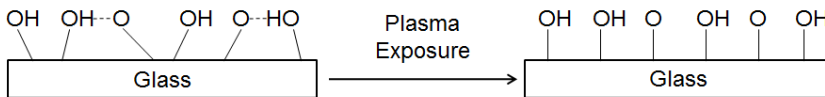


Figure 5-8: The effect of oxygen plasma activation on the glass surface

[†] To avoid confusion between the contact angle from the hydrophobic valving calculation and the one from the contact angle measurement by a sessile drop method, it is worth mentioning that the contact angle determined from the hydrophobic valving concept is *the advancing contact angle* which is different from *the static contact angle* measured by a sessile drop method.

The effect of irradiation on polydimethylsiloxane (PDMS) molecules has been reported earlier in the literature.⁵¹ Silicone oil has the same molecular structure as PDMS. Upon UV exposure, photons from the UV lamp with a wavelength of 254 nm have an energy of 469 kJ/mol (4.88 eV) which is enough to break some bonds in the silicone oil molecules forming radicals of oil molecules. We propose that these radicals diffuse to the surface and react with the hydroxyl groups on the glass surface, leaving the non-polar tails of the oil molecules in contact with the solution forming the hydrophobic surface.

The application of oxygen plasma and subsequent exposure to silicone oil resulted in a higher contact angle (89°) despite the lack of UV irradiation. This increase was probably due to the effect of oxygen plasma on a hydroxylated silica surface (Si-OH). As mentioned before, the oxygen plasma can remove organic contaminants and break hydrogen bonds between hydroxyl groups (OH) and their neighboring oxygen atom causing more OH groups on the surface. Furthermore, hydroxylated silica (Si-OH) can form strained edge-shared tetrahedral Si-O-Si bonds by heating at high temperature (above 650°C)⁵² or by oxygen plasma treatment.⁵³ Dehydroxylated siloxane bonds were reported to have a greatly enhanced reactivity compared to hydroxyl groups on the silica surface.⁵²⁻⁵⁴ This strained form might be highly reactive to silicone oil molecules even without molecular radical formation of oil by UV irradiation.

Alternatively, the glass surface could be activated by a chemical approach i.e. application of basic solution of sodium hydroxide solution into the fluidic channels. This could be the alternative method to activate the surface inside nanochannel which possibly is too small for plasma can reach and activate.

A long exposure led to a decrease of the observed contact angle and increased the observed deviation. Long exposure times might lead to the creation of a multilayer of oil molecules or the formation of unexpected molecular products. The evaporation of oil or the formation of air bubbles occurring from heating upon UV-overexposure probably also inhibited a high surface coverage causing the higher deviation of the contact angle. From our measurement, after two hour UV irradiation, the silicone oil was heated to the temperature of 45°.

Conclusion

In micro- and nanofluidic technology, approaches to hydrophobize in-channel microfluidic systems have rarely been reported. Commonly-used modification methods are accomplished in a plane wafer before bonding and/or require skilful handling procedures. Moreover, nanofluidic networks are more problematic for any modification approach especially in the aspect of debris left over after modification. In our novel approach, in-channel fluidic networks were hydrophobized by filling with silicone oil in combination with plasma activation and UV irradiation. The treatment can reduce the surface energy resulting in contact angles of 100° or more remaining stably hydrophobic in solvents of different polarity for more than three weeks. Layers were characterized by XPS. Glass-based micro- and nanofluidic chips were successfully modified without the formation of particulate debris, and could be used to produce W/O emulsions verifying the homogeneity of modified surface. It was finally shown that this method lends itself to selective in-channel hydrophobization by the application of a UV mask.

References

1. L. L. Shui, A. van den Berg and J. C. T. Eijkel, *Lab on a Chip*, 2009, **9**, 795-801.
2. P. Abbyad, R. Dangla, A. Alexandrou and C. N. Baroud, *Lab on a Chip*, 2011, **11**, 813-821.
3. M. Chabert and J. L. Viovy, *Proc. Natl. Acad. Sci. U. S. A.*, 2008, **105**, 3191-3196.
4. J. Clausell-Tormos, D. Lieber, J. C. Baret, A. El-Harrak, O. J. Miller, L. Frenz, J. Blouwolff, K. J. Humphry, S. Koster, H. Duan, C. Holtze, D. A. Weitz, A. D. Griffiths and C. A. Merten, *Chemistry & Biology*, 2008, **15**, 427-437.
5. S. Koster, F. E. Angile, H. Duan, J. J. Agresti, A. Wintner, C. Schmitz, A. C. Rowat, C. A. Merten, D. Pisignano, A. D. Griffiths and D. A. Weitz, *Lab on a Chip*, 2008, **8**, 1110-1115.
6. N. Wu, F. Courtois, R. Surjadi, J. Oakeshott, T. S. Peat, C. J. Easton, C. Abell and Y. G. Zhu, *Engineering in Life Sciences*, 2011, **11**, 157-164.
7. V. Chokkalingam, B. Weidenhof, M. Kramer, W. F. Maier, S. Herminghaus and R. Seemann, *Lab on a Chip*, 2010, **10**, 1700-1705.
8. H. Hwang, S. H. Kim and S. M. Yang, *Lab on a Chip*, 2011, **11**, 87-92.
9. S. H. Kim, A. Abbaspourrad and D. A. Weitz, *Journal of the American Chemical Society*, 2011, **133**, 5516-5524.
10. S. H. Kim, S. J. Jeon, G. R. Yi, C. J. Heo, J. H. Choi and S. M. Yang, *Advanced Materials*, 2008, **20**, 1649-+.

11. S. H. Kim, J. W. Shim, J. M. Lim, S. Y. Lee and S. M. Yang, *New Journal of Physics*, 2009, **11**.
12. T. Nisisako, T. Torii, T. Takahashi and Y. Takizawa, *Advanced Materials*, 2006, **18**, 1152-+.
13. J. Wan, M. Sullivan and H. A. Stone, *Controllable production of gas/water/oil double emulsions in microfluidic devices*, 2007.
14. R. M. Lorenz, G. S. Fiorini, G. D. M. Jeffries, D. S. W. Lim, M. Y. He and D. T. Chiu, *Analytica Chimica Acta*, 2008, **630**, 124-130.
15. Y. Liu, S. Y. Jung and C. P. Collier, *Anal. Chem.*, 2009, **81**, 4922-4928.
16. J. C. Baret, F. Kleinschmidt, A. El Harrak and A. D. Griffiths, *Langmuir*, 2009, **25**, 6088-6093.
17. M. Y. He, J. S. Edgar, G. D. M. Jeffries, R. M. Lorenz, J. P. Shelby and D. T. Chiu, *Anal. Chem.*, 2005, **77**, 1539-1544.
18. P. R. Marcoux, M. Dupoy, R. Mathey, A. Novelli-Rousseau, V. Heran, S. Morales, F. Rivera, P. L. Joly, J. P. Moy and F. Mallard, *Colloids and Surfaces a-Physicochemical and Engineering Aspects*, 2011, **377**, 54-62.
19. S. A. Vanapalli, A. G. Banpurkar, D. van den Ende, M. H. G. Duits and F. Mugele, *Lab on a Chip*, 2009, **9**, 982-990.
20. A. R. Abate, A. Poitzsch, Y. Hwang, J. Lee, J. Czerwinska and D. A. Weitz, *Physical Review E*, 2009, **80**.
21. J. J. Agresti, E. Antipov, A. R. Abate, K. Ahn, A. C. Rowat, J. C. Baret, M. Marquez, A. M. Klibanov, A. D. Griffiths and D. A. Weitz, *Proc. Natl. Acad. Sci. U. S. A.*, 2010, **107**, 4004-4009.
22. P. Garstecki, M. J. Fuerstman, H. A. Stone and G. M. Whitesides, *Lab on a Chip*, 2006, **6**, 437-446.
23. B. Y. Kim, L. Y. Hong, Y. M. Chung, D. P. Kim and C. S. Lee, *Advanced Functional Materials*, 2009, **19**, 3796-3803.
24. J. N. Lee, C. Park and G. M. Whitesides, *Anal. Chem.*, 2003, **75**, 6544-6554.
25. R. Dangla, F. Gallaire and C. N. Baroud, *Lab on a Chip*, 2010, **10**, 2972-2978.
26. J. U. Shim, S. N. Patil, J. T. Hodgkinson, S. D. Bowden, D. R. Spring, M. Welch, W. T. S. Huck, F. Hollfelder and C. Abell, *Lab on a Chip*, 2011, **11**, 1132-1137.
27. P. Tremblay, M. M. Savard, J. Vermette and R. Paquin, *Journal of Membrane Science*, 2006, **282**, 245-256.
28. J. Lee, Y. K. Yun, Y. Kim and K. Jo, *Bulletin of the Korean Chemical Society*, 2009, **30**, 1793-1797.
29. M. M. J. Decre, P. H. M. Timmermans, O. van der Sluis and R. Schroeders, *Langmuir*, 2005, **21**, 7971-7978.
30. K. J. Hsia, Y. Huang, E. Menard, J. U. Park, W. Zhou, J. Rogers and J. M. Fulton, *Applied Physics Letters*, 2005, **86**.
31. S. M. Park, Y. S. Huh, H. G. Craighead and D. Erickson, *Proc. Natl. Acad. Sci. U. S. A.*, 2009, **106**, 15549-15554.
32. M. Beck, M. Graczyk, I. Maximov, E. L. Sarwe, T. G. I. Ling, M. Keil and L. Montelius, *Microelectronic Engineering*, 2002, **61-2**, 441-448.
33. E. M. Chan, A. P. Alivisatos and R. A. Mathies, *Journal of the American Chemical Society*, 2005, **127**, 13854-13861.
34. J. Moresco, C. H. Clausen and W. Svendsen, *Sensors and Actuators B-Chemical*, 2010, **145**, 698-701.

Chapter: 5

35. Y. X. Zhuang, O. Hansen, T. Knieling, C. Wang, P. Rombach, W. Lang, W. Benecke, M. Kehlenbeck and J. Koblitz, *Journal of Microelectromechanical Systems*, 2007, **16**, 1451-1460.
36. A. Hibara, M. Nonaka, H. Hisamoto, K. Uchiyama, Y. Kikutani, M. Tokeshi and T. Kitamori, *Anal. Chem.*, 2002, **74**, 1724-1728.
37. X. A. Mu, Q. L. Liang, P. Hu, K. N. Ren, Y. M. Wang and G. A. Luo, *Microfluidics and Nanofluidics*, 2010, **9**, 365-373.
38. R. D. Oleschuk, L. L. Shultz-Lockyear, Y. B. Ning and D. J. Harrison, *Anal. Chem.*, 2000, **72**, 585-590.
39. M. Watanabe, *Sensors and Actuators B-Chemical*, 2007, **122**, 141-147.
40. B. Zhao, J. S. Moore and D. J. Beebe, *Science*, 2001, **291**, 1023-1026.
41. H. Andersson, W. van der Wijngaart, P. Griss, F. Niklaus and G. Stemme, *Sensors and Actuators B-Chemical*, 2001, **75**, 136-141.
42. Y. Y. Feng, Z. Y. Zhou, X. Y. Ye and H. J. Xiong, *Sensors and Actuators a-Physical*, 2003, **108**, 138-143.
43. E. T. Castellana, S. Kataoka, F. Albertorio and P. S. Cremer, *Anal. Chem.*, 2006, **78**, 107-112.
44. T. Vong, J. ter Maat, T. A. van Beek, B. van Lagen, M. Giesbers, J. C. M. van Hest and H. Zuilhof, *Langmuir*, 2009, **25**, 13952-13958.
45. M. Fukuyama and A. Hibara, *Anal Sci*, 2011, **27**, 671-672.
46. M. Loughran, S. W. Tsai, K. Yokoyama and I. Karube, *Curr Appl Phys*, 2003, **3**, 495-499.
47. J. ter Maat, R. Regeling, M. L. Yang, M. N. Mullings, S. F. Bent and H. Zuilhof, *Langmuir*, 2009, **25**, 11592-11597.
48. J. F. Moulder, W. F. Stickle, P. E. Sobol and K. D. Bomben, *Handbook of X-ray Photoelectron Spectroscopy*, Perkin-Elmer Corporation, 1992.
49. T. Yamamoto, M. Okubo, N. Imai and Y. Mori, *Plasma Chemistry and Plasma Processing*, 2004, **24**, 1-12.
50. K. G. Marinova, D. Christova, S. Tcholakova, E. Efremov and N. D. Denkov, *Langmuir*, 2005, **21**, 11729-11737.
51. S. W. Hu, X. Q. Ren, M. Bachman, C. E. Sims, G. P. Li and N. Allbritton, *Anal. Chem.*, 2002, **74**, 4117-4123.
52. B. C. Bunker, D. M. Haaland, T. A. Michalske and W. L. Smith, *Surf Sci*, 1989, **222**, 95-118.
53. R. F. Hicks, S. B. Habib and E. Gonzalez, *J Vac Sci Technol A*, 2010, **28**, 476-485.
54. A. Grabbe, T. A. Michalske and W. L. Smith, *J Phys Chem-US*, 1995, **99**, 4648-4654.

CHAPTER 6:

Single-molecule Encapsulation and Detection in a Droplet-based Micro- and Nanofluidic Device

In this chapter, the encapsulation of a single molecule of enzyme into a droplet-based carrier in a microfluidic device is performed for single enzyme kinetic analysis. The single-enzyme detection from our device is discussed in aspects of the concept of detection, the design of the device, the device material, etc. Devices are produced and operated and finally, the successful encapsulation of single enzyme into a droplet is validated by fitting to the Poisson distribution. The obtained enzymatic activity is furthermore compared to a result from a bulk experiment by fluorescence spectroscopy.

Single-molecule detection

Recently, many researchers have investigated the behavior of biomolecules in the single-molecular level to unravel the phenomena which remain hidden in the conventional bulk experiment.¹⁻³ For instance, they attached or confined individual molecules by means of attachment to a polymer-coated substrate.¹⁻³ Alternatively, microfluidic technology provides better and simpler confinement of the single molecule (i.e. enzyme) in numerous methods such as PDMS microwells,⁴ surface-immobilized droplets⁵ or liposomes.^{6, 7} Moreover, droplet-based microfluidics can be employed to generate scalable carriers to encapsulate individual molecules with high-throughput results. In addition, the microfluidic device also potentially provides precisely-controllable manipulation of the generated carriers in a miniaturized and automated fashion.

Generally, the measurement of single or a few molecules in solution is hindered by the background signal from the environment such as the solvent surrounding the target molecule(s) as well as the material of the device. In the first case, at low concentrations of target molecules, the background noise from the solvent becomes larger than that from the target molecules. However, this issue can be avoided by compartmentalization of the solution into tiny carriers and the signal from these tiny carriers is consequently detected as described in chapter 3 of this thesis (See Fig.6-1). Hereby smaller carriers allow higher concentrations of enzymes to be used and consequently higher signal-to-noise ratios.

In the latter case, the materials used to make a device can create some noise disturbing the measurement of the target signal. The polymer-based materials expressing high levels of background noise are therefore unsuitable to make devices for low-signal detection. Thus a glass material (Borofloat type) was used to fabricate the device in our system due to its excellent properties including the lower auto-fluorescence compared to polymer-based materials as discussed in chapter 3.^{8,9}

Droplet-based microfluidics will be used to provide the tiny compartmented aqueous droplets which are used as isolated enzyme carriers. This system is advantageous due to its flexibility to change the types of reactions and the amounts of the reagents.^{10, 11} In addition, the dimensions of these generated droplet carriers can be made monodisperse.^{12, 13} Moreover,

Single-enzyme Encapsulation and Detection

our platform fabricated from a glass borofloat material does not encounter the problem of the evaporation/dissolution into the chip material which is generally unavoidable in the device made from polymer-based materials such as polydimethyl-siloxane (PDMS).¹⁴

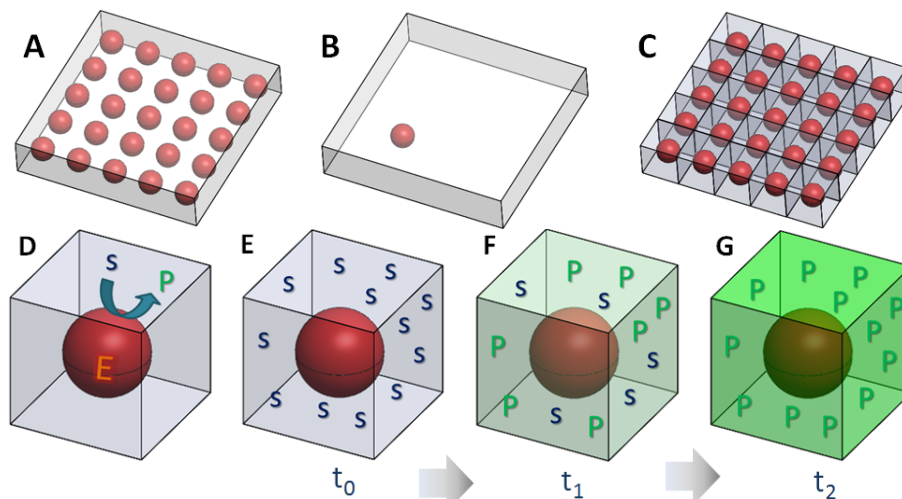


Figure 6-1: (A) An illustration of the enzyme solution dissolved in an aqueous carrier (enzyme: red and water: grey). (B) By dilution, the single-molecule encapsulation can be achieved but the excess amount of solvent provides high background noise. (C) By compartmentalization, the enzyme solution is confined as tiny droplets containing single enzymes at high concentration. (D) One box represents one droplet encapsulating single enzyme (red sphere). In the presence of substrate molecule shown as “S”, the substrate molecule binds to the enzyme molecule and generate the product molecule shown as “P”. (E) In the beginning at t_0 , single droplet encapsulating one enzyme molecule and the excess amounts of substrate molecules express non-fluorescence intensity. When the fluorescent product molecules are produced, the fluorescence intensity inside each droplet will gradually increase from t_0 to t_1 and t_2 (E-G). The product formation rate is used to determine the kinetic activity of this enzyme.

The micro and nanofluidic platforms used for generating the aqueous droplet emulsions have been fabricated and subsequently hydrophobized as earlier mentioned in chapter 3 and 5 of this thesis. An enzyme which produces a fluorescent product was chosen as model molecule to verify the single-molecule encapsulation into these generated droplets. The evolution of the fluorescent product can then be related to the kinetic activity of this enzyme. In addition, the histogram of the increasing fluorescent intensity in each droplet can be used to determine the number of enzymes encapsulated in each compartment.

In our experiment, we used the enzyme of β -glucosidase extracted from the hyperthermophilic archaon *Pyrococcus Furiosus* (provided by Microbiology Group,

Chapter: 6

Wageningen University, The Netherlands). This enzyme is hyperthermostable meaning it can function at high temperature.^{15, 16} Two substrates were available, (i) *4-Methylumbelliferyl-β-D-glucopyranoside* and (ii) *Fluorescein-β-D-glucopyranoside* (FLDGLu), which after reaction with this enzyme formed as fluorescent products 4-Methylumbelliferone (4-MUF) or fluorescein, respectively, as illustrated in Fig.6-2.

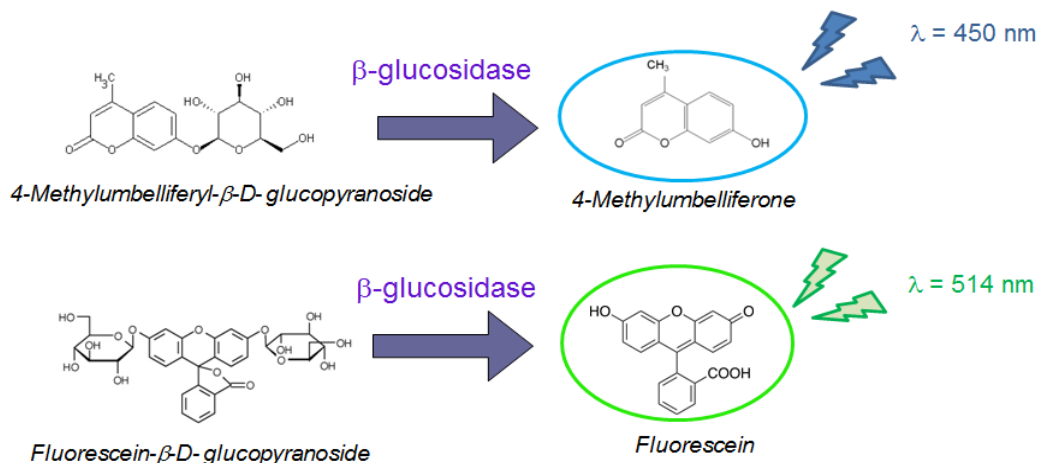


Figure 6-2: The two substrates reacting with the enzyme β -glucosidase; (Top) 4-methylumbelliferyl- β -D-glucopyranoside creating the product 4-methylumberriferone (4-MUF) whose emission wavelength is 450 nm; (Bottom) fluorescein- β -D-glucopyranoside creating as product fluorescein whose emission wavelength is 514 nm.

4-MUF has the maximal excitation and emission wavelengths at 360 and 450 nm, respectively, whereas fluorescein has those at 490 and 514 nm, respectively (Table 6-1).¹⁷⁻¹⁹ In addition, the intensities of the fluorescent products are pH-dependent, leading to significantly reduced intensities below the maximal intensity at the optimum pH.¹⁷⁻¹⁹

Table 6-1: The excitation and emission wavelength of the fluorophores 4-MUF and fluorescein as well as the optimum pH to express the highest fluorescence intensity.

Fluorescence	Excitation Wavelength (nm)	Emission Wavelength (nm)	Optimum pH
4-MUF	360	450	>10
Fluorescein	490	514	>8

The two major criteria used to select the substrate for our device are (a) the fluorescence intensity and (b) the autofluorescence from the borofloat at specific wavelength. Considering the first criterion, β -glucosidase expresses a maximal kinetic activity at pH 5 which activity

becomes lower at higher pH values. The fluorescence intensity of both fluorescein and 4-MUF is also pH-dependent, decreasing with pH values lower than the optimal one (Table 6-1). Fluorescein should thus be preferred due to smaller difference between its optimum pH condition and the pH for maximal kinetic activity. Initially, phosphate buffer saline (PBS) solution at pH 7 was used as the dispersed phase for our fluidic experimentations.

Considering the second criterion, devices made from borofloat glass (Borofloat Scott, Germany) can express autofluorescence, even though this auto-fluorescence is less than that from polymer-based devices. This autofluorescence can obstruct the optical observation of the samples especially in case of low concentrations of fluorescent molecules. The autofluorescence of borofloat glass is dependent on the excitation wavelength used and its emission spectra are shown in Fig.6-3, where also the emission wavelengths of 4-MUF and fluorescein are indicated.²⁰

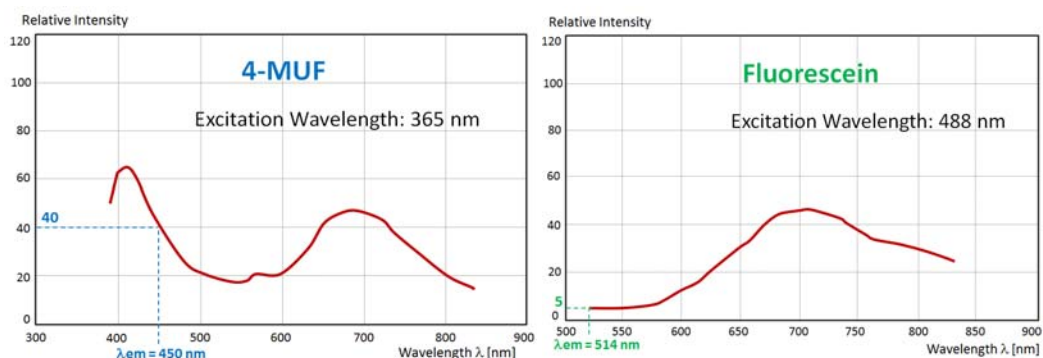


Figure 6-3: The autofluorescence of Borofloat 33 glass substrate at the excitation wavelengths of 365nm (Left) and 488 nm (Right). At the emission wavelength of 450 nm (light blue dot line, left), the relative autofluorescence intensity is around 40 while at the emission wavelength of 514 nm (green dot line; Right), the relative autofluorescence intensity is around 5. [fig. from ref.20]

In case of 4-MUF ($\lambda_{ex}=365\text{nm}$, $\lambda_{em}=450\text{nm}$), when the molecule is excited at 365 nm, the relative autofluorescence intensity from borofloat at the emission wavelength of 4-MUF is around 40 A.U. (Fig.6-3 Left). In case of fluorescein, when the molecule is excited at 488 nm, the relative autofluorescence at the fluorescein emission wavelength is just around 5 A.U. (Fig.6-3 Right). Therefore, also according to this second criterion fluorescein is preferred. Consequently, on the basis of both the high product fluorescence intensity at the pH of the solution and the autofluorescence from the material, *fluorescein- β -D-glucopyranoside* (FLDGlu) was selected as the substrate for the enzymatic reaction.

Chapter: 6

Calibration

Prior to the kinetic measurement of the enzymatic reaction, the fluorescent intensity of the product was calibrated to relate it to the concentration of the fluorescent product. To perform this calibration, a fluorescein solution in PBS buffer at pH 7 and silicone oil with 4 wt% Span 80 were loaded into the fluidic system to produce aqueous droplets in a continuous oil phase. The fluorescence intensities of the fluorescein solution were measured at different concentrations of fluorescein as depicted in Fig.6-4 showing that the fluorescence intensity is proportional to the concentration of fluorescein in the μM range. This calibration curve is used later to convert the measured increasing intensity to the increasing concentration of fluorescent product and hence the turnover number of the enzymatic reaction.

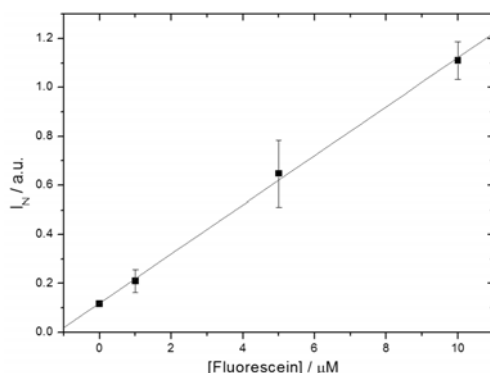


Figure 6-4: A calibration curve of the fluorescence intensity against the concentration of the fluorescein at pH 7.

Photobleaching

One drawback of the fluorescein molecule is the relatively high rate of photobleaching, due to the photo-induced chemical destruction during the exposure to the excitation light in the presence of oxygen molecules.²¹ Via this process, the fluorescence intensity reduces irreversibly leading to the misinterpretation of the amount of fluorescent molecules in the system. To avoid this problem, oxygen molecules should be removed from the system and an anti-oxidant reagent can be added to the solution. Addition of an anti-oxidant reagent e.g. n-propyl gallate (nPG) to a solution can hinder photobleaching especially in the fluorescein solution.²²⁻²⁴ Thus, in our study, nPG was added to the aqueous solution. The experimental details of the effect on photobleaching in our system are described in the appendix A. Generally, upon the observation the UV light was exposed to the system for a few seconds only for every single snapshot taken.

Kinetic activity in the bulk experiment determined with a fluorescence spectrometer

To verify the reliability of the experiment performed in our droplet-based microfluidic platform, we have to compare the enzyme kinetic activity obtained from our device to that from the bulk experiment under identical conditions. Therefore, the kinetic activity of the enzymatic reaction using FDGlu as substrate was first determined using a fluorescence spectrometer (Perkin Elmer). From this experiment, the obtained production rates of the reaction are plotted as a function of the concentration of substrate (Fig.6-5). To ensure obtaining a correct turnover number and K_m for the enzymatic reaction, we used different models to plot the data from the fluorescence spectrometer as summarized in Table 6-2. More details of each fitting methods are described in the appendix B. The data obtained from the *Michaelis-Menten Plot* was chosen due to the homogeneous distribution of the data along this fitting curve (Fig.6-5) as well as the R^2 value of almost 1 (see more details in the appendix B). Consequently, K_m and K_{cat} from the bulk experiment performed by a fluorescence spectrometer (*Michaelis-Menten Plot*) are around 26 μM and 5.7 sec^{-1} .

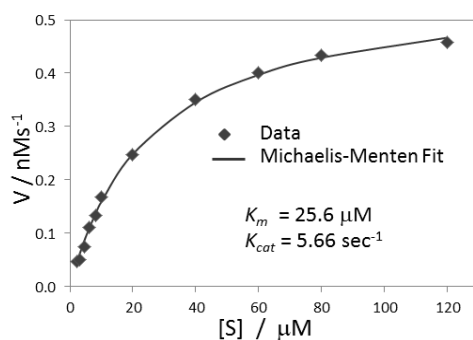


Figure 6-5: The experimental result of the enzymatic reaction of β -glucosidase using substrate FDGlu from a fluorescence spectrometer and a fitted Michaelis-Menten curve.

Table 6-2: Kinetic activity determined from the bulk experiment by a fluorescence spectrometer and plotted by different methods.

	Fitting Methods			
	<i>Michaelis-Menten</i>	<i>Lineweaver-Burk</i>	<i>Eadie-Hofstee</i>	<i>Hanes-Woolf</i>
K_{cat} (sec^{-1})	5.66	6.80	5.67	5.67
K_m (μM)	25.6	34.4	25.6	26.4

Single-enzyme kinetics in a droplet-based microfluidic device

As explained in the previous section, the single molecule should be encapsulated into miniaturized droplet carriers. For this purpose a fluidic platform consisting of a microfluidic network and a T-junction nanofluidic network was used (Fig.6-6). The oil solution and the aqueous solution were individually loaded into the device at positions 1 and 2 indicated in Fig.6-6 *Left*, respectively, and subsequently both fluids flowed to the microchannels as shown as large arrows in Fig.6-6 *Left*. When reaching the splitting channels between micro- and nanochannels at the positions 3 and 4 for the oil and aqueous phase networks, respectively, tiny portions of both fluids were split off into the nanochannels as indicated as the small arrows. Subsequently at the T-junction in the nanofluidic network (Fig.6-6 *Right*), shear was exerted on the tip of the dispersed phase stream by the continuous phase generating femtolitre droplets which flowed to the outlet nanochannels.

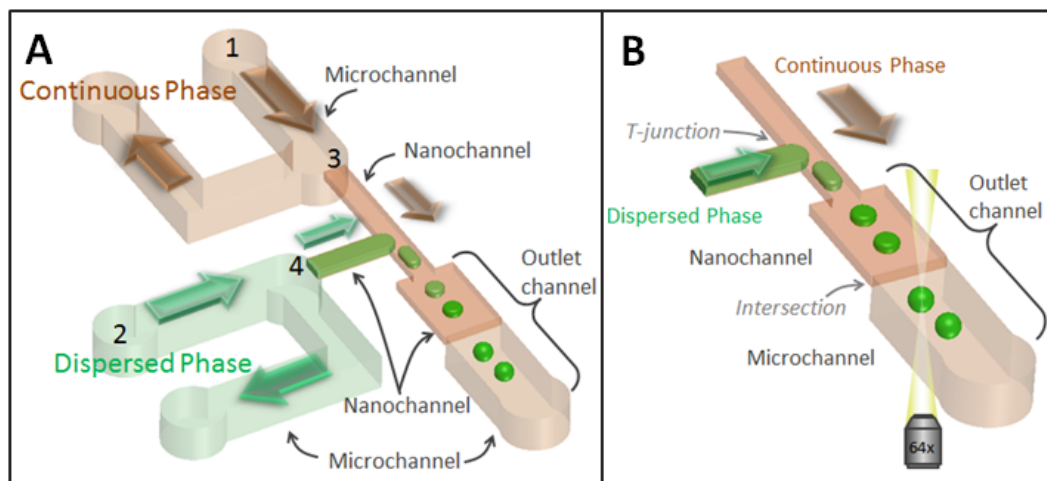


Figure 6-6: (A) Schematic of the droplet generator using a micro- and nanofluidic network. A dispersed phase (enzyme and substrate solution; shown in green) and a continuous phase (silicone oil; shown in orange) were separately loaded into the microchannels at position 0 and 1, respectively. Minute amounts of each phase split off into the nanochannels sections. A zoom-in view of the nanofluidic network as well as the outlet channel is shown in (B). At the T-junction, tiny droplets split off from the aqueous solution and flowed to the outlet nanochannel. Finally, at the intersection between nano and microchannels, the squeezed droplets obtained a spherical shape and entered the outlet microchannel where the time-resolved fluorescent measurement was performed. The arrows express the direction of the fluid flows. The depth of the microchannel and nanochannels are 3 and 0.5 μm , respectively.

After the droplet formation, the droplets were squeezed by the top and bottom walls of nanochannels, generating a non-spherical shape. The squeezed droplets in the nanochannels in principle would provide a larger detecting area as compared to spherical droplets with the same volume. The squeezed droplets were however less stable due to larger surface areas as compared to the spherical ones. As a result, the spherical droplets were preferably used as carriers for prolonged observation. Therefore, the outlet microchannel was added into our fluidic platform (Fig.6-6) at the downstream of the outlet nanochannel. At the intersection of micro- and nanochannels, the squeezed droplet transformed to a spherical shape driven by a reduction of the interfacial energy. Subsequently, a time-resolved measurement of the increasing fluorescence intensity of each droplet was performed.

Experimental Details

The micro- and nanofluidic chip was made from a Borofloat glass substrate by a standard etching technique and subsequently hydrophobized by the methods described in chapter 3 and 5 of this thesis, respectively. The hydrophobized chip was then mounted into the in-house built chip holder and placed onto an inverted fluorescence microscope (DMI 5000M, Leica) equipped with mercury lamp and high-sensitivity camera (EMCCD, Andor Ixon, UK). The solutions were loaded into the chip by using a flow-driven neMESYS pump. (Details and illustration of the optical and fluidic setups are previously described in chapter 3.) The enzymatic reaction of β -glucosidase was studied by using fluorescein- β -D-glucopyranoside (FDGlu) as a substrate, and yielding fluorescein as product. The increase in fluorescence intensity was used to determine the kinetic activity. Droplets were produced from a dispersed phase containing β -glucosidase (0.1 nM), FDGlu (200 μ M) in PBS solution (pH 7) and a continuous oil phase (silicone oil with 4% Span80), which were individually injected into the fluidic system by a syringe pump. In the experiment in the presence of an antioxidant reagent, n-propyl gallate (5% w/v) was added into the aqueous solution before injection into the fluidic device. The enzyme was provided by the Department of Microbiology, Wageningen University, The Netherlands. FDGlu was purchased from Invitrogen. The other chemicals were bought from Sigma-Aldrich, The Netherlands. Before mixing, each solution was degassed by placing into the desiccator to remove oxygen

Chapter: 6

molecules in the solution. The aqueous and oil solutions were separately loaded into the fluidic device to create droplets. After a large amount of generated droplets had entered the outlet channel, all syringe pumps were stopped to halt the movement of droplets. Upon the evolution of the fluorescence intensity in each droplet, snapshots of the array of droplets were imaged by using a high sensitive EMCCD camera and the fluorescence intensities in each droplet were later measured by using a program ImageJ (NIH Image). The data from droplets in the range of 2.5 - 3 μm in diameter were used for the analysis in this experiment.

Experimental results

Enzyme Kinetics in the presence of n-propyl gallate

After droplet formation, the fluorescence intensity of a single droplet was plotted against time (Fig. 6-7). The signal from the fluorescent product initially remained less than the background noise from the environment e.g. stemming from substrate (glass), solvent, or oil molecules. Thus, the signal which was measured in the beginning was a fluctuating background noise as shown in Fig.6-7. The time during which this signal was measured is labeled as “*delay time*”. After this delay time, the fluorescence intensity increased proportionally to the incubation time. The rate of increase of fluorescence intensity was then used to determine the kinetic activity of the enzymatic reaction. In this work, we took for this purpose the fluorescence intensity change from the 1200th to the 1335th minute.

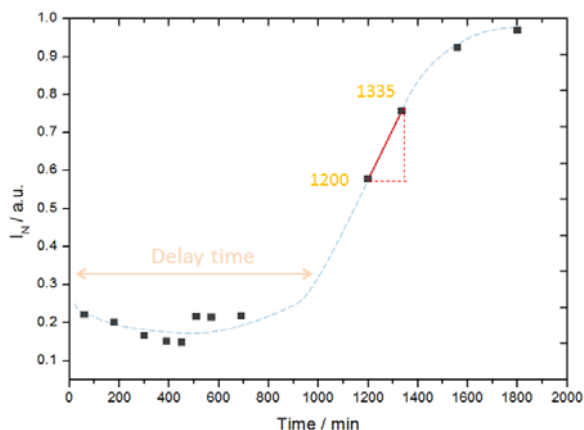


Figure 6-7: The evolution of the fluorescence intensity from the enzymatic reaction in the presence of nPG. In the first part, labeled as ‘*delay time*’, the signal from the fluorescein remains lower than the background noise. In the second part, the fluorescence intensity increases above the background noise and is used to determine the enzyme kinetics.

Single-enzyme Encapsulation and Detection

The images of the array of droplets containing the enzyme and substrate solution after the reaction had taken place are exemplified in Fig.6-8.

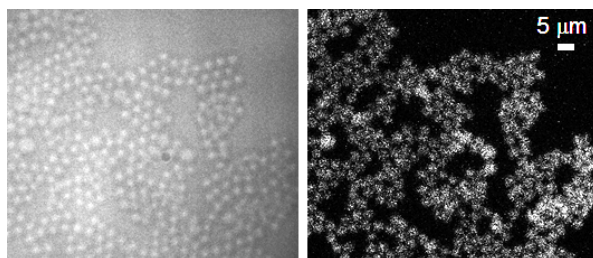


Figure 6-8: Encapsulation of enzyme and substrate into droplets. (Left) Bright-field image of the array of droplets; (Right) Fluorescence image of the same system after incubation for 1335 minutes. The droplet size is around 2.9 μm .

In this experiment, an approximately monodisperse emulsion was obtained. Only the fluorescence of the droplets ranging from 2.5 – 3.1 μm in diameter were counted (around 90%) for this analysis. We speculate that the remainder of the droplets (10 %) which were larger than 3.1 μm in diameter was produced from coalescence occurring during the prolonged measurement. This speculation was confirmed by the size distribution of the generated droplets (Fig.6-9). When the averaged diameter of generated droplets was around 2.9 μm , the coalescence of two, three and four droplets will create larger droplets with diameters of approximately 3.3, 4.0 and 4.6 μm , respectively. These dimensions correspond to the diameters of larger droplets in this droplet array (Fig.6-9).

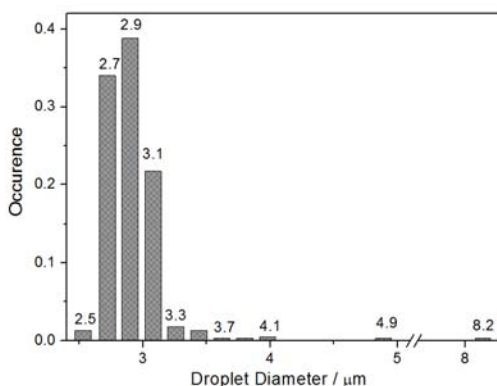


Figure 6-9: The size distribution of the generated droplets after incubation for 1335 minutes.

The increasing fluorescence intensity in each droplet between minutes 1200 and 1335 is plotted in a histogram (Fig.6-10) revealing that the increasing intensity is periodically enhanced and can be categorized into four peaks. We interpreted these peaks as generated by

Chapter: 6

0, 1, 2 or 3 enzyme molecules encapsulated in the droplets. The resulting turnover number for the enzyme activity is around 1.6 molecule of product per second.

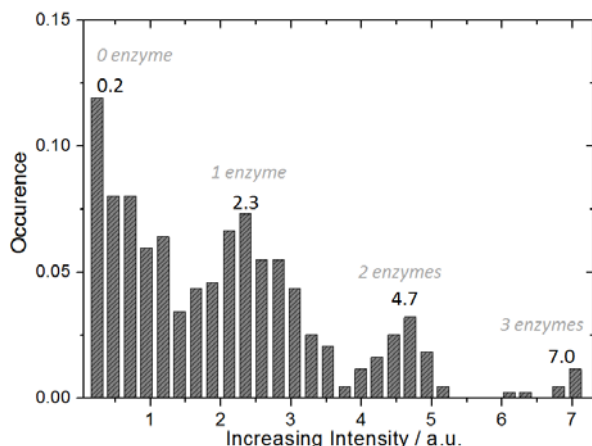


Figure 6-10: Histogram of the increasing fluorescence intensity from the 1200th to the 1335th minute. Four peaks can be interpreted as indicating the occupancy of droplets by (0, 1, 2 and 3) enzymes.

The histogram of the occupancy of this enzyme fits well to a Poisson distribution (Fig.6-11),

which is expressed by $f(\lambda, x) = \frac{\lambda^x e^{-\lambda}}{x!}$ where λ is a mean number of enzymes per droplet

and x is the number of enzymes per droplet. In this experiment a mean occupancy λ of 0.7 molecules/droplet was measured while the occupancy calculated for droplets with a diameter of 3 μm and an enzyme concentration of 0.1 nM is approximately 0.9 molecules/droplet. These data strongly suggest a successful encapsulation of single enzymes into the droplets.

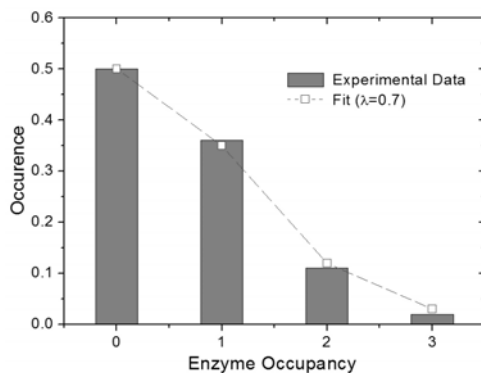


Figure 6-11: Distribution of the occupancy of enzyme in each droplet (bar chart) fitted to a Poisson distribution with a mean occupancy $\lambda = 0.7$ (dash line).

From these experiment results, the obtained K_{cat} from our droplet-based device (1.6 sec^{-1}) is significantly lower than that from the bulk experiment (5.7 sec^{-1}). We speculated that this difference of the kinetic activity resulted from the effect of n-propyl gallate (nPG) added as an anti-oxidant reagent. nPG might behave as an inhibitor in this enzymatic reaction. Therefore the further experiments were performed without the addition of nPG.

Enzyme Kinetics in the absence of n-propyl gallate

In this experiment, the aqueous solution containing the β -glucosidase (0.1 nM) and the substrate solution (200 μM), in PBS buffer solution without the addition of nPG. Then, this aqueous stream and the silicone oil were individually injected into a fluidic platform to generate tiny droplets. The evolution of the fluorescence intensity recorded in the absence of n-propyl gallate in the aqueous solution is illustrated in Fig.6-12. A shorter delay time was observed as compared to the previous experiment in the presence of nPG (Fig. 6-7).

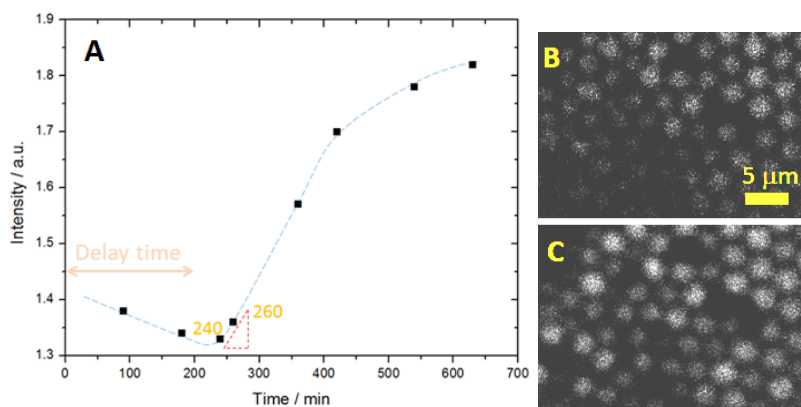


Figure 6-12: The evolution of the fluorescence intensity from the enzymatic reaction in the absence of nPG. The data at the 240th and 260th minute were used to estimate the enzyme kinetics. The snapshots of the array of droplets containing enzyme and substrate molecules without the addition of nPG at minute 240 (B), and 260 (C) are shown.

The increase in the fluorescence intensity and hence the enhancement of fluorescent product in each droplet from the 240th to the 260th minute is plotted in a histogram (Fig.6-13) when the concentration of the enzyme solution was 0.1 nM. From this histogram (Fig.6-13), the concentration of fluorescein was seen to be periodically increased in four peaks which can be interpreted as corresponding to different numbers of enzymes encapsulated into the droplets. The obtained K_{cat} from these experiments was around 3.8 sec^{-1} .

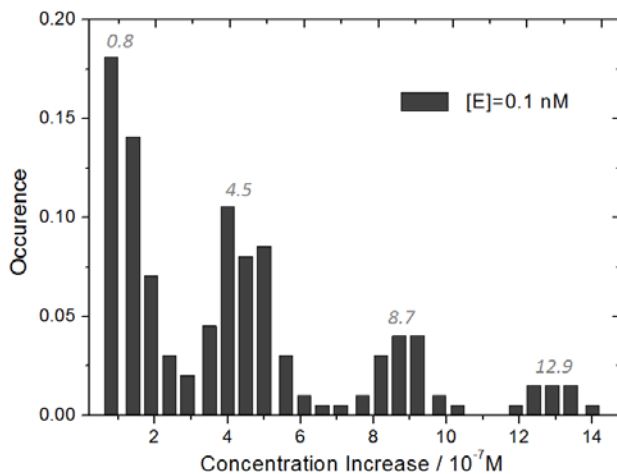


Figure 6-13: The increasing fluorescence intensity from the 240th to the 260th minute. Four peaks can be interpreted as indicating the occupancy of droplets by (0, 1, 2 and 3) enzymes. The continuous phase was silicone oil with 4% Span80 and the aqueous phase was FDGlu (200 μ M) and, β -glucosidase (0.1 nM) in PBS solution.

To confirm this single-enzyme encapsulation and our interpretation, another experiment was performed by using the two-fold greater concentration of the enzyme (0.2 nM) than that in the previous experiment. The histogram of the increasing concentration of fluorescein in each droplet is plotted in Fig.6-14. For this case the resulting K_{cat} was around 4.5 sec⁻¹.

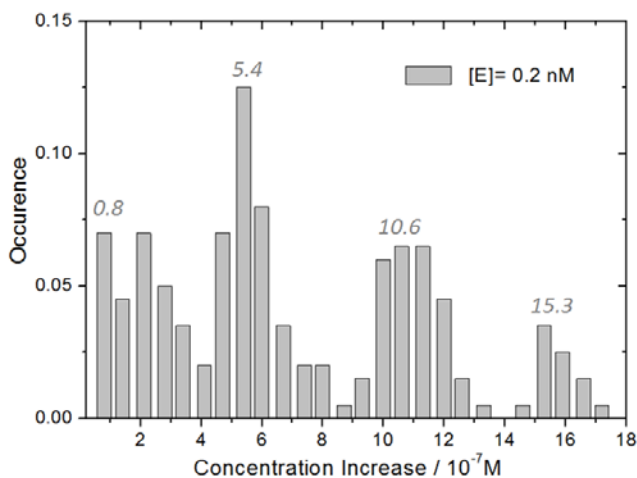


Figure 6-14: The increasing fluorescence intensity from the 20th to the 30th minute. Four peaks can be interpreted as indicating the occupancy of droplets by (0, 1, 2 and 3) enzymes. The continuous phase was a silicone oil with 4% Span80 and the aqueous phase was FDGlu (200 μ M) and β -glucosidase (0.2 nM) in PBS solution.

Single-enzyme Encapsulation and Detection

In Fig.6-15, the experimental data obtained from the enzyme solutions are plotted as fractional occurrence of droplets with enzyme occupancy (0, 1, 2 or 3) using bars of dark grey and light grey for the 0.1 and 0.2 nM of enzyme solution, respectively. The Poisson distributions for the first and second cases are depicted as dotted and straight lines, respectively. As shown, the histograms for both experiments can be well fitted to Poisson distributions (Fig.6-15) with mean occupancies λ of 0.62 and 1.24. Considering the amount of enzyme encapsulated into one droplet (diameter of 2.8 μm) by calculation, we found the averaged enzyme occupancies are around 0.7 and 1.4 molecules for the concentration of enzyme of 0.1 and 0.2 nM, respectively. These calculated values correspond well to the mean occupancies (λ) from the Poisson fitting curve. In addition, The size distributions of generated droplets for both experiment are highly monodisperse (approximately 97-98 %).

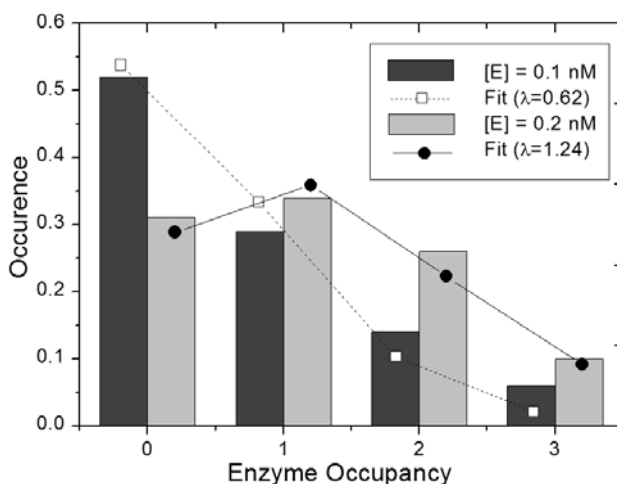


Figure 6-15: Two histograms express the distribution of the occupancy of enzymes (0, 1, 2 and 3) per droplet. The dark grey bar and the light grey bar depict the data distribution when the enzyme solution was 0.1 and 0.2 nM, respectively. The data for 0.1 and 0.2 nM enzyme solution were fitted to a Poisson distribution as shown by a dotted line and a solid line, respectively. The mean occupancy λ for these fitting was 0.62 and 1.24, respectively.

These data indicate that single-enzyme encapsulation was obtained into the tiny aqueous droplets generated in our device. The evolution of the fluorescence intensity as determined from the kinetic activity of the encapsulated enzymes ($3.8\text{-}4.5 \text{ sec}^{-1}$) was lower than the enzymatic kinetic activity observed in bulk experiments (5.7 sec^{-1}), but much higher than the kinetic activities observed in the presence of nPG as will be further discussed in the following section.

Discussion

From these experiments, the kinetic activity obtained from the experiments in droplets in our micro- and nanofluidic device is about 25% lower than the value obtained from a bulk experiment. This observation corresponds to several works reported before in the literature mentioning that the kinetic activity obtained in the droplets from microfluidic devices were marginally lower than that in the bulk experiment.^{25, 26}

Furthermore, during the first period of measurement, the intensity remained almost constant which is indicated as a *delay time* in Fig.6-7 and 6-12. In the second phase the intensity, however, enhanced approximately proportionally to the incubation time. Initially we thought this observation resulted from the fact that the signal of the fluorescein needed to be accumulated until it overcame the background noise. However, considering the lowest concentration of the fluorescein from the calibration curve, we found that the lowest amount of fluorescein molecules whose signal was distinguishable was approximately 7000 molecules. In case of a K_{cat} of 3.8 sec^{-1} , the fluorescence intensity should then start to increase at around 30th minute. In our experiment however, it took place only at around the 230th minute (Fig.6-12). Therefore the main cause of the delay is not the background noise. A possible explanation is that this delay time occurs because the fluorescent product which was generated by the reaction was consumed in a second process. Subsequently, after the delay time, this phenomena became less pronounced (for example due to saturation) in an increasing fluorescence concentration in the droplets.

As to the nature of this second process, firstly we can speculate that after the enzymatic reaction, the generated product diffuses to the interface between water and oil phases and was adsorbed by surfactant molecules. After the surface of a droplet became saturated by the fluorescein molecules ("*delay time*"), the increasing intensity in the droplet was then observed. However, in this hypothesis we need to assume that the fluorescein molecules which became adsorbed at the interface cannot fluoresce anymore. Apart from adsorption of the fluorescein molecules, a temporary adsorption of the enzyme and the substrate molecules is also possible. However, it would be hard to explain why the enzyme would adsorb to the interface only initially. Conversely, if it would be continuously adsorbed to the interface, we should see a continuous (partial) suppression of the activity.

Secondly, we can speculate that the fluorescein molecules diffuse into the oil phase. In general, when two immiscible fluids are partitioned, chemicals in one fluid can cross the partitioning border to another fluid until equilibrium is reached. From this hypothesis, the fluorescein molecules were produced and crossed the interface to the oil phase in the beginning (“*delay time*”). When reaching equilibrium, the fluorescein molecules produced from the enzymatic reaction then remained inside a droplet resulting in the increasing fluorescence intensity in each droplet. At present we cannot distinguish between both hypotheses, and they must be confirmed from further investigations such as by changing the types of surfactant and oil, performing the analysis from different dimensions of droplets and so on.

In the experiment in the presence of *n*-propyl gallate (nPG), the measured kinetic activity was only 1.6 sec^{-1} , while it increased to $3.8\text{-}4.5 \text{ sec}^{-1}$ in its absence. On the basis of this we speculate that the nPG can behave as an inhibitor for the enzymatic reaction. When considering the structure of nPG as shown in Fig.6-15A, its structure is somewhat similar to one side of the structure of cellobiose which is a natural substrate of β -glucosidase (see Fig.6-15). Thus, nPG might indeed inhibit or disturb the interaction between the glucosidase enzyme and the substrate molecules.

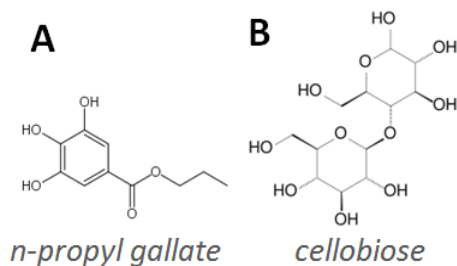


Figure 6-15: Molecular structures of (A) *n*-propyl gallate and (B) cellobiose.

Additionally, in the experiment in the absence of *n*-propyl gallate (nPG), the fluorescein molecules produced from the enzymatic reaction might undergo photobleaching. Indeed, the photobleaching effect might be less pronounced in our experiment since the half time of the fluorescein molecule under illumination from our setup is around 5 minutes (see Appendix A). Upon the observation, the UV light was, however, illuminated for a few seconds only for every single snapshot taken. Otherwise this photobleaching effect might be the reason of the

Chapter: 6

relative low value of the enzyme kinetic activity from our experiment. The effect of photobleaching should be further investigated by experiments with other anti-oxidant reagents.

Conclusion

We have demonstrated a micro- and nanofluidic platform for creating droplet arrays encapsulating single enzyme molecules. The enzyme β -glucosidase was selected for a first demonstration generating fluorescent product. Single-molecule detection is generally prohibited by the background noise from the environment such as the solvent and the device material which are larger than the signal from the molecule of interest. The reduction of the background noise by compartmentalization of the system into tiny carriers allowing high enzyme and product concentrations and selection of the proper materials played a role to achieve single-molecule detection. Droplets were generated in a hydrophobized glass-based device. In case of low enzymatic reaction rates, the generated droplets have to be stable upon prolonged measurement, making it necessary to create spherical droplets. The histogram of the rate of fluorescence intensity increase and hence the turnover number of the enzymatic reaction in each droplet showed periodically-increased peaks revealing the occupancy of droplets by multiples of a single enzyme. The distributions fitted well to a Poisson distribution verifying the achieved encapsulation of single enzymes. The resulting kinetic activity was somewhat lower than that from the bulk experiment.

Acknowledgement

We would like to thank to Serve Kengen (Microbiology Group, Wageningen University, The Netherlands) for providing the substrate, (4-methylumbelliferyl- β -D-glucopyranoside) and the enzyme (β -glucosidase) for these experiments as well as arranging the essential discussions and the practical work. Also, we appreciate the training and technical support from Richard Egberink (Molecular Nanofabrication; MNF, University of Twente, The Netherlands) for the fluorescence spectrometer.

References

1. H. P. Lu, L. Y. Xun and X. S. Xie, *Science*, 1998, **282**, 1877-1882.
2. W. Min, I. V. Gopich, B. P. English, S. C. Kou, X. S. Xie and A. Szabo, *J Phys Chem B*, 2006, **110**, 20093-20097.
3. K. Velonia, O. Flomenbom, D. Loos, S. Masuo, M. Cotlet, Y. Engelborghs, J. Hofkens, A. E. Rowan, J. Klafter, R. J. M. Nolte and F. C. de Schryver, *Angew Chem Int Edit*, 2005, **44**, 560-564.
4. Y. Rondelez, G. Tresset, K. V. Tabata, H. Arata, H. Fujita, S. Takeuchi and H. Noji, *Nat Biotechnol*, 2005, **23**, 361-365.
5. S. Sakakihara, S. Araki, R. Iino and H. Noji, *Lab Chip*, 2010, **10**, 3355-3362.
6. T. M. Hsin and E. S. Yeung, *Angew Chem Int Edit*, 2007, **46**, 8032-8035.
7. S. M. Christensen, P. Y. Bolinger, N. S. Hatzakis, M. W. Mortensen and D. Stamou, *Nat Nanotechnol*, 2012, **7**, 51-55.
8. B. Lu, S. Y. Zheng, B. Q. Quach and Y. C. Tai, *Lab Chip*, 2010, **10**, 1826-1834.
9. A. Piruska, I. Nikcevic, S. H. Lee, C. Ahn, W. R. Heineman, P. A. Limbach and C. J. Seliskar, *Lab Chip*, 2005, **5**, 1348-1354.
10. T. T. Fu, D. Funfschilling, Y. Ma and H. Z. Li, *Microfluid Nanofluid*, 2010, **8**, 467-475.
11. S. J. Zeng, B. W. Li, X. O. Su, J. H. Qin and B. C. Lin, *Lab Chip*, 2009, **9**, 1340-1343.
12. A. J. C. Kuehne and D. A. Weitz, *Chem Commun*, 2011, **47**, 12379-12381.
13. L. L. Shui, A. van den Berg and J. C. T. Eijkel, *Microfluid Nanofluid*, 2011, **11**, 87-92.
14. Y. S. Heo, L. M. Cabrera, J. W. Song, N. Futai, Y. C. Tung, G. D. Smith and S. Takayama, *Anal Chem*, 2007, **79**, 1126-1134.
15. S. W. M. Kengen, E. J. Luesink, A. J. M. Stams and A. J. B. Zehnder, *Eur J Biochem*, 1993, **213**, 305-312.
16. J. H. G. Lebbink, T. Kaper, S. W. M. Kengen, J. van der Oost and W. M. de Vos, *Method Enzymol*, 2001, **330**, 364-379.
17. D. M. Broadhead and J. Butterworth, *Clin Chim Acta*, 1977, **75**, 155-161.
18. J. W. M. Visser, A. A. M. Jongeling and H. J. Tanke, *J Histochem Cytochem*, 1979, **27**, 32-35.
19. D. W. Fink and W. R. Koehler, *Anal Chem*, 1970, **42**, 990-&.
20. www.schott.com.
21. L. L. Song, E. J. Hennink, I. T. Young and H. J. Tanke, *Biophys J*, 1995, **68**, 2588-2600.
22. H. Giloh and J. W. Sedat, *Science*, 1982, **217**, 1252-1255.
23. A. K. Gaigalas, L. Wang, K. D. Cole and E. Humphries, *J Phys Chem A*, 2004, **108**, 4378-4384.
24. M. Battaglia, D. Pozzi, S. Grimaldi and T. Parasassi, *Biotech Histochem*, 1994, **69**, 152-156.
25. Y. Liu, S. Y. Jung and C. P. Collier, *Anal Chem*, 2009, **81**, 4922-4928.
26. L. Mazutis, J. C. Baret, P. Treacy, Y. Skhiri, A. F. Araghi, M. Ryckelynck, V. Taly and A. D. Griffiths, *Lab Chip*, 2009, **9**, 2902-2908.

CHAPTER 7:

Summary and Perspective

In the last chapter, a brief description of every chapter is given and the achieved results are summarized. Additionally, we propose several aspects to improve our device as well as recommend possible applications.

Summary

In this thesis, we have demonstrated the application of micro- and nanofluidic devices to generate an array of aqueous droplets in oil phase for single-enzyme encapsulation and activity measurement. We chose droplet-based microfluidics for this purpose of monitoring single-enzyme reactions since the generated droplets can be modulated by changing the fluidic flows as well as the geometry of the micro- and nanofluidic channels. This droplet-based microfluidics was discussed regarding the aspects of the generation and manipulation of droplets, their applications, and the recent work which has been performed by many researchers. The enzymatic reaction of beta-glucosidase to produce fluorescein was chosen as the model reaction for this assay. Glass material was used to fabricate the devices to avoid a high background noise for the optical measurements. In addition, a femtolitre compartmentalization of the aqueous system was achieved by using devices with both nanochannels and microchannels to diminish the background signal from solvent molecules and substrate.

Since the glass-based micro- and nanofluidic device is inherently hydrophilic, it requires to be hydrophobized for facilitating the formation of an water-in-oil emulsion. Conventional hydrophobization methods were performed on plain substrates and then multisubstrates were integrated by several integration techniques. We propose an integration technique operated at room temperature at the chip level by using an UV adhesive. However, our integration method puts a limit to the geometry of the fluidic channels which should be above 10 μm wide and 15 μm high and therefore is not suitable to implement on devices containing nanofluidic channels. Subsequently therefore, a new in-channel hydrophobization method was developed by using a silicone oil and UV light. After the thermal bonding of two patterned glass substrates, the glass-based micro- and nanofluidic device can be hydrophobized by our method at the chip level. Finally, the hydrophobized chip can be used to generate water-in-oil emulsions.

For the single-enzyme activity measurements, we demonstrated the successful encapsulation of single enzymes into femtolitre carriers. The histograms of the enhancing fluorescence intensity express the periodic increase in the fluorescence intensity, and hence the turnover

number of the enzymatic reaction. The occupancies of the enzyme per droplet were determined by fitting to the Poisson distribution and were found to be in agreement with the calculated values. The obtained kinetic activity was somewhat lower than the value observed from the experiment in bulk probably due to effects of the confined volume.

Perspectives

Droplet Fusion

Our micro- and nanofluidic device can in principle be modified for loading enzyme and substrate solutions separately before fusion by application of shear force as shown in Fig.7-1. This scheme is especially suitable for fast enzymatic reactions where the reaction rapidly proceeds after the two aqueous streams are merged as the preliminary test of this system can be seen in appendix C

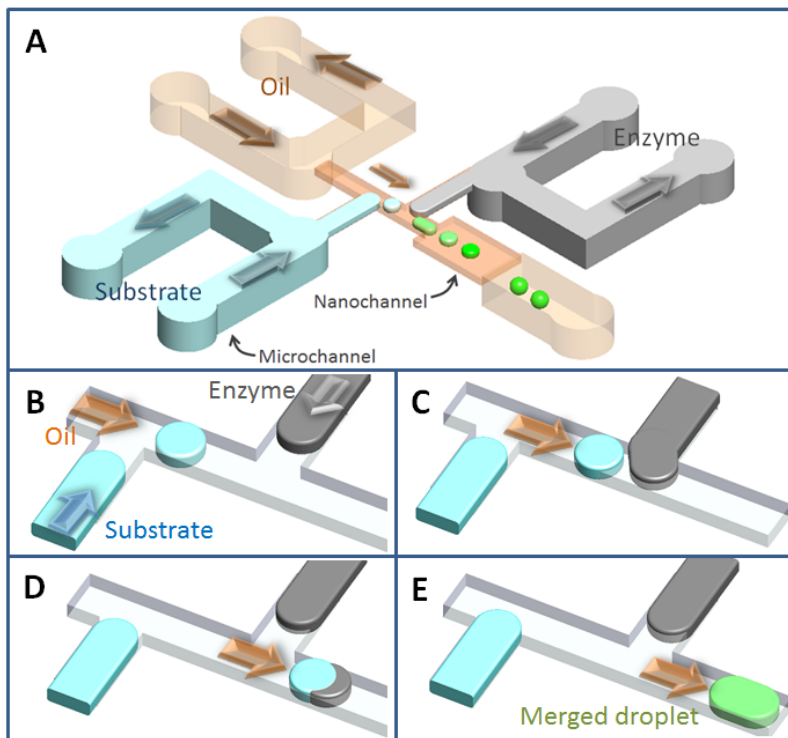


Figure 7-1: Schematic of a nanofluidic network consisting of two T-junctions; A: at the first junction, the first aqueous droplet (blue) is created in the oil phase. B: The first droplet flows to contact the tip of a second aqueous stream (green). C and D: The two aqueous solutions merge creating the product droplet (purple). The arrows express the fluidic direction.

Expansion chamber to enhance the efficiency of droplet fusion

One drawback of the droplet fusion by the passive approach as shown in Fig.7-1 is the low success rate of fusion as shown in Appendix C resulting from, for instance, the generation of a droplet by the second water stream before the upcoming droplet merges to this stream, as well as the short contact time between the two aqueous streams leading to a lower possibility of coalescence of the two streams. In order to retard the droplet formation by the second water stream and increase the contact time between droplet and second stream, an extra chamber could be integrated just downstream of the second T-junction¹ as shown in Fig.7-2.

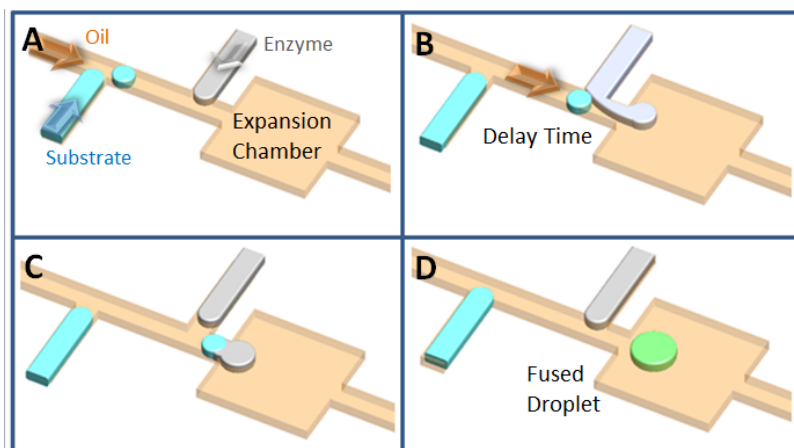


Figure 7-2: Illustration of a fluidic network with an expansion chamber located downstream of the T-junction to enhance the droplet fusion. The arrows express the fluidic flows. The expansion chamber can retard the droplet formation and slow down the movement of the second stream resulting in a longer time for the first droplet to contact with the second stream.

In general, a droplet is generated when the tip of the dispersed stream enters a T-junction far enough to make the shear force from the continuous stream large enough to break up that tip. When an extra expansion chamber would be used (Fig.7-2A), the tip of the second stream (illustrated in grey color in Fig.7-2) enters the T-junction and the expansion chamber, and the pressure exerting on the tip is relieved and hence this pressure takes a longer time (*delay time*) to build up and become large enough to break up this tip (Fig.7-2 B). The tip of the second water stream thus has more time to form a larger droplet. When reaching the extra chamber, the tip of the second stream furthermore undergoes a slower movement due to the change in the hydrodynamics, giving the consecutive droplet of the first stream (illustrated in blue color in Fig.7-2) more time to contact and eventually coalesce with the second

Chapter: 7

stream (Fig.7-2 B and C). After complete fusion, the fused droplet travels along this chamber and then enters the outlet channel. (Fig.7-2 D).

Study of the effect of inhibitors

The effect of a range of inhibitors on the enzymatic reaction can be studied on the single-enzyme level in a microfluidic platform as earlier reported in the literature for larger numbers of enzymes.² In our device, a mixture of enzyme and substrate solution can be injected into the platform to generate the first droplet and another aqueous stream containing an enzyme inhibitor can be separately injected into the platform and then merge with the first droplet. This scheme is similar to the schematic shown in Fig.7-1.

Alternatively, by adjusting fluidic networks for four fluidic flows (i.e. oil, enzyme, substrate, inhibitor), all solutions can be separately loaded into the device generating droplets for enzymatic analysis in the presence or in the absence of inhibitor in one single array as depicted in Fig.7-3.

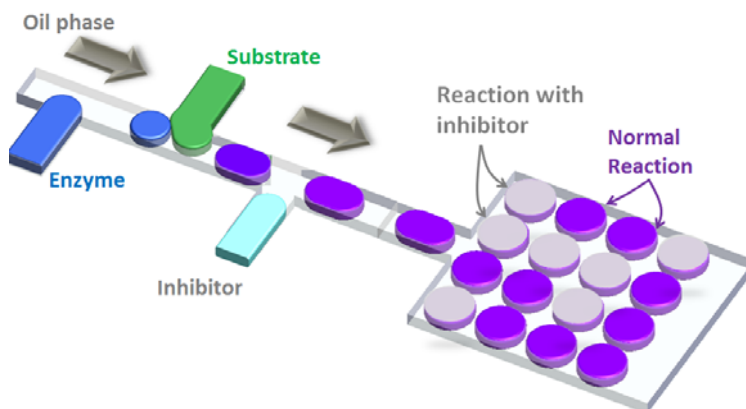


Figure 7-3: Illustration of a fluidic network with four branches of nanochannels for individually loading the oil, enzyme, substrate and inhibitor solutions. This platform can be used to study the effect of a range of inhibitors on the enzymatic reaction in one single array.

Break-up of a large droplet to generate small droplets

Though the nanofluidic networks can be fabricated and used for generation of femtolitre droplets, the multiple steps of fluidic operations inside this nanofluidic network is not so straightforward to implement. As compared to larger fluidic channels, the nanofluidic channels can easily become clogged by debris or any contaminants. The fluidic resistance in the nanofluidic network is dominant in the entire fluidic chip, therefore, when the dimension

of nanochannel is smaller, a higher applied pressure is required to inject fluids into the device. This higher pressure can create the leakage in the fluidic setup especially at the connectors between the capillary tubing and the fluidic device. To reduce the fluidic resistance and avoid the aforementioned issues, we propose the idea to generate small droplets from the break-up of a larger droplet.^{3,4}

In this thesis, the tiny droplets were generated using a narrow and shallow channel (for instance, 4 μm wide and 500 nm deep) where the droplet is confined from two directions (width and height). We think that the droplets can also be generated from a larger droplet in a wider channel (for instance, 50 μm wide and 500 nm deep) which then undergoes droplet fusion of two reagents. Subsequently the large merged droplet is homogeneously split up to form uniform tiny droplets. Two designs for a break-up of a large droplet which are proposed here are (i) the array of pillars and (ii) the intersection between the nano- and microchannels.

(i) *An array of pillars inside the outlet channel:* In this design, the nanofluidic network comprises the inlet nanochannels, two T-junctions and a wide outlet channel containing the array of pillars as shown in Fig.7-4A. After droplet fusion, a merged large droplet (shown in green in Fig.7-4B) enters the outlet channel and collides with a pillar and breaks up into smaller droplets which flow further and collide with other pillars generating smaller droplets until they pass through this array in the outlet. The dimension of the obtained droplets will be related to the applied flow rate and the size of the pillars.³

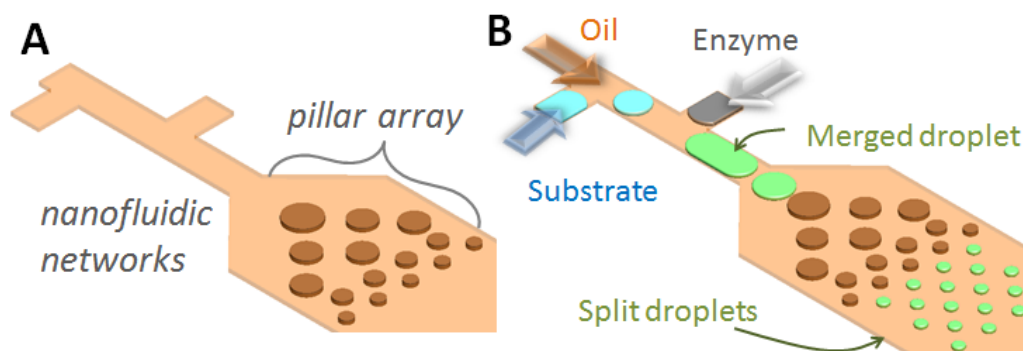


Figure 7-4: Illustration of a nanofluidic network containing an array of pillars in the outlet channel (A). Two reagents as shown in blue and grey colors are separately injected into a fluidic device to generate water-in-oil emulsions. After coalescence of the two reagents, the merged droplet (green color) enters the outlet channel containing the array of pillars. The merged droplet is then broken up after colliding with these pillars creating the smaller droplets.

Chapter: 7

(ii) *An intersection between nano- and microchannels:* This design is similar to our current design. At the intersection between nano- and microchannels, the Laplace pressure induces the break-up of the large droplets or even a stratified stream to generate monodisperse smaller droplets. The dimension of the smaller droplets obtained from this system is governed either by the depth of the nanochannel when the Laplace pressure is dominant or by the applied flow rate when the shear force is dominant.⁴ Therefore, it is not necessary for the initial merged droplets to be very small as they can later at this intersection be broken up to form highly-monodisperse tiny droplets.

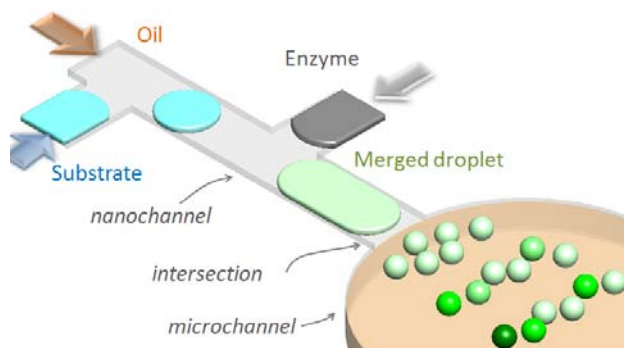


Figure 7-5: Illustration of a micro- and nanofluidic network with an intersection between micro- and nanochannel. When flowing through this intersection, a merged large droplet is broken up due to the Laplace pressure to form smaller droplets which are highly monodisperse. The size of the obtained tiny droplets is governed by the height of the nanochannel.[ref.4]

Reduced background from a device

One prospect for improvement of our micro- and nanofluidic platform for monitoring fast enzymatic reactions is by using a thin fused silica glass substrate for the fabrication of the device, which expresses significantly lower auto-fluorescence than borofloat glass. The thin fused silica glass substrate can highly reduce the background noise as compared to the borofloat glass substrate.⁵ It is however noteworthy that the fused silica substrate is generally less preferential for microfabrication since it is more expensive and difficult to handle due to its worse mechanical properties compared to a borosilicate substrate as well as its considerably higher fusion temperature.

Enzymatic reactions at elevated temperature

In addition, in the microfluidic platform, the study of thermally induced reactions in a precisely-controlled mode is plausible by integrating a thin-layer heater into the microfluidic

device. During the fabrication of the microfluidic platform, a metal thin film can be deposited and patterned onto the glass substrate to be used as the heating wire. The integrated wire(s) can be activated by, for example, an applied electric field to precisely modulate the temperature inside the microchannel. This integrated device might be promising for the study of the enzymatic reaction at different temperatures.

Surfactant and Oil

Lastly, different types of surfactant and oil should be considered and further studied for their compatibility with the biomolecules used in each reaction. In our experiments, when the generated droplets encapsulating enzyme and substrate solution were incubated for a long time (a few days), we found that the fluorescence intensity of all droplets became equalized. This observation seems to suggest that the fluorescein molecules underwent diffusion through the layer of surfactant and the oil phase. Furthermore, it was reported before that surfactant bilayers can be permeable for small molecules and these molecule can be transported to other droplets by diffusion.⁶ On the other hand, this phenomena might be interesting since such a device could be used for studying the diffusion of drug(s) or small molecules from one droplet compartmented by the lipid molecules to another compartmented droplet, in a manner that shows similarity to transport processes in the human body.

References

1. J. Sivasamy, Y. C. Chim, T. N. Wong, N. T. Nguyen and L. Yobas, *Microfluid Nanofluid*, 2010, **8**, 409-416.
 2. O. J. Miller, A. El Harrak, T. Mangeat, J. C. Baret, L. Frenz, B. El Debs, E. Mayot, M. L. Samuels, E. K. Rooney, P. Dieu, M. Galvan, D. R. Link and A. D. Griffiths, *P Natl Acad Sci USA*, 2012, **109**, 378-383.
 3. A. R. Abate and D. A. Weitz, *Lab Chip*, 2011, **11**, 1911-1915.
 4. L. L. Shui, A. van den Berg and J. C. T. Eijkel, *Microfluid Nanofluid*, 2011, **11**, 87-92.
 5. L. M. Davis, B. K. Canfield, X. X. Li, W. H. Hofmeister, G. Q. Shen, I. P. Lescano-Mendoza, B. W. Bomar, J. P. Wikswo, D. A. Markov, P. C. Samson, C. Daniel, Z. Sikorski and W. N. Robinson, *P Soc Photo-Opt Ins*, 2008, **7035**.
 6. J. C. Baret, *Lab Chip*, 2012, **12**, 422-433.
-

APPENDIX A

Photobleaching Experiment

In this appendix, we present the experiment results to test the photobleaching effect on the fluorescein solution in our existing setup. Also, an optimization of the addition of anti-oxidant reagent (n-propyl gallate, nPG) was performed to reduce this effect.

Photobleaching Effect

One drawback of the fluorescein molecule is its relative high rate of photobleaching by which the fluorescent molecules lose their ability to fluoresce due to the photo-induced chemical destruction during the exposure to the excitation light in the presence of oxygen molecules.¹ Via this process, the fluorescent intensity reduces irreversibly leading to the misinterpretation of the amount of fluorescent molecules in the system. To avoid this problem, oxygen molecules should be removed from the system and anti-oxidant reagent should be added to the solution. Addition of the anti-oxidant reagent e.g. n-propyl gallate (n-PG) into a solution can diminish the photobleaching effect especially in a fluorescein solution.²⁻⁴ Therefore, the photobleaching effect on the fluorescein molecules from our existing setup and the optimization of the amount of this anti-oxidant reagent added into the solution have to be studied. The water-in-oil emulsions were prepared from fluorescein solution (50 μ M fluorescein in PBS solution at pH 7) with or without n-PG as an aqueous phase and the silicone oil as a continuous phase. Then, the emulsion was placed between two glass substrates for the excitation by UV lamp and observation by a fluorescence microscope (DMI 5000M, Leica) equipped with mercury lamp and high-sensitivity camera (EMCCD, Andor Ixon, UK). Before mixing, each solution was degassed by placing into the desiccator to remove oxygen molecules in the solution. Firstly, no anti-oxidant reagent was added into the fluorescent solution. The light from UV lamp was exposed to one area (red circle in Fig.A-1) and the fluorescence intensity was measured upon UV exposure (from 0 to 1080 sec) as can be seen in Fig.A-1 and Fig.A-2 *Left*.

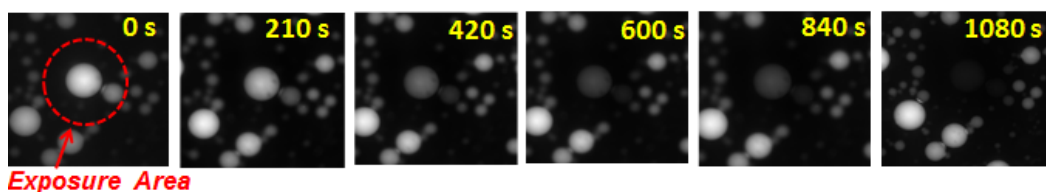


Figure A-1: The decreasing fluorescent intensity due to the photobleaching effect on an aqueous droplet in oil without the addition of n-PG.

Then, the decreasing fluorescence intensity was plotted against the exposure time as shown in Fig.A-2 *Left*. The fluorescence intensity decreased exponentially as a function of the exposure time corresponding to the following equation,

Appendix: A

$$I = I_0 e^{-t/T} \quad \text{Eqn.(A-1)}$$

When I = Fluorescence Intensity
 I_0 = Initial fluorescence intensity
 t = Exposure time
 T = Life time of a fluorescent molecule

From Eqn.(A-1),

$$\log(I) - \log(I_0) = \log(e^{-t/T}) \quad \text{Eqn.(A-2)}$$

$$\log(I) - \log(I_0) \cong -0.434\left(\frac{t}{T}\right) \quad \text{Eqn.(A-3)}$$

A plot of the logarithm of the intensity against the exposure time (Fig.A-2 *Right*) can thus determine the half time ($t_{1/2}$) of this fluorescent molecule under the illumination conditions of our existing setup and is found to be 5 minutes.

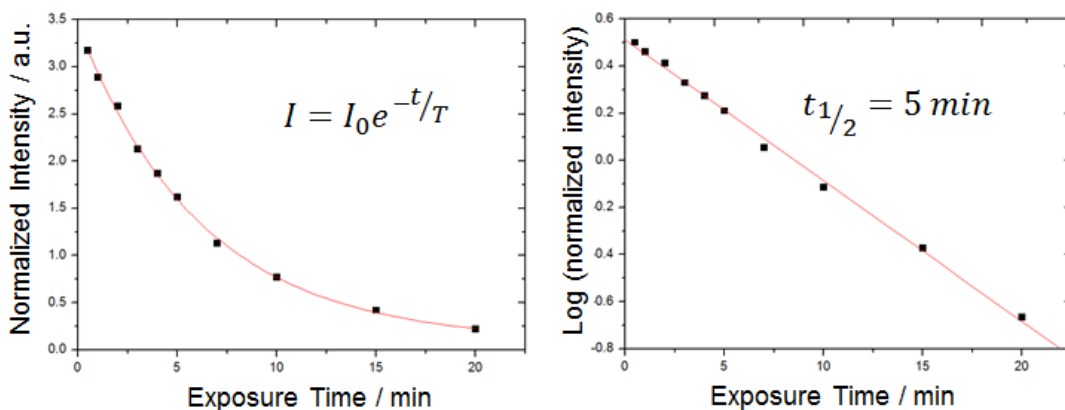


Figure A-2: The exponential decay of the fluorescence intensity under illumination by a UV-lamp from our setup (Left). The half time ($t_{1/2}$) of this fluorophore can be determined from the plot of the logarithm of the intensity against the exposure time.

In addition, we performed the same experiment with other concentrations of fluorescein solution and found, interestingly, that when the concentration of fluorescein was lower, the half time ($t_{1/2}$) became relatively higher as illustrated in Fig.A-3. We speculate that this might be the self-quenching effect by which the fluorescence intensity reduced due to the interaction between fluorescent molecules and another fluorescent molecule or other species molecules in the environment.

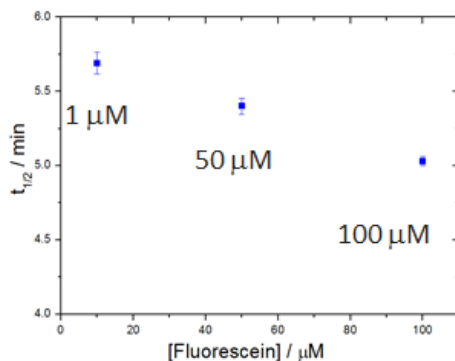


Figure A-3: The life time ($t_{1/2}$) of the fluorescein solution (pH 7) at different fluorescein concentrations.

Next, the amount of the anti-oxidant reagent added into the fluorescein solution was optimized. A solution of n-PG was prepared by dissolving n-PG powder in pure glycerol at a concentration of 50 g/L, and then diluted with an equal volume of PBS buffer (pH 7). All chemicals in these experiments were purchased from Sigma Aldrich, The Netherlands. The reduction in the rate of photobleaching was then plotted against the added concentration of n-PG as shown in Fig.A-4.

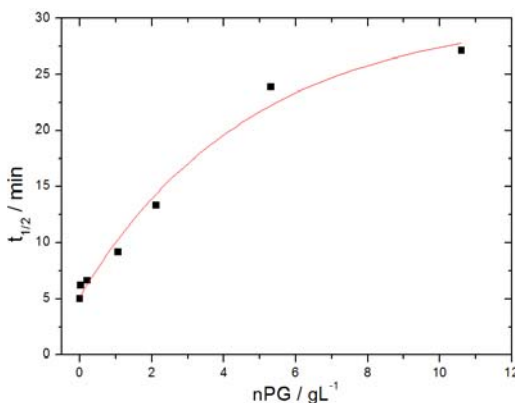


Figure A-4: The half time ($t_{1/2}$) of the fluorescent molecule increases proportionally with the concentration of added n-propyl gallate.

From this experiment it is clear that the addition of n-PG to the fluorescein solution can reduce the photobleaching effect. The higher the amount of n-PG, the smaller the photobleaching effect in the solution. However, when the amount of n-PG was higher than 5 g/L, the photobleaching effect was found to be only marginally further reduced. Thus, the optimal amount of n-PG in our solution was found to be around 5 g/L.

References

1. L. L. Song, E. J. Hennink, I. T. Young and H. J. Tanke, *Biophys J*, 1995, **68**, 2588-2600.
 2. H. Giloh and J. W. Sedat, *Science*, 1982, **217**, 1252-1255.
 3. A. K. Gaigalas, L. Wang, K. D. Cole and E. Humphries, *J Phys Chem A*, 2004, **108**, 4378-4384.
 4. M. Battaglia, D. Pozzi, S. Grimaldi and T. Parasassi, *Biotech Histochem*, 1994, **69**, 152-156.
-

APPENDIX B

Enzyme Kinetic Activity in Bulk Experiment by a Fluorescence Spectrometer

In this appendix, the experimental results to determine the enzyme kinetic activity of beta-glucosidase in bulk solution using a fluorescence spectrometer are detailed and fitted by different fitting methods.

Kinetic Activity in the bulk experiment determined from Fluorescence Spectrometer

Basically, the production rate (V) of the enzymatic reaction increases when the concentration of substrate, $[S]$, enhances until this concentration is high enough and the production rate reaches the maximal value (V_{max}). The production rate obeys the *Michaelis-Menten* equation (Eqn.B-1) and is illustrated in Fig.B-1. The turnover number (K_{cat}) which is defined as the number of substrate molecules converted to product per one enzyme molecule per unit of time is equivalent to the V_{max} divided by the concentration of enzyme $[E]$ as expressed in Eqn.B-2.

$$v = \frac{V_{max} [S]}{K_m + [S]} \quad \text{Eqn.(B-1)}$$

$$K_{cat} = \frac{V_{max}}{[E]} \quad \text{Eqn.(B-2)}$$

Where

v	=	Production rate
V_{max}	=	Maximum production rate
$[S]$	=	Concentration of substrate
K_m	=	<i>Michaelis-Menten</i> Constant
K_{cat}	=	Turnover number
$[E]$	=	Concentration of enzyme

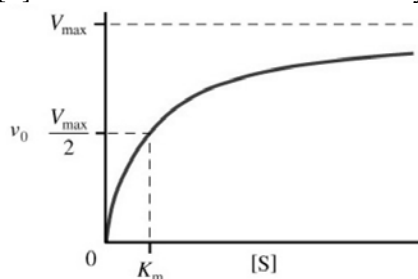


Figure B-1: An illustration showing the dependence of the production rate (v) on substrate concentration ($[S]$). K_m is the concentration of substrate at $v=V_{max}/2$.

To verify the reliability of the experiment performed in our droplet-based microfluidic platform, we have to compare the kinetic activity obtained from our device to that from the bulk experiment. Therefore, the kinetic activity of the enzymatic reaction was determined from a bulk experiment using a fluorescence spectrometer (Perkin Elmer). From the experiment on the fluorescence spectrometer, the obtained production rates of the reaction

Enzyme Kinetics in Bulk Experiment

are plotted as a function of the concentration of substrate (Fig.B-2). From the displayed fitting curve, the resulting K_m and K_{cat} are $25.6 \mu\text{M}$ and 5.7 sec^{-1} , respectively.

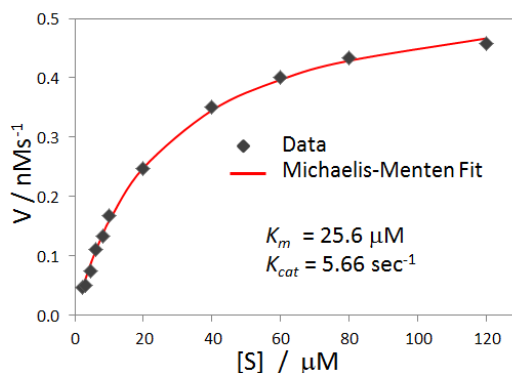


Figure B-2: The experimental result of the enzymatic reaction from a fluorescence spectrometer and the Michaelis-Menten fitting curve.

To ensure obtaining the correct turnover number and K_m from the enzymatic reaction, we use different models to plot the data from the fluorescence spectrometer. Another fitting method can be employed when the reciprocal of the production rate ($1/V$) is plotted against the reciprocal of the concentration of substrate ($1/[S]$) resulting in a so-called *Lineweaver-Burk plot*. The slope and y-intercept of this figure are then equivalent to (K_m/V_{max}) and $(1/V_{max})$, respectively, as shown in Fig.B-3.

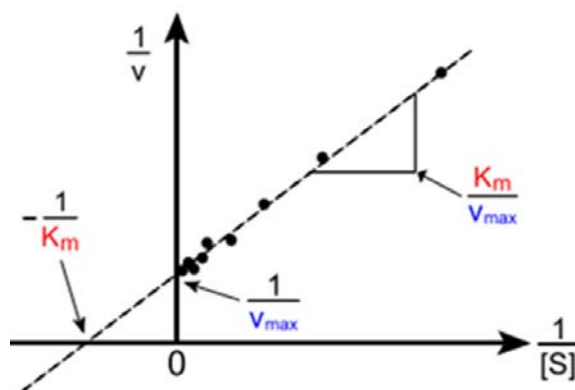


Figure B-3: Lineweaver-Burk plot for determining the V_{max} and K_m of the enzymatic reaction.

Thus, the experimental data from Fig.B-2 were rearranged to obtain a *Lineweaver-Burk plot* as shown in Fig. B-4. From the *Lineweaver-Burk plot*, the K_m obtained is $35 \mu\text{M}$ and K_{cat} is around 6.8 sec^{-1} .

Appendix: B

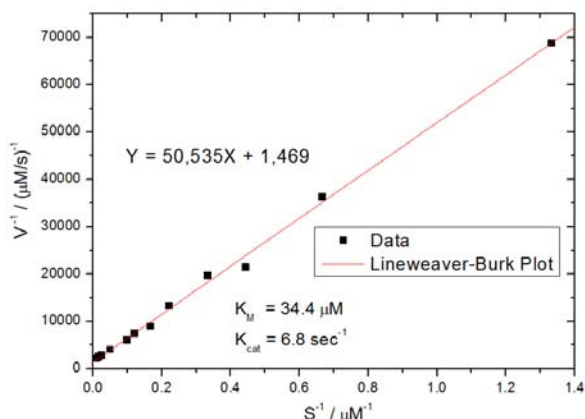


Figure B-4: A plot of the reciprocal of the production rate and concentration of enzyme fitted to the Lineweaver-Burk plot. The obtained K_m and K_{cat} are $34.4 \mu\text{M}$ and 6.7 sec^{-1} , respectively.

Additionally, when the *Michaelis-Menten* equation is inverted and multiplied by V_{max}

$$\frac{V_{max}}{v} = \frac{V_{max}(K_m + [S])}{V_{max}[S]} \quad \text{Eqn.(B-3)}$$

$$\frac{V_{max}}{v} = \frac{K_m + [S]}{[S]} \quad \text{Eqn.(B-4)}$$

$$V_{max} = \frac{vK_m}{[S]} + v \quad \text{Eqn.(B-5)}$$

$$v = -\frac{vK_m}{[S]} + V_{max} \quad \text{Eqn.(B-6)}$$

Therefore, a plot of V and $V/[S]$ can also determine K_m and V_{max} and is known as a *Eadie-Hofstee diagram* (See Fig.B-5).

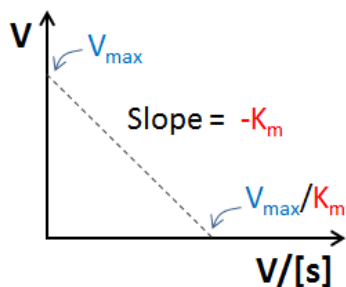


Figure B-5: Eadie-Hofstee diagram determining the K_m and V_{max}

Thus, the experimental data is plotted as the production rate (V) against $V/[S]$ as depicted in Fig.B-6. The obtained K_m and K_{cat} now are $25.6 \mu\text{M}$ and 5.6 sec^{-1} , respectively.

Enzyme Kinetics in Bulk Experiment

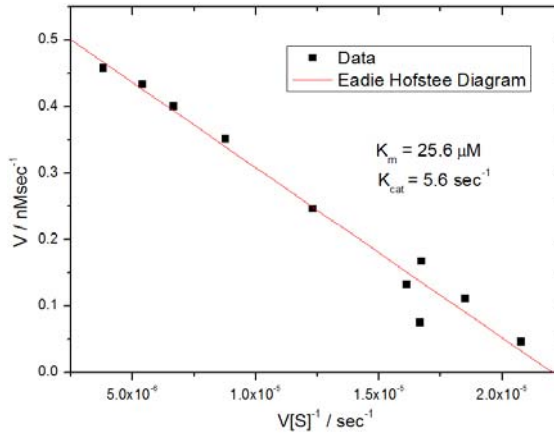


Figure B-6: A plot of the production rate against the ratio of production rate to the concentration of enzyme fitted to the so-called Eadie-Hofstee plot. K_m and K_{cat} are $25.6 \mu\text{M}$ and 5.6sec^{-1} , respectively.

Alternatively still, the *Michaelis-Menten* equation (Eqn.B-1) can be rearranged as

$$K_m + [S] = \frac{V_{max} [S]}{v} \quad \text{Eqn.(B-7)}$$

$$\frac{V_{max} [S]}{V_{max} v} = \frac{1}{V_{max}} [S] + \frac{K_m}{V_{max}} \quad \text{Eqn.(B-8)}$$

$$\frac{[S]}{v} = \frac{1}{V_{max}} [S] + \frac{K_m}{V_{max}} \quad \text{Eqn.(B-9)}$$

A plot of $[S]/V$ against $[S]$, so-called *Hanes-Woolf plot*, can now estimate the value of K_m and V_{max} as illustrated in Fig. B-7.

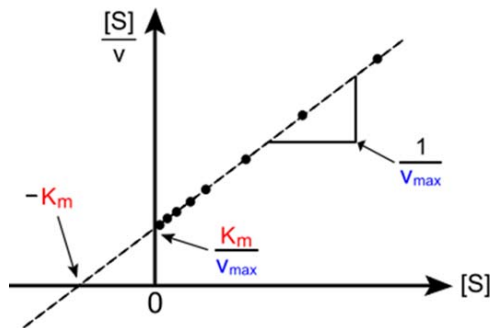


Figure B-7: The *Hanes-Woolf plot* determining the K_m and V_{max} .

Therefore, the experimental data is plotted of $[S]/V$ against $[S]$ and fitted to *Hanes Woolf plot* as shown in Fig.B-8. The resulting K_m and K_{cat} now are $26.4 \mu\text{M}$ and 5.67sec^{-1} , respectively.

Appendix: B

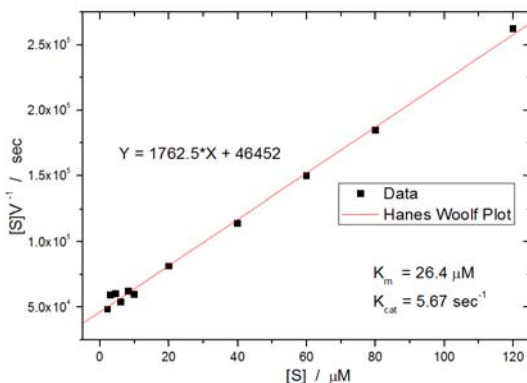


Figure B-8: A plot of $[S]V$ and $[S]$ fitted to a Hanes Woolf plot estimates the values of K_m and K_{cat} as $26.4 \mu\text{M}$ and 5.67 sec^{-1} , respectively.

Consequently, the results obtained in bulk experiments using a fluorescence spectrometer can be fitted to determine the values of K_m and K_{cat} of the enzymatic reaction with different fitting methods as summarized in Table B-1. The table B-1 also includes the coefficient of determination (R^2) from the different methods.

Table B-1: Enzyme kinetic activity determined from the bulk experiment by a fluorescence spectrometer and plotted by different methods.

	Fitting Method			
	<i>Michaelis-Menten</i>	<i>Lineweaver-Burk</i>	<i>Eadie-Hofstee</i>	<i>Hanes-Woolf</i>
$K_{cat} (\text{sec}^{-1})$	5.66	6.80	5.67	5.67
$K_m (\mu\text{M})$	25.6	34.4	25.6	26.4
R^2	0.99869	0.99642	0.97198	0.99656

From these fitting data, we regard the K_m and K_{cat} obtained from *Michaelis-Menten Plot* as the most reliable as compared to other fitting methods since the data is homogeneously distributed along the fitting curve (See Fig.B-2) and the R^2 obtained from this fitting plot is almost equivalent to 1 indicating the best fit of data to this fitting method. In addition, in this case, the data from *Lineweaver-Burk* is less trustworthy since the fitting curve was highly affected by the high value of the reciprocal of the concentration of substrate ($[S]^{-1}$) meaning that in this method the data at low concentration of the substrate is very essential. Practically, the error from a preparation of the reagent at low concentration, however, can occur which can strongly influence the fitting data from this method in an adverse manner.

APPENDIX C

Droplet Fusion

In this appendix, the preliminary test to investigate the droplet fusion behaviour of a micro- and nanofluidic device is described. Two aqueous phases containing fluorescein solution and PBS solution were used to generate two droplets for droplet fusion. The fusion mechanism was visualized by using a high speed camera. The change in the dimension and fluorescence intensity can identify the merged droplets from the original droplets. The droplet fusion can be achieved by using this platform, however, the efficiency of this fusion should be further improved.

Droplet fusion by a passive approach

A glass-based micro- and nano-fluidic chip was fabricated and hydrophobized by the methods which are described in chapter 3 and 5 of this thesis, respectively. This hydrophobized chip was mounted into the in-house chip holder and placed onto the inverted fluorescence microscope equipped with the mercury lamp and the high-sensitivity EMCCD camera. The solutions were loaded into the chip by using a flow-driven neMESYS pump. (Details and illustration of the optical and fluidic setups are described in chapter 3 of this thesis.) In this preliminary test, the aqueous solution of the first water stream was a PBS buffer solution (pH 7) and the second aqueous stream was a 25 μ M fluorescein solution in PBS solution (pH 7); the oil phase was silicone oil with 4% wt Span80. Snapshots of droplet fusion were visualized by a high-speed camera (Photron SA3) connected to the inverted microscope.

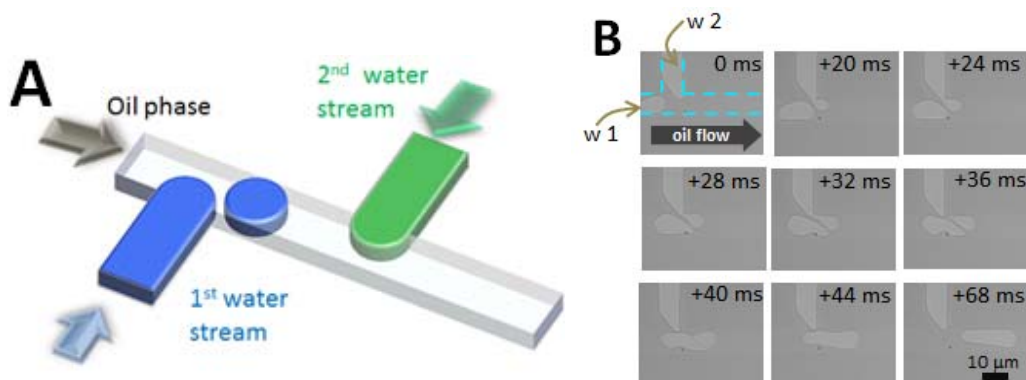


Figure C-1: (A) Configuration of double T-junctions in the nanofluidic network. At the first junction, the first droplet (blue) was formed and flowed to touch the tip of the second water stream (green) resulting in a merged droplet. The depth of the nanochannel is around 500 nm.

After the generation of the first droplet as shown in blue in Fig.C-1A, the generated droplet flowed to hit the tip of the second stream (in green in Fig.C-1A). Snapshots of the subsequent droplet fusion are shown in Fig.C-2B. The first droplet flowed to contact with the tip of the second stream ($t=20$ ms). Then, the shear force exerted by the continuous phase and the first droplet narrowed the neck of this tip ($t=24-32$ ms). Eventually a second droplet was generated by the second aqueous stream and merged with the first droplet ($t=36-44$ ms). The process however mostly proceeded in a different manner, with the second stream

generating a droplet before the arrival of the first droplet. The size of the first droplet is around threefold larger than the size of the second droplet.

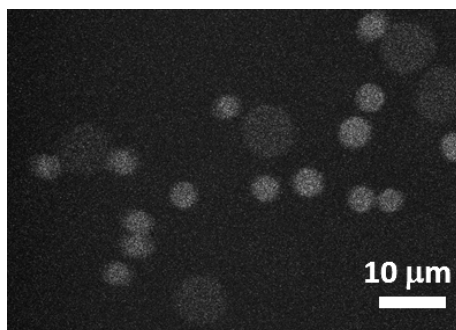


Figure C-2: A snapshot of the generated droplets after droplet fusion. The smaller and brighter droplets represent the droplets containing fluorescein solution. The larger and darker droplets represent the merged droplets. The droplets containing only PBS solution were invisible in this measurement and their dimensions are around threefold larger than the size of the fluorescein-containing droplets. The depth of the nanochannel is around 500 nm.

When entering the outlet nanochannel, the generated droplets of the first and second streams as well as the merged droplets were visualized by a high sensitivity EMCCD camera as shown in Fig.C-2. The smaller and brighter droplets represent non-merged droplets containing fluorescein solution which is the second aqueous stream in Fig.C-1. The droplets from the first aqueous stream containing PBS solution are invisible in this measurement; their dimensions are around threefold larger than the dimensions of the fluorescein droplets. The merged droplets are the larger but darker droplets in Fig.C-2 since, after merging two droplets, the concentration of fluorescein is diluted resulting in a lower fluorescence intensity.

From this preliminary test, two droplets can be merged using the generation of droplets at two consecutive T-junctions. The fusion can be achieved by modulating the flow rates of two streams. However, in our experiment, the success rate of droplet fusion is merely 10 %. The cause of this is the generation of droplets by the second aqueous stream before arrival of the first droplet. The improvement of the droplet fusion should therefore be further studied such as the integration of the expansion chamber downstream the second T-junction as described in the perspective section in chapter 7 of this thesis.



Acknowledgements

In the past four years of my doctoral research in the Netherlands, I have undergone tremendously memorable and marvelous learning experiences. To complete this research study, I owe my sincere gratitude to a number of people who have helped me over the course of this work.

Above all, I am truly thankful to Jan (Prof. Jan C.T. Eijkel) for his superb daily supervision as well as his excellent guidance and sense of humor. He instructed me and showed me scientific attitudes and methodology as well as inspiring me to grow professionally and become an independent researcher. I am also very grateful that he provided me with the freedom to make my own decisions in this study.

I would like to acknowledge Albert (Prof. Albert Van den Berg) for his great supervision and management. He is a vibrant and enthusiastic leader in the BIOS group who always demonstrated to us how to be a successful scientist. I am thankful for all of the social events arranged by him and his family as well as BIOS werkweek. Thanks to all the BIOS werkweek committees for these well-organized activities (both in the USA and France), as well.

All the work related to enzymatic reaction could not have been achieved without the help of Servé Kengen (Microbiology Group, Wageningen University). He provided me with the enzyme and substrate, organized many fruitful discussions on the enzymatic reaction, and arranged the practicum in Wageningen for me. For this, I am sincerely thankful for his help and hospitality.

Lingling Shui, I would like to thank to you for all your suggestions and support in both technical and theoretical aspects of the fluidic phenomena (two-phase flow) and fluidic

Acknowledgements

manipulation and connections. Séverine, I am very appreciative for your kindness in providing me with the opportunity as well as your constant encouragement. Edwin Carlen, thanks for the many vital suggestions both on technical and social aspects.

I am very grateful for the help of Johan and Daniel during my first year in the clean room in MESA+. I learned numerous technical protocols and tricks from both of you. Also, I would like to pay special thanks to Henk for his support with the optical instrument and Focus Ion Beam (FIB) equipment, and to Jan Van and Lennart for their help in solving problems with the optical instrument and fabrication in the clean room. I cannot forget the tremendous support from Hans de Boer whose mechanical tools were always magnificent and helpful. And to Georgette and Wouter Sparreboom for their helps in the software for the high sensitive camera. Many special thanks to all technical staff in the clean room. I am sincerely thankful to several people for their technical support with specific equipment; Gerard Kip for X-ray Photoelectron Spectroscopy (XPS), Mark Smithers for Scanning Electron Microscopy (SEM), and Richard Egberrink (MNF group) for a fluorescence spectroscopy.

I would like to acknowledge all of my office mates (Kanesh, Iris, Arpita, Mingling, Masood, Yanbo Xie, Lonneke, Martin) for all of their cooperative help and support during the last four years. Special thanks to Kanesh for several suggestions during my first two years in Enschede. For the enormously helpful discussion from Masood particularly on the chemical aspect, I also give my sincere gratitude. Special thanks for all night-and-weekend-shift workers (Kanesh, Masood, Arpita) who were always on standby in the lab and cooperated and helped whenever needed. Big thanks to Loes who gave me many suggestions for the preparation of this thesis as well as regularly organized many BIOS activities. Many thanks to Eddy for his scientific and technical suggestions. I would like to thank Hermine for helping especially with official documents and tasks as well as translating Dutch information for me. Also, thanks to all BIOSers and former members who participated or cooperated with me on any occasions. Apart from BIOS, thanks to my Dutch friends (Tom, Andre, Steef) who helped me with many things during my first year in Enschede. Thanks to the Japanese students (Naito and Mao) who cooperated with me in many tasks and shared many scientific – and non-scientific – ideas with me.

Acknowledgements

Charles Baroud (École Polytechnique, France), my first instructor in Microfluidics, who inspired and showed me how wonderful microfluidics is. I am very appreciative that you are on my graduation committee as well. Prof. Isabelle Ledoux-Rak (ENS Cachan, France), it was a very great kindness on your part to offer me the opportunity and provide truly helpful advice during my Master's study in France. Big thanks to all of my dear friends in Cachan as well, you all made my life in France memorable. I am truly grateful to Dominique Chauvat (ENS Cachan, France). He was not only the fantastic researcher and advisor of "Light and Matter" but is also the beloved brother to all Monabiophot students. Dominique, vous remercions vivement pour tous les supports de vous, vous serez dans la mémoire de Monabiophot jamais, reposer en paix.

I would like to give a big hug to all Thai students in Enschede (Aj.Kan, P'May, P'Tom, P'Siti, P'Nu, P'Weaw, P'Took, P'Odd, P'Lek, Pipe, Wisut, Nueng, Gift, Kanda, Ton, Linda, ...) who always arrange "*the star*" dinners and lively rendezvous. These events re-energized my life and opened another window on the world through the sharing of ideas with you all.

Lastly, I would like to pay my sincere gratitude to my parents, brothers and sisters who always listen to me and support me. Thanks for all the encouragement; life is an adventure. Mama, in my dreams, you always stand by me.

Rerngchai Arayanarakool
Enschede, 2012

Curriculum Vitae

Personal Information

Date and Place of Birth : 4th Feb 1981, Nakorn Ratchasima, Thailand
Personal Contact : rerngchaia@yahoo.com

Education

Doctoral Degree Oct.2008 - Sep.2012
University of Twente, The Netherlands
Thesis: Toward Single Enzyme Analysis in a Droplet-based Micro and Nanofluidic System

Master's Degree Sep.2006 - Aug.2008
École Normale Supérieure de Cachan, France
Program: Molecular Nano and Biophotonics
Project: Integration of Magnetic Sensor into Lab-on-a-Chip System

Bachelor's Degree May.1998 - Mar.2002
Chulalongkorn University, Thailand
Program: Chemical Engineering
Project: Regeneration of Catalyst for Hydrogenation

Employment

Post-doctoral Researcher, IFW Dresden, Germany Oct.2012 - Present
Engineer, Technip Engineering, Thailand Sep.2003 - Jul.2006
Engineer, Thai Petrochemical Industry, Thailand Sep.2002 - Aug.2003

Publications

International Journal Articles

1. **Rerngchai Arayanarakool**, Lingling Shui, Servé Kengen, Albert van den Berg, and Jan C.T. Eijkel, “Single-enzyme analysis in a droplet-based micro and nanofluidic system”, (in preparation).
2. Toyohiro Naito, **Rerngchai Arayanarakool**, Séverine Le Gac, Takao Yasui, Noritada Kaji, Manabu Tokeshi, Albert van den Berg, Yoshinobu Baba, “Temperature-driven self-actuated microchamber sealing system for highly integrated microfluidic devices”, *Lab on a chip*, 2012, (submitted)
3. **Rerngchai Arayanarakool**, Lingling Shui, Albert van den Berg, and Jan C.T. Eijkel, “A new method of UV-patternable hydrophobization of micro- and nanofluidic networks”, *Lab on a chip*, 2011, 11 (24). pp. 4260-4266.
4. **Rerngchai Arayanarakool**, Séverine Le Gac, and Albert van den Berg, “Low-temperature, simple and fast integration technique of microfluidic chips by using a UV-curable adhesive”, *Lab on a chip*, 2010, 10 (16). pp. 2115-2121.

Conference Proceedings

1. **Rerngchai Arayanarakool**, Lingling Shui, Servé Kengen, Albert van den Berg, and Jan C.T. Eijkel, “Single-enzyme analysis in a droplet-based micro and nanofluidic system”, *Conference on Miniaturized Systems for Chemistry and Life Sciences, μ TAS 2012, 28 October – 1 November 2012, Okinawa, Japan*.
 2. **Rerngchai Arayanarakool**, Lingling Shui, Albert van den Berg, and Jan C.T. Eijkel, “A new method of UV-patternable hydrophobization of micro- and nanofluidic networks”, *Conference on Miniaturized Systems for Chemistry and Life Sciences, μ TAS 2011, 2-6 October 2011, Seattle, Washington, USA*.
 3. Toyohiro Naito, **Rerngchai Arayanarakool**, Noritada Kaji, Yokohiro Okamoto, Manabu Takeshi, Séverine Le Gac, and Albert van den Berg, Lingling Shui, Albert van den Berg, and Yoshinobu Baba, “Temperature-driven self-actuated microvalve for PCR”, *Conference on Miniaturized Systems for Chemistry and Life Sciences, μ TAS 2011, 2-6 October 2011, Seattle, Washington, USA*.
 4. **Rerngchai Arayanarakool**, Severine Le Gac, and Albert van den Berg, “Low-temperature, simple and fast integration technique of microfluidic chips by using a UV-curable adhesive”, *NanoBioTech Montreux 2009, 16-18 November 2009, Switzerland*.
-

“We should seek the greatest value of our action”

...Professor Stephen Hawking...
